Design of a Low Enrichment, Enhanced Fast Flux Core for the Massachusetts Institute of Technology Research Reactor

By

Tyler Shawn Ellis

S.B. Nuclear Science and Engineering, Massachusetts Institute of Technology, 2006
S.M. Nuclear Science and Engineering, Massachusetts Institute of Technology, 2006

Submitted to the Department of Nuclear Science and Engineering
in partial fulfillment of the requirements for the degree of

Doctor of Philosophy
at the
Massachusetts Institute of Technology

December 2008

Signature of Author: _____
Department of Nuclear Science and Engineering
December 9, 2008

Certified by: _____
Professor Mujid S. Kazimi, Supervisor
TEPCO Professor of Nuclear Science and Engineering
Director, Center for Advanced Nuclear Energy Systems

Certified by: _____
Professor Benoit Forget, Supervisor
Assistant Professor of Nuclear Science and Engineering

Certified by: _____
Dr. Thomas H. Newton, Jr., Reader
Reactor Physicist, MIT Nuclear Reactor Laboratory

Certified by: _____
Dr. Edward E. Pilat, Reader
Research Scientist, Department of Nuclear Science and Engineering

Accepted by: _____
Professor Jacquelyn C. Yanch
Chairman, Department Committee on Graduate Students

Design of a Low Enrichment, Enhanced Fast Flux Core for the Massachusetts Institute of Technology Research Reactor

by

Tyler Shawn Ellis

Submitted to the Department of Nuclear Science and Engineering on December 9, 2008 in Partial Fulfillment of the Requirements for the Degree of Doctor of Philosophy in Nuclear Science and Engineering

Abstract

Worldwide, there is limited test reactor capacity to perform the required irradiation experiments on advanced fast reactor materials and fuel designs. This is particularly true in the U.S., which no longer has an operating fast reactor but depends upon two aging thermal reactors for testing the behavior of various materials in an irradiation environment. The MIT research reactor is planning for a new core to end the need for highly enriched uranium and operate the reactor with uranium enrichments under 20%. This study explores the use of the central region in the newly proposed MIT reactor core to boost the production of fast neutrons, thus making the new core more beneficial for materials testing.

The Fast Flux Trap introduces a region of fissile material surrounding a central irradiation facility which is cooled by liquid lead-bismuth eutectic. This arrangement maximizes the fast neutron production by avoiding neutron moderation in the center. The fissile material, arranged in a tight hexagonal pin array, can be uranium enriched in either ^{235}U or ^{233}U, to the limit allowable for non-proliferation. Insertion of the Fast Flux Trap in the proposed low enriched uranium core operated at a 10 MW power level, can provide a 252%-271% higher fast neutron flux than the previously proposed designs with low enriched fuel for the MIT research reactor and a 235%-253% higher fast neutron flux than the existing highly enriched uranium MITR-II core at 5 MW. This new core fast flux capability is within a factor of 2 to 4 of the much larger national test reactors, the Advanced Test Reactor and the High Flux Isotope Reactor, and hence can allow the MIT research reactor to be more useful for fast irradiation.

The work covered both steady state and transient events involving the Fast Flux Trap, using the Monte Carlo N-Particle (MCNP) transport code. It was shown that the power distribution within the Fast Flux Trap pins as well as the plates in the rest of the core will be satisfactory; or in other words, no excessive power peaking will develop. The limits of the Fast Flux Trap lifetime were found to exceed the expected licensing time of the new core. Furthermore, the reactivity implications of metallic coolant leaks, water flooding of the Fast Flux Trap and various possible test materials were all found to be acceptable. The loss of flow following a pump trip event was analyzed using the RELAP5-3D code, and found not to result in excessive temperatures with regards to materials strength and corrosion resistance.

While the specific design developed in this dissertation is particular to the MIT research reactor core, the Fast Flux Trap design concept can potentially be applied in other reactor cores so that other thermal spectrum research and test reactor facilities can benefit from this enhanced capability.

Thesis Supervisor:	Mujid S. Kazimi TEPCO Professor of Nuclear Science and Engineering Director, Center for Advanced Nuclear Energy Systems
Thesis Supervisor:	Benoit Forget Assistant Professor of Nuclear Science and Engineering

Acknowledgements

I've always found in life that the more challenging the journey, the more worthwhile and spectacular the culmination. This thesis is the capstone of my seven and a half year journey at MIT and I would like to recognize all of those who have helped me along the way. First and foremost, I'd like to acknowledge the guidance and support of my thesis supervisors Professor Mujid Kazimi and Professor Benoit Forget. Professor Kazimi has been an unwavering source of support throughout both my undergraduate and graduate career. I certainly would not have arrived at where I am today without his direction. Professor Forget has also provided invaluable insight and encouragement in the formulation of this thesis. I'd like to thank my thesis readers, Dr. Thomas Newton, Jr. and Dr. Edward Pilat, who have spent a large amount of time answering all my questions and carefully reviewing this work in order to ensure that everything is correct. Thanks are also deserved to Dr. John Bernard for all of his support over the years and to Professor Michael Driscoll for the original inspiration of this thesis. Finally, a multitude of thanks belongs to Dr. Pavel Hejzlar, who is another integral part of my success in this journey. Whether hoisting the Phi Cup victoriously over our heads as ANS Atomsmashers or figuring out the ins and outs of every nuclear analysis code imaginable, I have always enjoyed our time together. It has been an honor and a privilege to work with all of you.

Out of the original twelve, I'd also like to acknowledge the camaraderie of my remaining four NSE compatriots who have truly made this journey enjoyable along the way; David Carpenter, Erik Johnson, Mike Short and Michael Stawicki. Between MSR design sessions at the Asgard, January reconnaissance missions, various start-up companies or just discussing life in general; I've cherished all of the memories with you guys. I wish you all the very best of luck and I'll look forward to seeing the magnitude of our impact upon the world.

I'd also like to thank Clare Egan for all of her support, Peter Brenton for working with me on various department related endeavors and everyone else in the NSE department over the years. Seven and a half years is the longest I've ever lived in one place and you all have helped make it a home.

The financial support for this work was provided by the Reduced Enrichment for Research and Test Reactors (RERTR) Program of the National Nuclear Security Administration at the U.S. Department of Energy.

Finally, last but certainly not least, I'd like to acknowledge the love and support of my family, Randy, Carol, Laura-bean, Chance, Riley and everyone else in the Ellis and VanGarven clans. Though we are now spread out all over, I feel that the love between us is as strong as ever. And to Chance, who saw me embark on this journey but didn't live long enough to see me complete it, I know you're still watching from above.

For Chance

Table of Contents

Abstract 3

Acknowledgements 5

Table of Contents 7

List of Figures 10

List of Tables 13

Chapter 1 - Introduction 16

1.1 Background and Motivation 16

1.2 Review of Previous Work on Fast Flux Facilities 21

1.3 Review of Previous Work on LEU Fuels 25

1.4 Constraints 27

1.5 Objective 28

1.6 Organization 28

Chapter 2 – Design Description 31

2.1 Existing MITR-II Description 31

2.2 Proposed MITR-III Description 34

2.3 Fast Flux Trap Design Evolution 41

2.4 Proposed Fast Flux Trap Description 47

Chapter 3 – Neutronic Evaluation 53

3.1 Steady-state Analyses 53

3.1.1 Flux Spectrum Enhancement 54

3.1.2 Power Peaking Profiles for Fast Flux Trap Amplifier Pins 59

3.1.3 Cadmium Filter Optimization 63

3.1.4 Reactivity Worth of Typical Experimental Samples 65

3.1.5 Power Peaking Profiles for Fuel Plates 67

3.2 Reactivity Insertion Analyses 73

3.2.1 Initial Fast Flux Trap Insertion 73

3.2.2 Reactivity Worth of Fast Flux Trap 73

3.2.3 Reactivity Worth of Control Mechanisms 74

3.2.4 Pb-Bi/Primary H_2O Leakage Effects 75

3.2.5 Flooding of the Central Irradiation Facility 76

3.3 Lifetime Analyses 77

3.3.1 F1 Fast Flux Trap Design Lifetime Analysis 78

3.3.2 F2 Fast Flux Trap Design Lifetime Analysis 81

3.3.3 Coolant Activation 85

Chapter 4 – Thermal Hydraulic Evaluation 86

4.1 Coolant Selection 86

4.2 Structural Material Selection 88

4.3 Steady-state Analyses 89

4.4 Transient Analyses 100

Chapter 5 - Summary 110

5.1 Conclusions 110

5.2 Recommendations for Future Work 113

References 115

Appendix A: MCNP/MCODE Input Files 118

A.1 F1 Design 118

A.2 F2 Design 118

Appendix B: RELAP Input Files 119

B.1 F1 Design 119

B.2 F2 Design 119

Appendix C: Computational Modeling Tools 120

C.1 Neutronic Modeling Tools 120

C.2 Thermal Hydraulic Modeling Tools 121

Appendix D: Experimental Sample Total Absorption Cross Sections 123

List of Figures

Figure 1: Typical Neutron Flux Spectra for Fast and Thermal Reactor Systems [adapted from DOE] 17

Figure 2: Neutron Energy Spectrum at the Peak Flux Position in the Irradiation Zone of the MTS Compared to that of a Fast Reactor (ABTR) [Pitcher 2008] 23

Figure 3: Neutron Flux Spectra within the Flux Trap Region of HFIR and the Tri-Pin Fast Irradiation Facility [Ellis, Gehin *et. al.* 2008] 24

Figure 4: MITR-II Cutaway View 33

Figure 5: MITR-II Core Cross Section 34

Figure 6: LEU LSSS Power for Fuel Thickness of 0.762mm [Ko 2008] 36

Figure 7: Proposed MITR Whole Core Cross Section 37

Figure 8: Cross Section of core design with Fast Flux Trap and an Amplifier Ring [Ellis and Newton 2008] 42

Figure 9: Fast Flux versus Outer Radius of the Amplifier Ring 45

Figure 10: Fast Flux Trap Ring Assembly [Ellis and Newton 2008] 46

Figure 11: Fast Flux Trap XY Cross-section 48

Figure 12: LEU Enrichment Standard Curves [von Hippel and Kang 2001] 50

Figure 13: Vertical Diagram of Fast Flux Trap Loop 52

Figure 14: Flux Spectrum Comparison of F1, F2, and HEU/LEU Reference Designs for a 10 MW Core 55

Figure 15: Numbering Scheme for Amplifier Pin Flux Profiles 57

Figure 16: Neutron Flux Comparison of Amplifier Pin Rings and Core Elements 58

Figure 17: F1 Design Radial Peaking Factors 60

Figure 18: F2 Design Radial Peaking Factors 61

Figure 19: Cadmium Filter Effect on the Neutron Flux Spectrum 64

Figure 20: Neutron Energy Spectrum in the Middle H2O Channel in the B-6 Fuel Element 72

Figure 21: F1 Design Neutron Spectra in the Central Irradiation Facility during Operational Lifetime 79

Figure 22: F2 Design Neutron Spectra in the Central Irradiation Facility during Operational Lifetime 82

Figure 23: RELAP5-3D Fast Flux Trap Nodalization Diagram 91

Figure 24: Sub-channel Geometry 92

Figure 25: Steady-state Coolant Pressure Profile for F1 FFT 94

Figure 26: Steady-state Coolant Velocity Profile for F1 FFT 95

Figure 27: Steady-state Coolant Temperature Profile for F1 FFT 96

Figure 28: Steady-state Coolant Pressure Profile for F2 FFT 97

Figure 29: Steady-state Coolant Velocity Profile for F2 FFT 98

Figure 30: Steady-state Coolant Temperature Profile for F2 FFT 99

Figure 31: Pb-Bi Coolant Pump Coastdown Curve [Memmott 2008] 100

Figure 32: F1 FFT Design Fuel Temperature at Side Sub-channel Outlet 103

Figure 33: F1 FFT Design Clad Temperature at Side Sub-channel Outlet 104

Figure 34: F1 FFT Design Pb-Bi Temperature at Side Sub-channel Outlet 105

Figure 35: F2 FFT Design Fuel Temperature at Side Sub-channel Outlet 106

Figure 36: F2 FFT Design Clad Temperature at Side Sub-channel Outlet..... 107

Figure 37: F2 FFT Design Pb-Bi Temperature at Side Sub-channel Outlet..... 108

Figure 38: Total Absorption Cross Section for Isotopes of Iron 123

Figure 39: Total Absorption Cross Section for Isotopes of Chromium..... 124

Figure 40: Total Absorption Cross Section for Natural Graphite..... 125

Figure 41: Total Absorption Cross Section for Natural Tungsten..... 126

Figure 42: Total Absorption Cross Section for Natural Titanium 127

List of Tables

Table 1: U.S. Nuclear Facilities Which Don't Require High Uranium Density Fuels to Convert [Newton 2006] 19

Table 2: U.S. Nuclear Facilities Which Require High Uranium Density Fuels to Convert [Newton 2006] 20

Table 3: Non-U.S. Nuclear Facilities Which Require High Uranium Density Fuels to Convert [Newton 2006] 21

Table 4: Properties of UAlx and U-10Mo Fuels [Newton 2006 and IAEA] 25

Table 5: Fuel Assembly Design Parameters 38

Table 6: Y-12 Chemical Specification of Uranium Metal Supplied to Research Reactors [adapted from Y-12 2005] 38

Table 7: Flowrate Effect on Core Tank Pressure Loading 39

Table 8: Estimated Peak Neutron Fluence for the MITR-II Reactor Core Tank [Kohse 2008a] 40

Table 9: Neutronic Properties of Am-242m, U-233 and U-235 44

Table 10: U-233 as a Fissile Material [Kazimi 2003] 49

Table 11: Fast Flux Enhancement of F1 Design 56

Table 12: Fast Flux Enhancement of F2 Design 56

Table 13: Neutron Flux Profile across Rings of Amplifier Pins 59

Table 14: F1 Design Amplifier Pins Axial Peaking Profile 62

Table 15: F2 Design Amplifier Pins Axial Peaking Profile 62

Table 16: Cadmium Filter Thickness Affect Study 63

Table 17: Reactivity Effect of Various Samples 65

Table 18: Core Plate Hot Channel Factors for the F1 Design 69

Table 19: Core Plate Hot Channel Factors for the F2 Design 70

Table 20: Axial Power Production Profile for Core Plates in the F1 Design 71

Table 21: Reactivity Difference from Installation of Fast Flux Trap Loop 73

Table 22: Reactivity Worth of Fast Flux Trap 74

Table 23: Control Rod Insertion Worth 74

Table 24: Control Rod Insertion plus Reflector Dump Worth 74

Table 25: Control Blade Shutdown Margin Calculation of FFT and LEU Reference Designs 75

Table 26: Fast Flux Trap Water Ingress Reactivity Difference 76

Table 27: F1 Design Flooded Central Irradiation Facility Reactivity Insertion 77

Table 28: F2 Design Flooded Central Irradiation Facility Reactivity Insertion 77

Table 29: Neutron Flux Changes during Operational Lifetime of the F1 FFT 80

Table 30: Fissile and Fertile Vector Changes during Operational Lifetime of the F1 FFT 80

Table 31: Heat Production Changes during Operational Lifetime of the F1 FFT 81

Table 32: Neutron Flux Changes during Operational Lifetime of the F2 FFT 83

Table 33: Fissile and Fertile Vector Changes during Operational Lifetime of the F2 FFT 84

Table 34: Heat Production Changes during Operational Lifetime of the F2 FFT 84

Table 35: Reactor Coolant Basic Characteristics [Todreas 2004] 86

Table 36: Decay Heat Curves for U-235 (F1) and U-233 (F2) FFT Designs..... 101

Table 37: Fast Flux Comparison between the MITR-III FFT Design, ATR and HFIR. 111

Chapter 1 - Introduction

1.1 Background and Motivation

At the beginning of an era which promises to be the second great expansion of nuclear energy worldwide, innovations in reactor design are to be expected. However, unlike the first era, there is limited test reactor capacity to perform the required irradiation experiments on new designs. This is particularly true in the U.S., which no longer has an operating fast reactor but depends upon two aging thermal reactors for testing materials' behavior under irradiation. It is the fast neutron flux that causes damage to the materials, and not having such a fast spectrum test capability has led to suggestions for using the existing reactors, such as the Advanced Test Reactor (ATR) or the High Flux Isotope Reactor (HFIR), to boost their fast neutron flux levels to the largest extent possible while the Department of Energy (DOE) develops plans for new fast reactor test facilities. As shown in Figure 1, thermal reactors have a significantly lower fast flux than fast reactors. Therefore in order to achieve comparable fast fluxes in a thermal reactor, significant design modifications will be necessary.

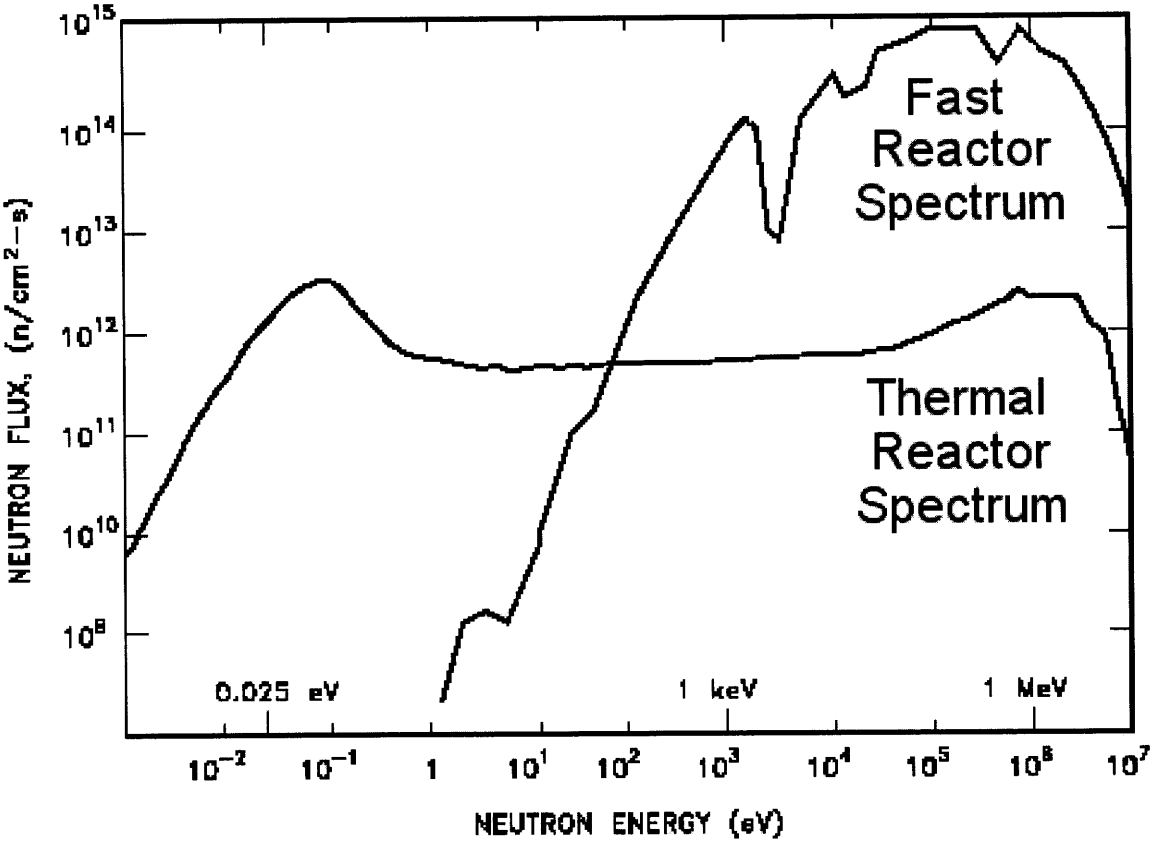

Figure 1: Typical Neutron Flux Spectra for Fast and Thermal Reactor Systems [adapted from DOE]

This happens to coincide with ongoing planning for a new core at the MIT research reactor to end the need for highly enriched uranium and operate the reactor with uranium enrichments under 20%. The motivation for this change is to increase the proliferation resistance of the fuel, thus adding to both the international and homeland security. Among the many challenges for a terrorist group or rogue nation seeking to build a nuclear weapon, the procurement of weapons grade fissile material is one of the most financially and technically onerous. One potential source of this fissile material is the Highly Enriched Uranium (HEU) fuel intended for use in research and test reactor cores. While this fuel was originally developed to maximize the neutron flux in compact core designs, the rising concern about prospective nuclear terrorists using diverted HEU

for a crude nuclear weapon necessitates the rapid conversion of all research and test reactors who use this fuel.

On December 8th, 1953, United States President Dwight Eisenhower gave a famous speech entitled "Atoms for Peace" in which he hoped to hasten the day when fear of the atom will begin to disappear from the minds of people [Eisenhower 1953]. One of the proposals to accomplish this worthy goal was the exportation of research reactors of varying power levels worldwide. Since the cores were typically small in physical size, several of them were built utilizing HEU.

In the 1970s during the early Carter administration, a political realization was made that the HEU from these reactors could potentially be diverted for nuclear weapons purposes. Thus began the political impetus for minimizing the use of HEU in the international civilian nuclear sector. The US sought to accomplish this by promoting a switch of all current research and test reactors throughout the world from highly enriched fuel designs to low enriched designs. By keeping the ^{235}U content to less than 20 weight percent, the attractiveness of the Low Enriched Uranium (LEU) for nuclear weapon purposes is virtually non-existent since the critical mass is on the order of several hundreds of kilograms. Although the ^{239}Pu production increases by an order of magnitude from the vast presence of the ^{238}U in LEU fuel, this change does put the fissile isotopes in a significantly less usable form since reprocessing ^{239}Pu is considerably more expensive and difficult to perform than the enrichment process of ^{235}U.

In 1978 the Reduced Enrichment for Research and Test Reactors (RERTR) program was established with the expressed desire to 'develop the technical means to convert the reactors and isotope production processes from the use of HEU to the use of

low enriched uranium through the development of new LEU fuels and targets' [U.S. DOE]. The RERTR program pursues this goal by initially helping to develop LEU fuels and the necessary targets for isotope production and then by aiding fuel suppliers, such as BWXT, to produce and sell LEU fuels. The main focus of the RERTR program now is in developing high uranium density fuels for high power density reactors.

Out of the remaining nine research reactors in the United States which currently use HEU, three have sufficiently low power density that they can convert over to LEU using currently existing LEU fuels. These reactors are listed below in Table 1.

Table 1: U.S. Nuclear Facilities Which Don't Require High Uranium Density Fuels to Convert [Newton 2006]

Name of Facility	Power Level (MW)	Scheduled to Convert by
DOE NRAD Reactor	1	2009
University of Wisconsin	1	2009
General Electric NTR Reactor	0.1	To Be Determined

The other six research reactors listed in Table 2, present a larger conversion challenge due to the fact that their small size and sufficiently high power density does not allow them to use any of the currently qualified LEU fuels. This necessitates that a program for a new high uranium density fuel be developed and the fuel qualified to appreciable burnup.

Table 2: U.S. Nuclear Facilities Which Require High Uranium Density Fuels to Convert [Newton 2006]

Name of Facility	Power Level (MW)
ATRC	Critical
Massachusetts Institute of Technology	5
University of Missouri at Columbia	10
National Institute of Standards and Technology	20
High Flux Isotope Reactor	85 actual (100 capable)
Advanced Test Reactor	110 actual (250 capable)

It's also important to note that these reactors were specifically designed and optimized to deliver large neutron fluxes to adjoining experimental facilities. The experiments performed in these reactors directly support basic scientific research and the nuclear industry; these experiments ensure adequate funding for the reactor and its personnel. It is thus critical that these new core designs be able to deliver either equivalent or higher neutron fluxes. Failure to meet this design goal will jeopardize the long-term financial viability of the reactor and lead to an eventual shutdown of important nuclear testing facilities.

Finally, since the U.S. has been the main driving force behind the conversion effort internationally, it is essential that the U.S. provide leadership in developing innovative LEU designs which can be applied to the other 24 high power density HEU reactors located throughout the rest of the world (shown in Table 3). This transfer of knowledge by the U.S. will directly help to strengthen the nuclear non-proliferation regime worldwide.

Table 3: Non-U.S. Nuclear Facilities Which Require High Uranium Density Fuels to Convert [Newton 2006]

Country	Name of Facility	Power Level (MW)
Belgium	BR-2	100
Czech Republic	LWR-15 (Rez)	10
	VR-1	0.005
France	ORPHEE	14
	RHF	58.3
Germany	FRM-II	20
Kazakhstan	VVR-K	10
	VVR-K critical facility	6
Poland	MARIA	30
Russia	CA.MIR-M1	Critical
	CA.SM-3	Critical
	IR-8	8
	IRT-ME Ph. Inst.	2.5
	IRT-T	6
	IVV-2M	15
	MIR-M1	100
	PIK	Critical
	PIK Physical Model	Critical
	RBT-6	6
	RBT-10/2	7
	SM-3	100
	VVR-M	18
	VVR-TS	15
Uzbekistan	VVR-CM	10

1.2 Review of Previous Work on Fast Flux Facilities

In February 2006, the United States federal government announced a plan called Global Nuclear Energy Partnership (GNEP) which sought to reduce the risks of nuclear proliferation while simultaneously expanding the use of nuclear energy worldwide. One of the central tenants in this plan was the construction of a fast spectrum sodium cooled reactor which would have the capability of transmuting minor actinides in a closed fuel

cycle. This necessitated the development of new fuel forms which have the capability of accommodating large quantities of minor actinides while surviving high neutron fluence in a fast spectrum. Since new fuel forms must be tested prior to certification from the Nuclear Regulatory Commission (NRC), a domestic testing facility capable of appreciable fast neutron flux was needed. Unfortunately, no fast reactor testing facilities are available in the United States and very few are available internationally. This lack of proper facilities prompted the nuclear research community to investigate novel avenues of developing this capability.

Researchers in Los Alamos National Laboratory have proposed the design of a 1 MW proton beam called the Materials Test Station (MTS) which generates neutrons through spallation reactions resulting from the interaction of 800-MeV protons with tungsten targets. The theoretical models indicated that a fast flux of over $1.2x10^{15}$ n cm^{-2} s^{-1} and a fluence over $2x10^{22}$ n cm^{-2} per year are possible [Pitcher 2008]. As shown in Figure 2, the neutron energy spectra of the MTS and a typical fast reactor are similar. The x-axis is given in units of neutron flux per unit lethargy where lethargy is defined as the natural logarithm of the ratio of a reference energy to the energy of the neutron. The reference energy is typically the maximum energy that a neutron can have in a particular reactor facility. In the case of the Advanced Burner Test Reactor (ABTR), this reference energy is ~10 MeV; for the case of the MTS, the value is ~800 MeV. The (a.u.) stands for 'arbitrary units' which reflects the dimensionless nature of these numbers.

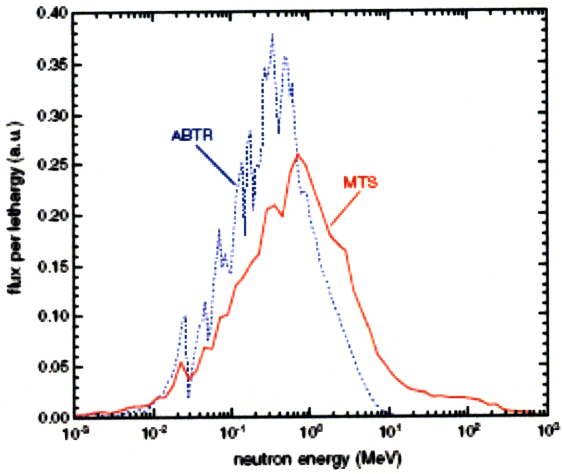

Figure 2: Neutron Energy Spectrum at the Peak Flux Position in the Irradiation Zone of the MTS Compared to that of a Fast Reactor (ABTR) [Pitcher 2008]

The main technical challenge which needs to be addressed is the ramification of the high energy tail for the MTS neutron spectrum. Normally in a fast reactor the neutron energy spectrum drops off to nearly zero after 10 MeV. However with the MTS system there is a high every tail which extends all the way up to the incident 800 MeV beam energy. This higher energy neutron flux increases hydrogen and helium production in metals. In iron, for example, the helium production rate is approximately 60 times higher in the MTS system than in a typical fast reactor. This is important because higher concentration of helium can lead to embrittlement and since ferritic/martensitic are being considered for fast reactor cladding, extra consideration will have to be given if this facility is used for cladding material testing. On the practical side, this facility will optimistically take 4.5 years to construct; provided all $73 million of funding is available from the federal government. Since this is more of a longer term proposition, the nuclear research community has started to investigate alternative shorter term solutions which utilize currently operating thermal reactors.

Researchers at Oak Ridge have proposed the design of a fast spectrum irradiation facility in the HEU fueled High Flux Isotope Reactor (HFIR). This fast spectrum irradiation facility design was essentially the existing core but with replacement of seven target pin irradiation spots with a single europium lined tube in which samples can be inserted. As shown in Figure 3, the europium liner was included to absorb most of the thermal neutrons so that the samples will see a more pure fast flux.

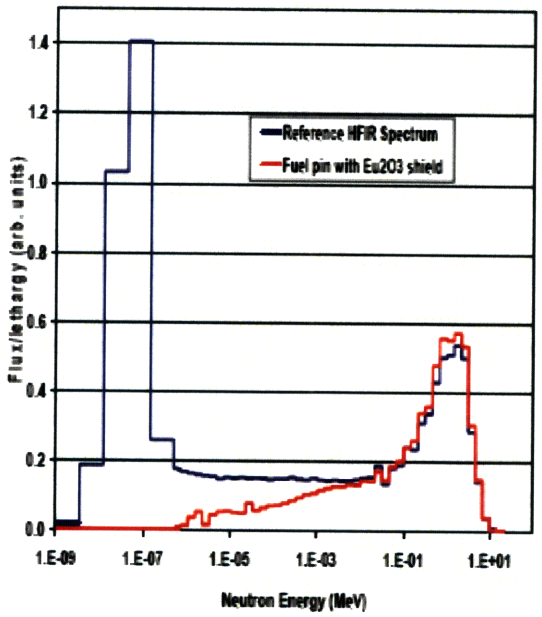

Figure 3: Neutron Flux Spectra within the Flux Trap Region of HFIR and the Tri-Pin Fast Irradiation Facility [Ellis, Gehin *et. al.* 2008]

Their analyses show that a fast flux of $1x10^{15}$ n/cm^2 s can be achieved with an acceptable impact on HFIR operation [Ellis, *et. al.* 2008]. It's important to note that the fast flux quoted in this paper is based upon the existing HFIR core which operates with HEU. It is not known how the LEU conversion process will affect HFIR's ability to deliver this fast flux. Research is needed to develop innovative mechanisms to amplify the fast flux post-conversion. To date there are no studies which have investigated innovative mechanisms

of amplifying the fast flux potential of currently operating high power density thermal research reactors after the conversion process.

1.3 Review of Previous Work on LEU Fuels

On the LEU fuels development side, several low uranium density fuels in the range of 2-4 g/cm^3 have already been developed. These include uranium-aluminum, uranium-oxygen and uranium-zirconium hydride alloys. U_3Si_2-Al dispersion fuel has also been developed and qualified with uranium densities in the range of 4.8 to 6 g/cm^3 but unfortunately this is still not high enough for high power density reactors such as the MITR.

More recently, U-10Mo monolithic fuel has been developed with uranium densities well over 15 g/cm^3, which is more than enough to support the conversion of all existing high power density reactors. Due to its superior irradiation performance during lifetime burnup as well as minimal problems with fuel/clad bonding, U-10Mo has been selected as the leading candidate for high power density research reactor fuel [Wachs *et al.* 2008]. Table 4 summarizes the more important differences between the HEU fuel currently used in the reactor and the proposed U-10Mo LEU fuel.

Table 4: Properties of UAlx and U-10Mo Fuels [Newton 2006 and IAEA]

Property	UAl_x	U-10Mo
Melting Point (°C)	1400	~1200
Unirradiated Conductivity (W/m K)	72.8	17.6
Allowable Burnup (fissions/cm^3)	2 x 10^{21}	3 x 10^{21}
Total Density (g/cm^3)	3.7	17.55

In his recently completed PhD dissertation, Thomas Newton Jr. [Newton 2006] has already designed a low enriched 5 MWth core utilizing the currently under development Uranium-Molybdenum alloy for the fuel matrix, while keeping the core size and geometry the same. Thus, a reactor internals redesign for the conversion process is not necessary. Unfortunately in this redesign, the flux in experimental facilities at both fast and thermal energies was in most cases decreased from the previous highly enriched core, for the same power level. This is because in this LEU core, the amount of ^{235}U will be greater than that in a HEU for a fixed power level. Since this is a thermal reactor, most of the fissions (on the order of 99%) are caused by thermal neutrons; hence the thermal flux needed to maintain this equivalent power level will be lower even when taking into account the thermal neutron absorption in the ^{238}U which is now four times more abundant than the ^{235}U. Furthermore, the neutron spectrum will harden from the resonance absorption of the ^{238}U which acts to reduce the resonance escape probability. Since the neutron flux a research reactor can deliver to its experimenters is the bread and butter of the facility, the development of an alternative core design capable of higher neutron fluxes and not subject to the same constraints as the previous investigation is needed.

1.4 Constraints

The previously proposed design was developed to fit inside of the present HEU core with minimal changes to the internal core structures and to operate at the currently rated power level of 5 MWth [Newton 2006]. In the present work, both of these limitations will be lifted. The reflector tank diameter will be held constant so that the biological shield and graphite reflector do not have to be rebuilt but the core internals may be subject to redesign. Due to the large reactivity worth of the control mechanisms, the six shim blades, regulating rod and reflector tank dump capability will also be left unchanged so as to minimize the amount of retrofitting work needed for the core upgrade. The structural materials will be selected based upon current availability and compatibility with the materials in its surrounding environment.

In order for the new design to retain its status as a research reactor, the federal laws require that the facility stay at or below 10 MWth and the maximum size for any one experiment be 16 in^2. Additionally, as is required in the current Safety Analysis Report, boiling will not be allowed at any place within the core. Since the reactor primary system operates at atmospheric pressure, this limits the temperature of the primary water coolant under normal operation to approximately 100°C. Equivalent no boiling limits will be imposed for any other non-water coolant systems. In accordance with the goal of being able to readily implement this work, the pumping power and heat rejection equipment will also be limited to currently existing technology.

While the fuel matrix for the core proper will be U-10Mo, which is the current front-runner in high density LEU fuel qualification trials, the fissile material used for amplification of the fast flux can be any matrix. Finally in line with the initial motivation

of increasing the proliferation resistance for the reactor, the fuel enrichment must stay below 20% ^{235}U in the core proper or its equivalent in any fast flux amplification facility.

1.5 Objective

This study will develop an innovative core design providing a significantly higher fast neutron flux than the previously proposed designs with low enrichment fuel for the MIT research reactor. The goal is to enable the performance of a wider variety of experiments for advanced technological development as well as contribute to the strength of the international nuclear non-proliferation regime. Since the nuclear industry depends upon research and test reactors for advanced technological development in the field, it is critical that these facilities do not lose their *raison d'être* in the conversion process.

1.6 Organization

This work is divided into five chapters and three appendices. The first chapter has already presented basic background information and motivation for this work, followed by a short review of the previous work on both fast flux facilities and LEU fuels. This was followed by the constraints applied to the design effort in this thesis as well as the overall objective of the work. The central idea is to describe a potential design for the MITR core which is capable of significantly higher fast neutron flux than previously proposed designs.

The second chapter covers the physical description of the core design. It starts off with a description of the existing MITR-II HEU core which is currently in operation and is followed by a description of the MITR-III core design proposed in this thesis. Then the design evolution of the Fast Flux Trap is discussed along with an explanation of the final design.

The third chapter contains the neutronic evaluation of the of the proposed core design. This chapter is broken down into steady-state, reactivity insertion and lifetime analyses. The steady-state analyses include the flux spectrum enhancement, cadmium filter optimization, reactivity worth of typical experimental samples and power peaking profiles for both the core fuel plates as well as the Amplifier Pins in the Fast Flux Trap. The investigated reactivity insertion analyses include initial insertion of the Fast Flux Trap into the core, leakage between the Pb-Bi and primary water coolant and flooding of the central irradiation facility. This subsection also characterizes the reactivity worth of the Fast Flux Trap as well as all control mechanisms for the core. The lifetime analyses describe how the neutron flux and heat production change with time for both the ^{235}U (F1) and ^{233}U (F2) Fast Flux Trap designs.

The fourth chapter contains the thermal hydraulic evaluation of the proposed core design. This chapter was split into four subsections, coolant selection, structural materials selection, steady-state analyses and transient analyses. The coolant selection describes how Pb-Bi came to be selected for the coolant. The structural materials selection section describes the T91 reference material in addition to the suitability of incorporation for a new alloy currently being developed at MIT. The steady-state analyses contain a description of the hydrodynamic model for the Pb-Bi loop in addition to the temperature,

pressure and velocity profiles during normal operation. The transient analyses show how these parameters change with time after a pump trip.

The fifth chapter summarizes the completed work, gives some concluding remarks and makes recommendations for future analyses. Appendices A and B give the input files for MCODE and RELAP respectively. Appendix C describes the computational tools used for both the neutronic and thermal hydraulic analyses. Appendix D shows the total absorption cross sections for the various experimental samples investigated in section 3.1.4.

Chapter 2 – Design Description

2.1 Existing MITR-II Description

The MITR-I, which used heavy water as both a moderator and as a coolant, first went critical in 1958. This reactor successfully operated for over 14 years before it was shutdown and replaced with a more optimized design. This new core design, called the MITR-II, first went critical in 1975 and has been operating continually ever since. The MITR-II, shown in Figure 4, is a light water cooled and heavy water reflected design. The heavy water reflector is surrounded by an additional graphite reflector and then by a high density concrete (280 lbs/ft^3) biological shield.

The MITR-II has a hexagonal core which is made up of rhomboid-shaped fuel elements as shown in Figure 5. Although there are 27 fuel element spaces total, typically only 24 are occupied by fuel elements. The other three spots are either filled with dummy elements or in-core experiments. The 27 fuel element spots are arranged in three rings; the A-ring which has three element spots, the B-ring which has 9 element spots and the C-ring which has 15 element spots. The A-ring typically contains two of the three dummy elements due to power peaking concerns.

The reactivity of the core is normally controlled with 6 boron impregnated stainless steel shim blades and one regulating rod, which are located around the periphery of the core. These absorbers are held up with electromagnets so that if power to the facility gets cut, they fall into the core via gravity. If additional negative reactivity is desired to be inserted into the core, such as during a refueling procedure, the heavy water reflector can also be dumped by opening an electromagnetic solenoid valve located below

the reflector tank. All of these control systems were developed with the fail-safe design philosophy in mind.

Each fuel element is constituted of fifteen 93% enriched HEU fuel plates with 6061 aluminum cladding. This aluminide cermet matrix fuel has a thickness of 0.76 mm and a length of 610 mm. The cladding has a thickness of 0.38 mm with 0.25 mm by 0.25 mm fins, which were incorporated into the fuel design to enhance the heat transfer capability by a factor of 1.9. The coolant channels have a width of 4.0 mm between plates (from the top of one coolant fin to the other). This core design is appreciably undermoderated primarily because of safety concerns but also to harden the neutron spectrum for experimental purposes. Since the fuel has a density of 3.7 g/cm^3 and a $\rho_{uranium}$ equal to 1.44 g/cm^3, the total uranium loading per element is 506 g of U^{235}. The core typically has 12 kg of ^{235}U.

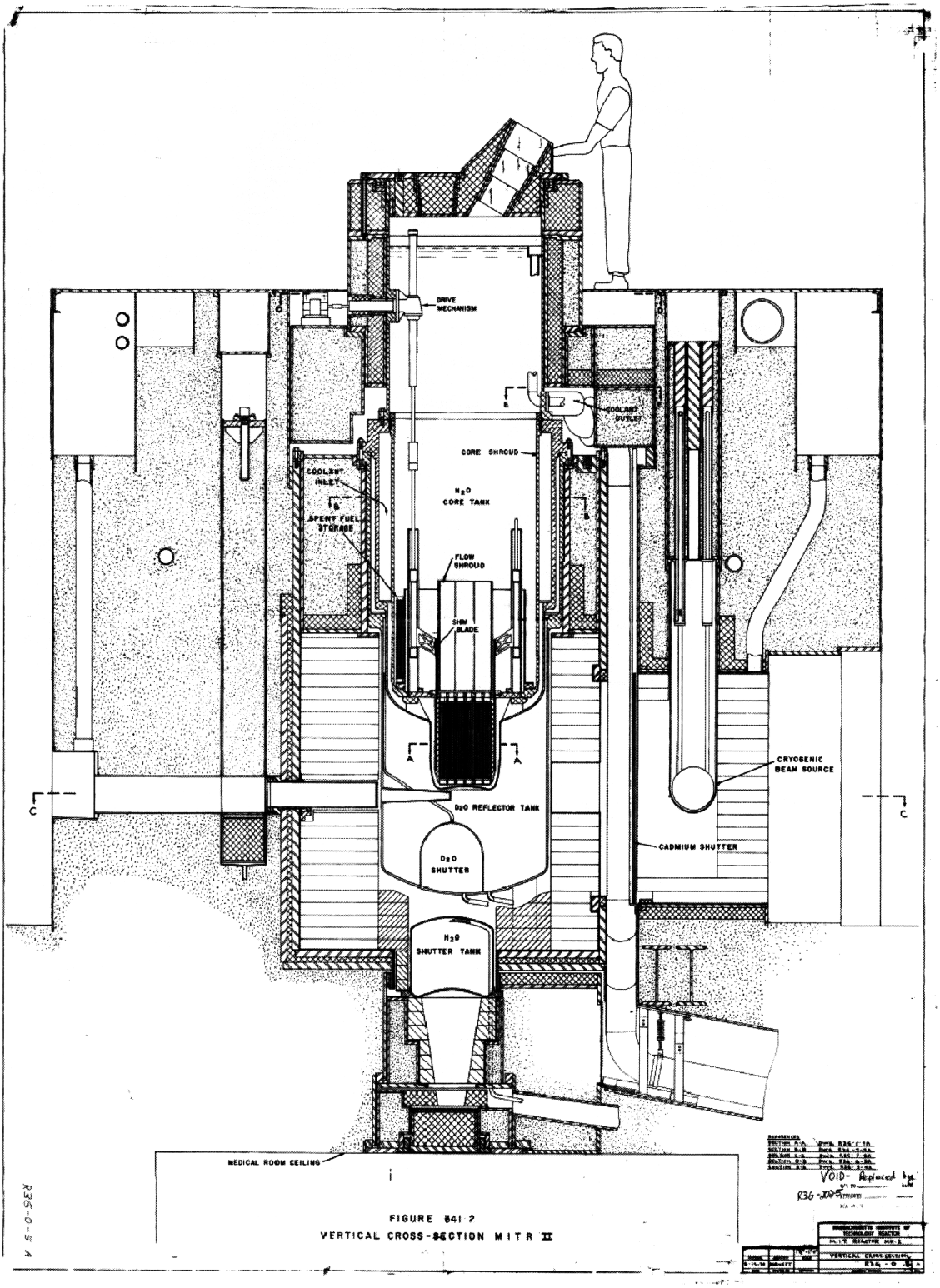

Figure 4: MITR-II Cutaway View

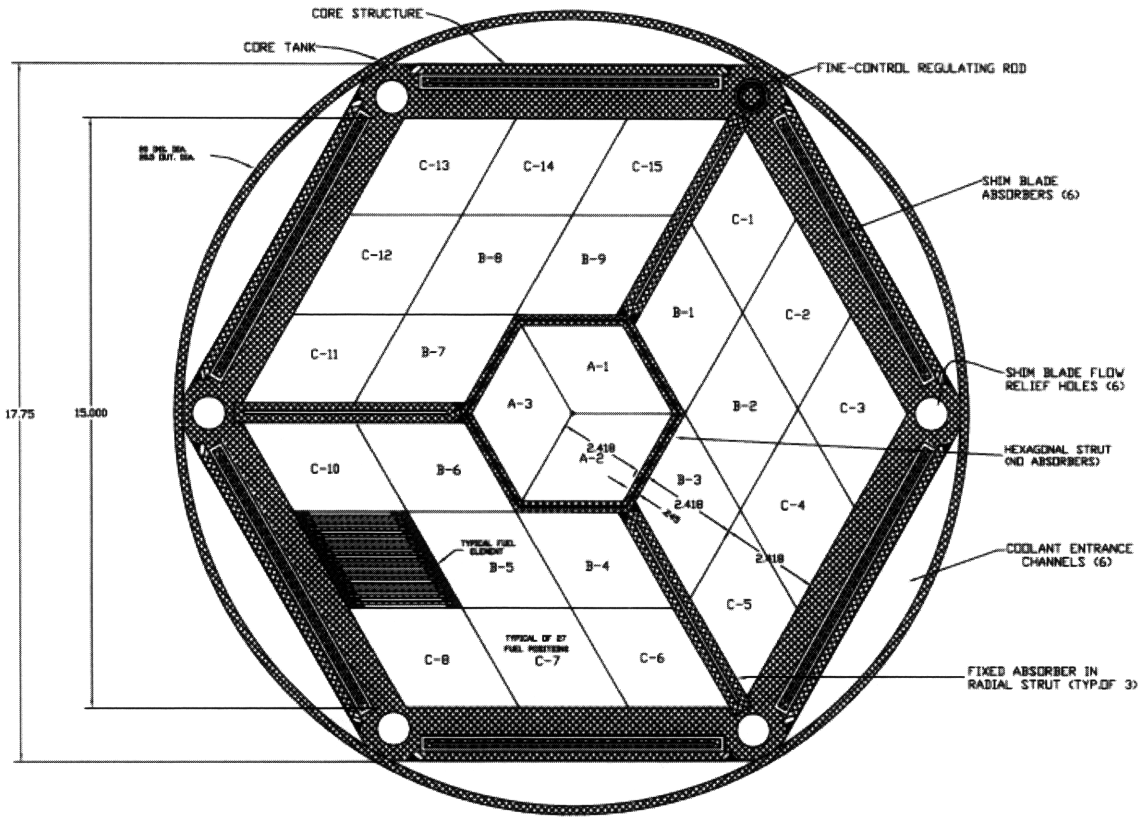

Figure 5: MITR-II Core Cross Section

2.2 Proposed MITR-III Description

Of the various mechanisms to maximize the fast flux in the MITR core, a core power uprate is the most obvious option since higher power equals higher flux. Given that the MITR was licensed as a research reactor, the maximum power level allowed by the NRC is 10 MWth. While it is possible to design a facility of higher power (bringing the facility into the test reactor range), the current regulatory requirements would necessitate a licensing process akin to licensing a brand new reactor. Since this process would take many years and many more millions of dollars than currently available, this option was ruled out.

There have been two major theses which have looked at developing a LEU core for the MITR. The first, a PhD dissertation completed by Thomas Newton, investigated the neutronic aspects of several LEU core designs [Newton 2006]. The second, a S.M. thesis completed by Yu-Chih Ko [Ko 2008], investigated the thermal hydraulic aspects of the LEU core designs developed by Newton. The thermal hydraulic analysis found that the hot channel factor of 1.76, defined as the ratio of peak power in any fuel plate to average power in all the fuel plates, was the main limiting parameter for increasing the core power. Another important parameter was the maximum allowable pressure on the core tank which was limited to equal or below that of the existing HEU core because of unknowns surrounding the condition of the core tank. The thesis by Ko concluded that in light of these constraints, the MITR can safely operate at a power level slightly greater than 6 MWth. An upgrade to 6 MW operation was submitted to the NRC and is expected to be approved in the near future. Ko also inferred that if a new LEU core could be designed with a hot channel factor at or below 1.6 and more information was known about the current state of the reactor vessel, than operation at 10 MWth could be possible. The MITR design proposed in this thesis has a hot channel factor of 1.37 in the B-3 element, which is well below the 1.6 limitation, and a recent study has shown that the reactor vessel has actually gotten stronger instead of weaker [Kohse 2008a], so operation at 10 MW should be feasible provided the appropriate heat removal systems are upgraded.

Currently the MITR-II maintains its Limiting Safety System Settings (LSSS) power settings at 6.0 MW which is a 20% margin above the currently licensed power level of 5 MW. Figure 6 shows that for a 20 plate per element design with a hot channel

factor of 1.6, the LSSS power is over 12 MW which gives appropriate margin for 10 MW operation.

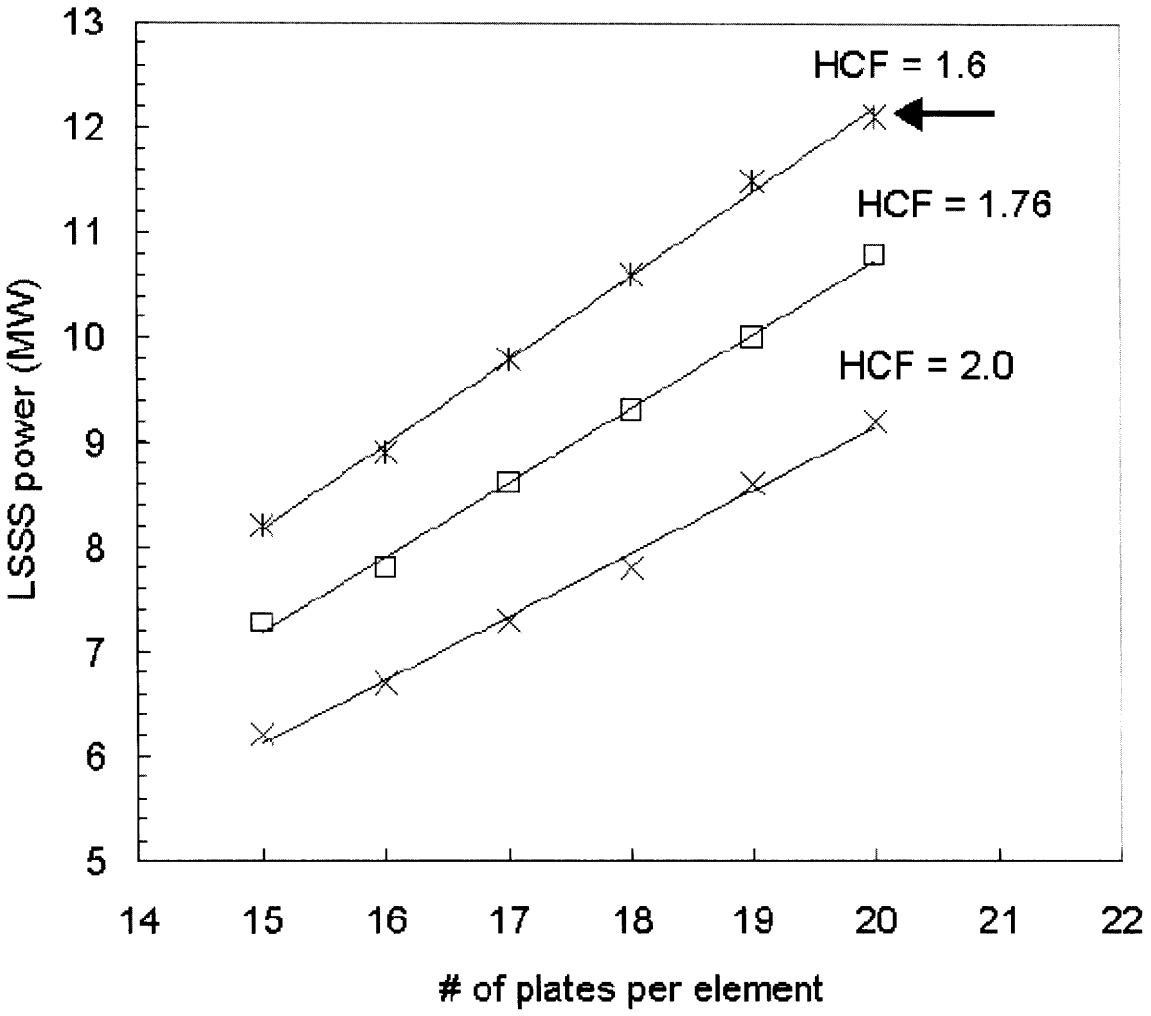

Figure 6: LEU LSSS Power for Fuel Thickness of 0.762mm [Ko 2008]

The proposed MITR core design is shown in Figure 7. The core is comprised of 24 hexagonal fuel elements surrounding a Fast Flux Trap (which will be described in the next section) located in the middle of the core. The fuel element dimension envelope from the MITR-II core was held constant to minimize the required redesign for the core

internals. Due to the large reactivity worth of the existing control absorbers from the MITR-II, the same control absorbers were also used in this redesign.

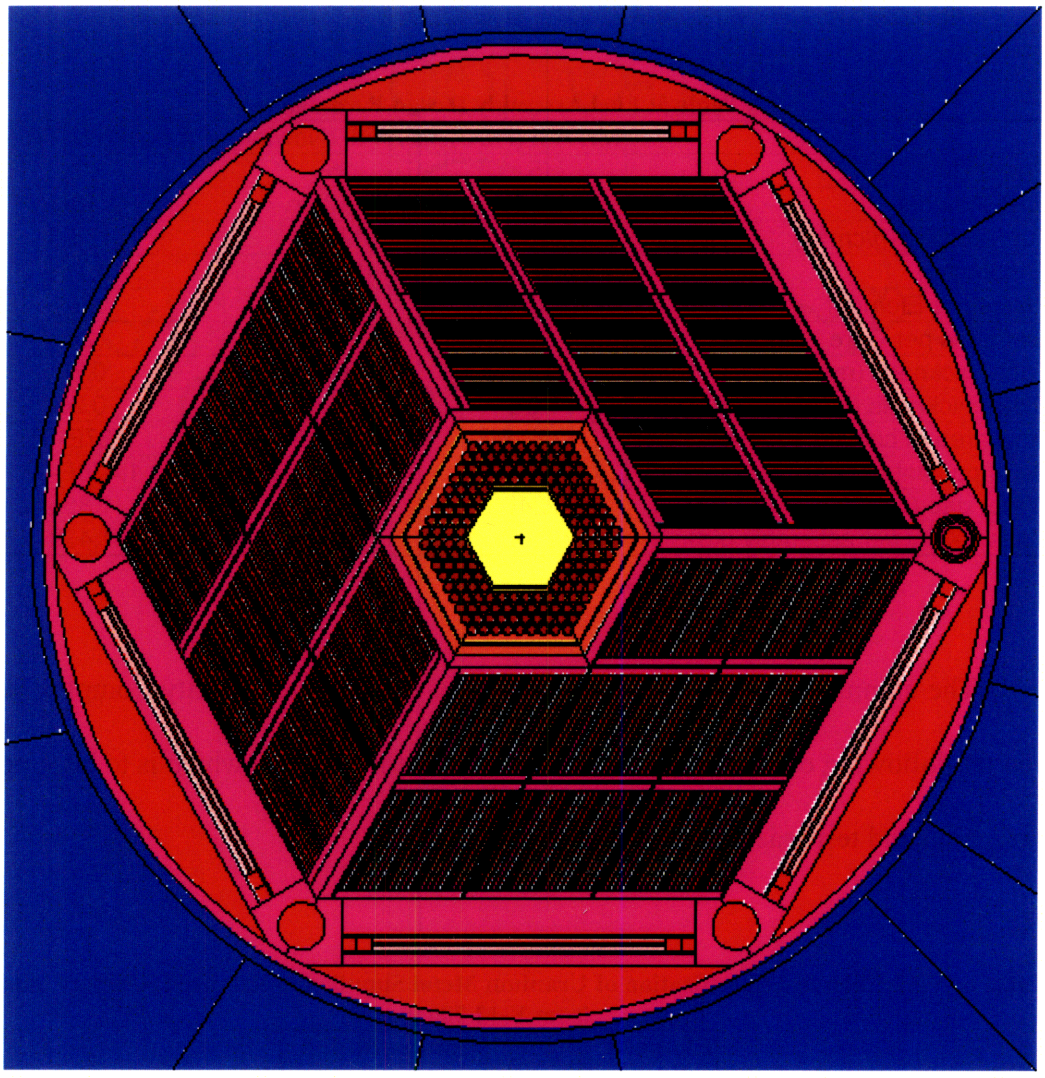

Figure 7: Proposed MITR Whole Core Cross Section

Each fuel element has twenty plates which contain a 0.762 mm (or 30 mil) thick fuel meat of U-10Mo and a clad which is 0.25 mm thick on both sides. The interior coolant channel gap has a thickness of 0.186 cm. Each coolant channel has an area of $8.37*10^{-5}$ m^2 and a hydraulic diameter of $1.47*10^{-3}$ m. Table 5 summarizes the physical

design parameters of the current HEU core (the HEU reference core or MITR-II), the LEU core proposed by Thomas Newton (the LEU reference core or MITR-III) and the MITR core proposed in this dissertation.

Table 5: Fuel Assembly Design Parameters

	MITR-II (HEU)	MITR-III (Newton)	Proposed MITR (Ellis)
Power (MWth)	5	5	10
Fuel Material	UAlx	U-10Mo	U-10Mo
Fuel Density (g/cm^3)	3.7	17.55	17.55
Enrichment	93%	19.75%	19.75%
Plates per Element	15	18	20
Elements per Core	23	24	24
Fuel Thickness (mm)	0.76	0.51	0.76
Clad Thickness (mm)	0.38	0.25	0.25
Flow area of coolant channel (m^3)	1.25E-04	1.14E-04	8.37E-05
De of coolant channel (m)	2.186E-03	1.996E-03	1.470E-03
Water gap (mm)	2.240	2.054	1.855
Mass U-235 per assembly (kg)	0.506	0.864	1.439

The uranium fuel specification from the Y-12 National Security Complex has given the following constitution (shown in Table 6) for the LEU which is to be supplied for research and test reactors.

Table 6: Y-12 Chemical Specification of Uranium Metal Supplied to Research Reactors [adapted from Y-12 2005]

Element	Concentration
Uranium (Metal)	≥ 99.880 wt%
U-232	≤ 0.002 µg/gU
U-234	≤ 0.260 wt%
U-235 ± 0.20 wt%	19.75 wt%
U-236	≤ 4600 µg/gU

In order to remove the full 10 MW worth of heat, the core will need a minimum flow rate of 2900 gallons/minute which is approximately 60% higher than the existing MITR-II minimum flow rate of 1800 gallons/minute and approximately 32% higher than

our current operational flow rate of 2200 gallons/minute [Newton 2006]. Calculations have shown that at a temperature of 50°C and a K factor of 2.05, the 2900 gallon/minute flow rate will cause a pressure of ~13 psig on the core tank. Even if the flow rate is raised to 3600 gallons/minute, which is much higher than needed for 10 MW operation, the pressure on the core tank is ~16.7 psig. Table 7 shows the effect of changing the total core flowrate for the HEU reference, LEU reference (Newton's design) and the MITR proposed in this thesis.

Table 7: Flowrate Effect on Core Tank Pressure Loading

Total Core Flowrate (gal/min)	Core Tank Pressure (psi) of HEU Reference	Core Tank Pressure (psi) of LEU Reference	Core Tank Pressure (psi) of Proposed MITR
2600	10.44	9.51	11.56
2700	10.80	9.81	12.01
2800	11.18	10.13	12.47
2900	11.57	10.45	12.94
3000	11.98	10.78	13.43
3100	12.39	11.12	13.93
3200	12.82	11.47	14.45
3300	13.26	11.83	14.98
3400	13.71	12.20	15.52
3500	14.17	12.57	16.08
3600	14.64	12.96	16.65

The total core tank pressure loading was calculated by adding the gravity pressure head of 3.8 m of primary coolant, which is equivalent to 5.33 psi at 50°C, to the friction pressure drop which was calculated with the total core flowrate indicated in the table. For purposes of comparison, the same calculation was applied to the current 5 MW MITR-II HEU reference core and its results are reported alongside the values for the LEU reference core at 5 MW and the proposed MITR at 10 MW. The current MITR-II was

designed for a maximum allowable pressure of 24 psig on the reactor vessel under ASME Section VIII requirements.

As mentioned previously, the maximum allowable pressure on the core tank in prior studies was conservatively limited to equal or below that of the existing HEU core because of unknowns surrounding the condition of the core tank. Recent work has shown that the reactor vessel has actually increased in strength with time rather than decreased [Kohse 2008a]. Table 8 shows the estimated neutron fluence for the MITR-II from initial criticality through June 2007 and estimated future total fluence provided the MITR-II operates at 10 MW for an additional 20 years.

Table 8: Estimated Peak Neutron Fluence for the MITR-II Reactor Core Tank [Kohse 2008a]

	Thermal	E > 0.1 MeV	E > 1.0 MeV
Initial Criticality → June 2007 (n/cm^2)	$3.2*10^{22}$		$2.9*10^{21}$
Initial Criticality → June 2007 + 20 years at 10 MW (n/cm^2)	$1.2*10^{23}$	$2.4*10^{22}$	$1.1*10^{22}$

For the neutron fluence level projected after 20 years of operation at 10 MW, papers by [King 1973] and [Farrell 1979] have found that the 6061-T6 aluminum alloy, used in the MITR-II reactor vessel, demonstrated an increase of approximately 40% in 0.2% offset yield stress and a 30% increase in ultimate tensile strength. Additionally, the total elongation was reduced by approximately 40% and uniform elongation was reduced by nearly 50%. Interestingly, both the yield and ultimate stresses continued to increase with neutron fluence while the reduction in ductility saturated at a fluence of 10^{22} n/cm^2 for E > 0.1 MeV. Kohse observed that the increases in both the yield and ultimate strength will obviously not affect the reactor vessel pressure load capability. Furthermore, since the ductility losses were not sufficient to change the material fracture mode and the reactor

vessel is expected to operate in the elastic region, the projected ductility changes should not affect the pressure load capability of the reactor vessel. Thus it was concluded that the pressure load capability of the MITR-II reactor vessel will not be significantly affected by irradiation induced changes in the mechanical properties over a projected additional 20 years of 10 MW operation.

2.3 Fast Flux Trap Design Evolution

The Fast Flux Trap design has undergone several iterations, both neutronic and thermal hydraulic, in order to arrive at its final form. Initially the design, represented by the XY cross section in Figure 8, was composed of a central irradiation facility (in yellow) surrounded by a thin ring of fissionable material called the Amplifier Ring (in brown), which was enclosed by a cylinder of lead (in white) [Ellis and Newton 2008]. This Fast Flux Trap occupies what used to be the entire A-ring of the core. Conversations with experimenters about future sample needs yielded a minimum of a 2 inch diameter for the central irradiation facility.

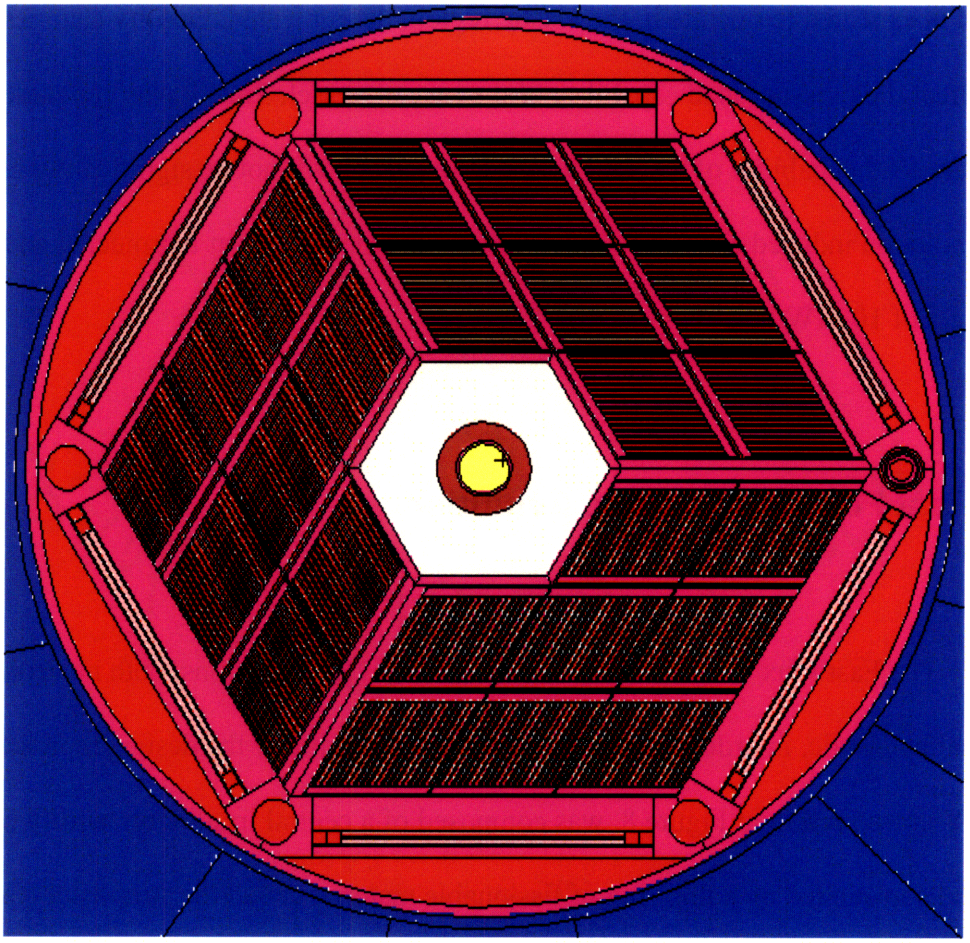

Figure 8: Cross Section of core design with Fast Flux Trap and an Amplifier Ring [Ellis and Newton 2008]

Lead serves as an excellent reflector for fast neutrons so in theory the fast neutrons produced in the amplifier ring are reflected back towards the central irradiation facility, thus enhancing the fast flux there. Gamma heating in the lead was thought to potentially pose some heat removal challenges but after several simulations the total amount of heat produced was on the order to 34 kW for a core power of 10 MW. Originally it was thought that the excess heat produced in the lead could be removed via a gaseous working fluid loop. Gaseous working fluid was selected because of its relative neutronic transparency as well as the low amount of heat needed to be rejected. The cooling loops were to run through the lead in the fast flux trap and back up to the top of

the reactor vessel to a heat exchanger and pump assembly which would remove the excess heat and pump the working fluid back to the fast flux trap in the core. The set-up and design of this apparatus was thought to be similar to the existing system for the Advanced Cladding Irradiation (ACI) experiment which has previously been installed and successfully operated in the MIT reactor core [Hu and Kohse 2008]. However after the fission heat was evaluated in the amplifier ring, the option of using gaseous coolant quickly dissipated since the heat removal requirements were on the order of 0.5 MW. This necessitated the change to a liquid metal coolant due to its superior heat transfer properties.

As previously mentioned, the amplifier ring is composed of a potent fissile material so as to provide a strong source of neutrons around the central irradiation facility. Some examples of the fissionable material which were under consideration for the Amplifier Ring included ^{233}U, ^{235}U, ^{239}Pu and ^{242m}Am. ^{242m}Am was considered for investigation because it has been previously identified for its superior neutronic properties [Shwageraus, *et al.* 2006]. This isotope has a 7000 b thermal neutron cross section which is approximately an order of magnitude higher than the other more common fissile materials. It also releases 3.26 prompt neutrons per fission as compared to 2.88 for ^{239}Pu or 2.43 for ^{235}U. Table 9 shows how the recoverable energy (Q) released per thermal fission and the number of neutrons per thermal fission compare with that of the other fissile isotopes considered in this study ^{233}U and ^{235}U.

Table 9: Neutronic Properties of Am-242m, U-233 and U-235

	Q/fission	Neutrons/Fission
U-235	180.884 MeV	2.44
U-233	180.847 MeV	2.50
Am-242m	190.479 MeV	3.26

The 13%-34% larger prompt neutron release for the ^{242m}Am has obvious implications for the maximization of the fast flux. However, usage of this isotope was eventually discarded because of concerns about the practicality of its supply.

The amount of fissile material loaded into the amplifier ring was optimized by conducting a ring thickness study, using all of the previously mentioned fissile and fertile fuel combinations, ranging from 0.01 cm all the way up to 3.5 cm. The results of this study are featured in Figure 9. It is important to note that the fast flux values here only range from 1-10 MeV. All of the fast flux numbers quoted in the rest of this dissertation assume that the fast flux ranges from 0.1-10 MeV. The calculated flux for Figure 9 was tallied in the Central Irradiation Facility, which was empty, and normalized to 10 MW. The outer wall of the Central Irradiation Facility has a radius of 2.54 cm so the x-axis in the figure below shows the Amplifier Ring thickness ranging between zero (on the left at 2.54 cm) all the way out to the entire radius of the Fast Flux Trap assembly (on the right at 6.1 cm).

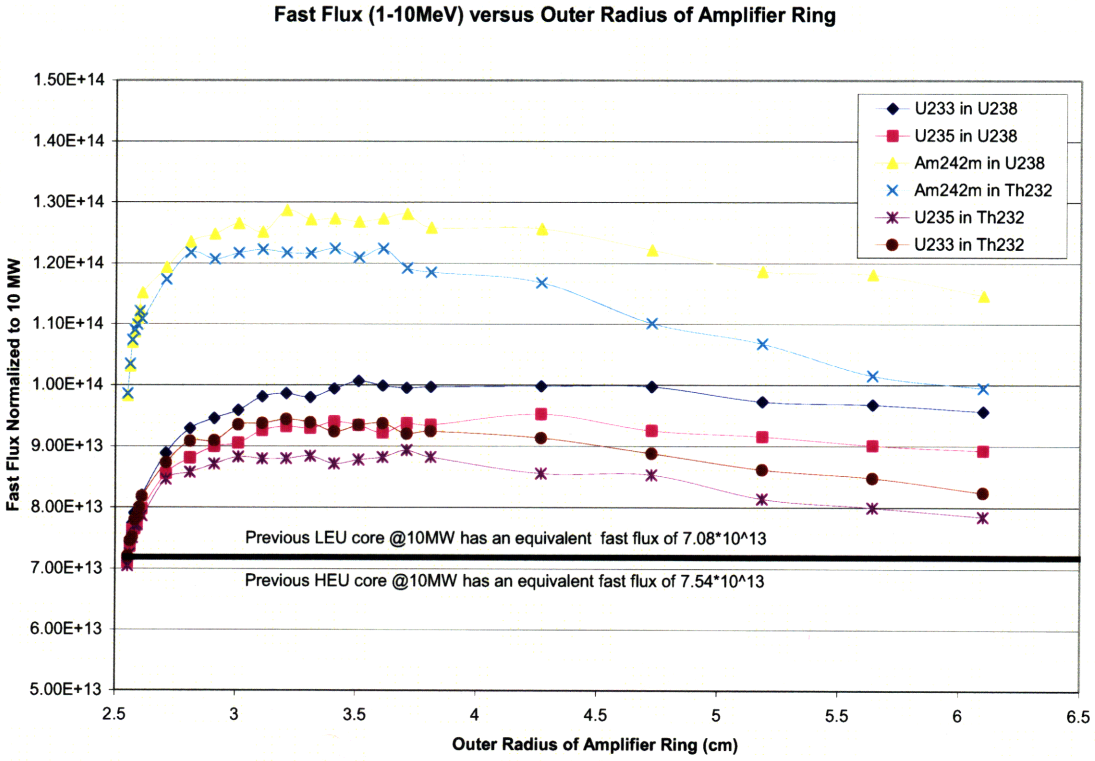

Figure 9: Fast Flux versus Outer Radius of the Amplifier Ring

This optimization study sought to ascertain the relative effectiveness of the proposed candidate materials for the Fast Flux Trap Amplifier Ring. The heavy metal enrichments are as follows: 20% for ^{235}U, 12% for ^{233}U and 4.5% for ^{242m}Am. All proposed candidate materials can be defended as 'proliferation resistant' since they adhere to the current definition of a 400 kg spherical critical mass surrounded by a 4 cm thick beryllium reflector (this definition is described in the next section). As shown in Figure 9 there is an optimum amount of fissile material for the amplifier ring which occurs at a ~3-3.5 cm outer radius of the amplifier ring. This established the optimal amount of fissile material since any addition beyond that point actually reduces the fast flux capability. This fast flux reduction is likely due to the reduced reflectivity capability

of the surrounding Pb-Bi and potentially also some self-shielding effects. This figure also shows that, at the beginning of life, ^{238}U is a better fertile material than the ^{232}Th because is absorbs less fast neutrons. The superior neutronic performance of the ^{242m}Am fissile material was also confirmed in both a ^{238}U and ^{232}Th fertile matrix. Finally, ^{233}U was shown to be a slightly better fissile material than ^{235}U.

The other investigated design feature was the idea of a cadmium filter. This filter was located in between the amplifier ring and the experimental irradiation facility. The cadmium filter, depicted in pink, is shown below in Figure 10.

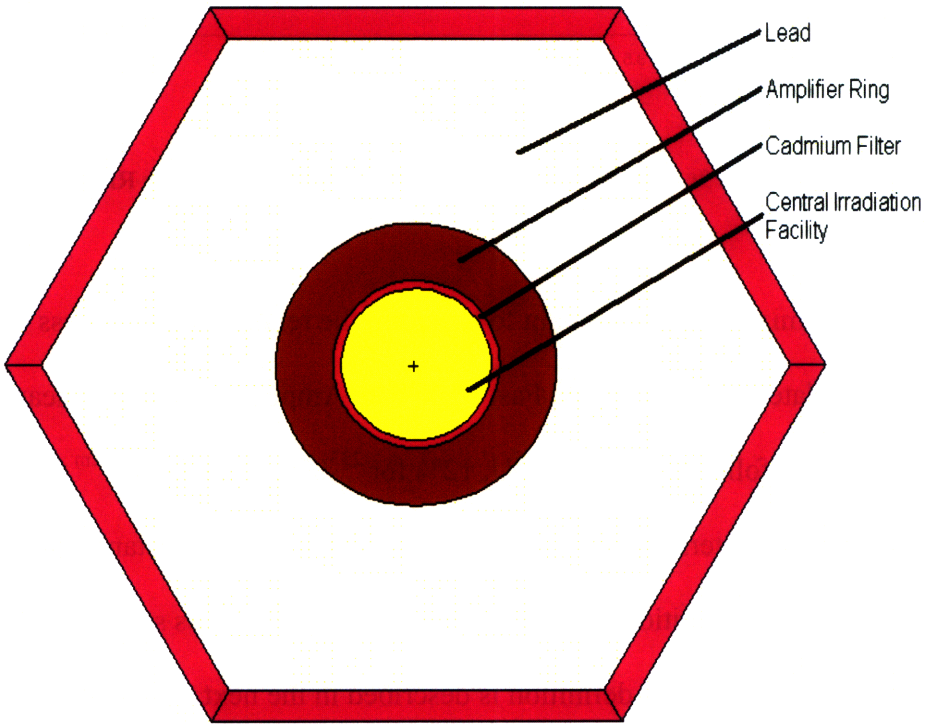

Figure 10: Fast Flux Trap Ring Assembly [Ellis and Newton 2008]

It was expected that, due to the considerable thermal neutron capture cross section for cadmium, this filter effectively removed a large portion of the low energy neutrons

while leaving the fast neutron population less reduced. Thus, experimenters desiring a more pure fast fluence will have that option at the MIT facility. The filter was also thought to be beneficial during accident analyses, where the presence of a strong absorber will help counteract the strong neutron production from the amplifier ring.

Subsequent thermal hydraulic analyses showed that the heat flux on the outside of the amplifier ring was far too large, even for a liquid metal coolant. This necessitated a design change to maximize the heat transfer surface area of the amplifier ring, so as to decrease the surface heat flux of the fueled portion of the Fast Flux Trap. Calculations showed that 164 pins with an outer diameter of 0.6 cm would allow for a low enough heat flux for liquid Pb-Bi coolant to be used. However these 164 pins had a slightly larger fuel volume than the previously determined optimal amount so the fuel matrix was switched from higher density U-10Mo to lower density UO_2. This geometry and material switch achieved the best balance of high performance and realistic design capability given the present state of the art. The final Fast Flux Trap design is described in the next section.

2.4 Proposed Fast Flux Trap Description

The final Fast Flux Trap design is featured in Figure 11. The hexagonal-shaped Central Irradiation Facility, located in the center of the fast flux trap and depicted in yellow, can be fitted with a thin 0.01 cm thick lining of cadmium which serves as an effective filter to remove most of the low energy neutrons. When the central irradiation facility is not being used, the interior part should be filled with helium gas or some other inert material. This central irradiation facility is surrounded by 164 amplifier oxide fuel

pins arranged in four rings of 32, 38, 44 and 50 pins respectively. The amplifier pins are both cooled and reflected by liquid Pb-Bi coolant. The fundamental concept of the Fast Flux Trap is that the Pb will reflect the fast neutrons produced in the amplifier pins back towards the middle, thereby concentrating or 'trapping' the fast neutrons in the central irradiation facility.

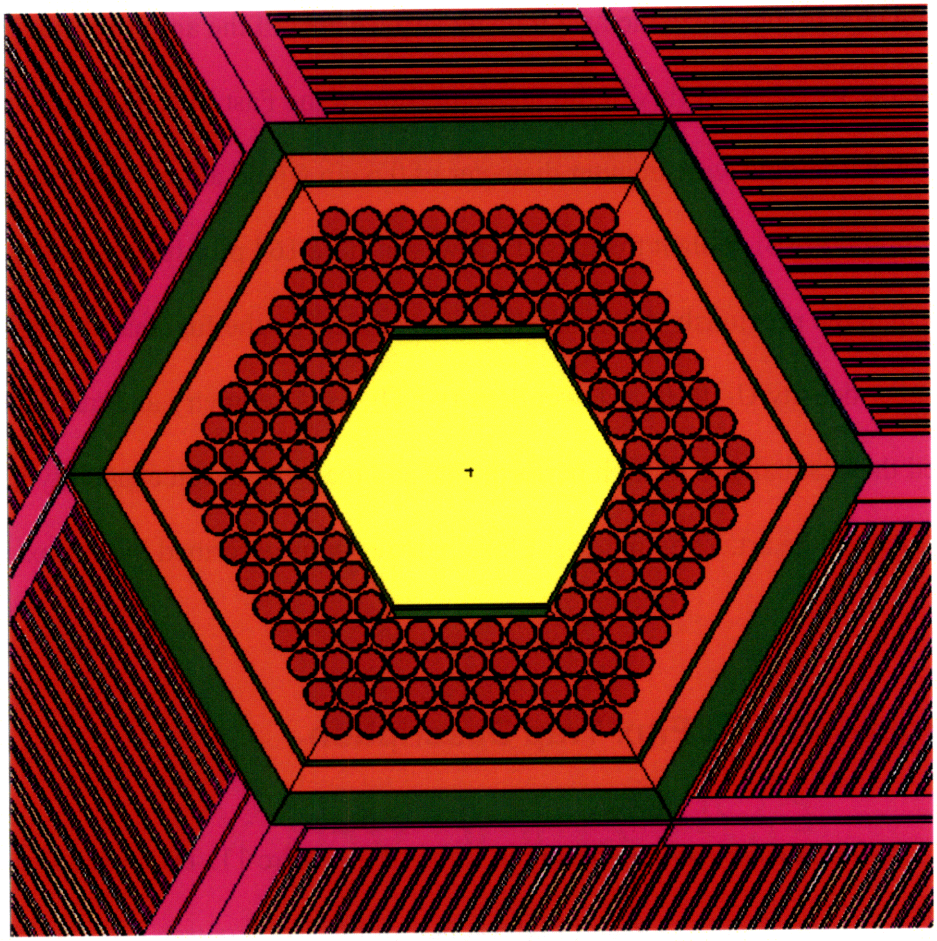

Figure 11: Fast Flux Trap XY Cross-section

The amplifier pins have an outer diameter of 0.6 cm, a pin to pin gap of 0.148 cm and a total length of 37 cm. The pins have 0.03 cm thick cladding of T91 alloy and a 0.006 cm thick helium gap. The 0.528 cm diameter fuel pellets are made of UO_2 with

either ^{235}U or ^{233}U as the fissile isotope and ^{238}U as the fertile isotope. The ^{233}U isotope was included in this analysis for two reasons. First, ^{233}U has superior nuclear properties to that of ^{235}U which makes higher fast neutron fluxes achievable. Table 10 shows that the number of neutrons produced per fission times the capture to fission ratio, or eta, is roughly 10% higher for ^{233}U than for either ^{235}U or ^{239}Pu.

Table 10: U-233 as a Fissile Material [Kazimi 2003]

	^{233}U	^{235}U	^{239}Pu	^{241}Pu
$\sigma_{capture}$, barns	46	101	271	368
$\sigma_{fission}$, barns	525	577	742	1007
$\alpha = \sigma_c/\sigma_f$	0.088	0.175	0.365	0.365
$\eta = \nu\sigma_c/\sigma_f$	2.300	2.077	2.109	2.151
Effective β factor, pcm	270	650	210	490

The second reason that ^{233}U was considered in this analysis is because of the availability of a large (two metric ton) stockpile of this material currently stored at Oak Ridge National Laboratory as a byproduct from the nuclear weapon manufacturing period. Thus, the ^{235}U supply can be assured. It would certainly be in line with the general goal of the LEU core to further strengthen the non-proliferation regime by downblending and using up leftover highly enriched ^{233}U.

Due to the differing nuclear properties of ^{233}U and ^{235}U, the same 20% LEU enrichment standard cannot be applied to ^{233}U. This necessitates the development of a new LEU enrichment standard in order to ensure proliferation resistance. The current LEU enrichment standard of 20% ^{235}U is based upon a ~400 kg sphere reflected with four

centimeters thick of beryllium assuming that ^{238}U is the fertile material. If a similar calculation is applied to ^{233}U the corresponding LEU enrichment limit decreases to 12% [von Hippel and Kang 2001].

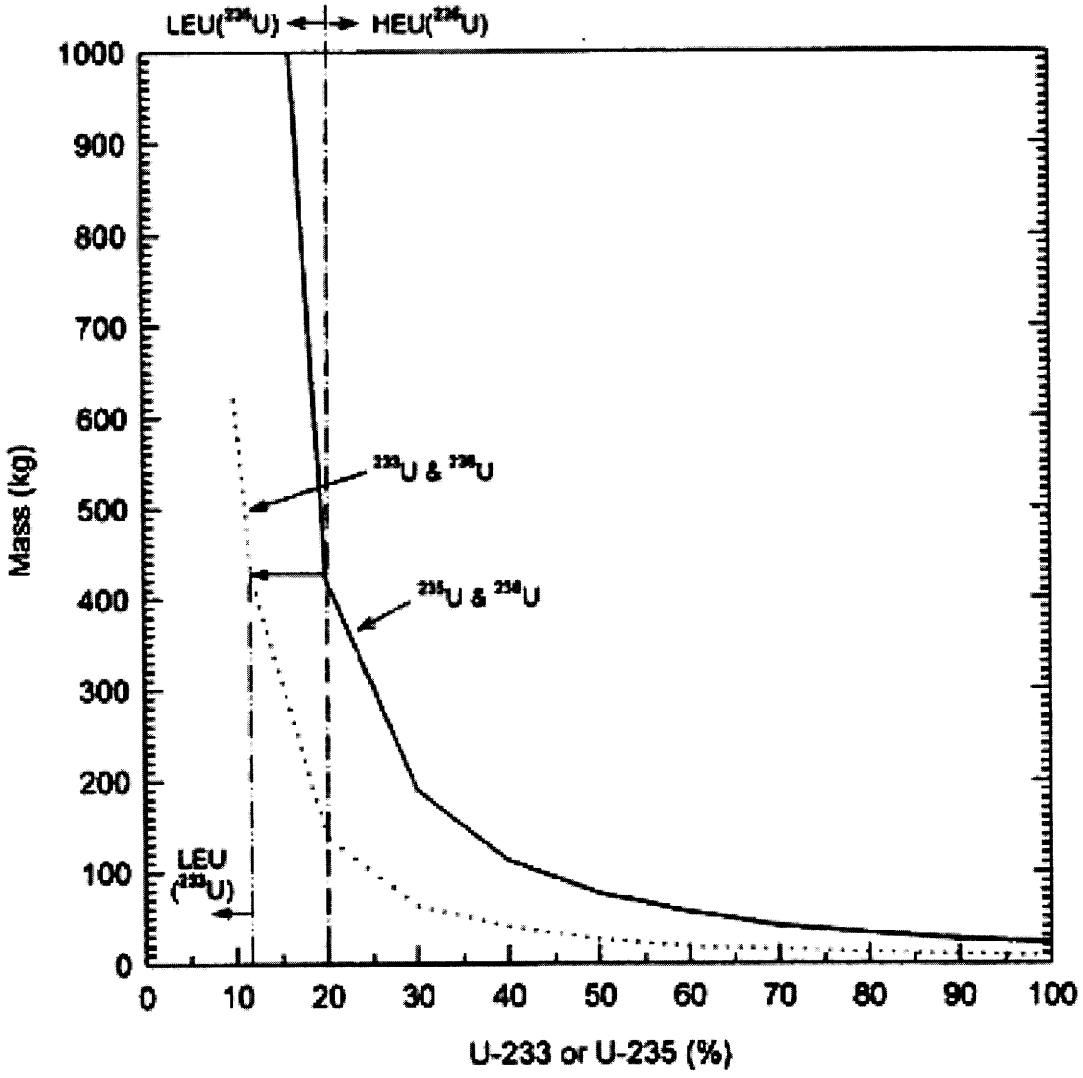

Figure 12: LEU Enrichment Standard Curves [von Hippel and Kang 2001]

Passive absorber type cadmium filters have been previously used in the Advanced Test Reactor's actinide fuel capsule design to simultaneously depress the linear heat generation rate as well as harden the neutron spectrum [Chang and Ambrosek 2005]. The

idea behind the filter is that the cadmium modifies the neutron spectrum by eliminating most thermal neutrons via absorption, while still keeping the intermediate/fast energy neutrons. Previous designs utilizing cadmium filters have been shown to effectively reduce the low energy neutrons while leaving the higher energy neutrons relatively unaffected.

The fission heat produced by the amplifier pins, as well as the much smaller amount of heat produced by gamma heating in the lead reflector, will be removed via a molten Pb-Bi coolant loop similar in design to the Advanced Cladding Irradiation (ACI) experimental loop which has previously been installed and operated in the MITR-II core [Hu and Kohse 2008]. The supporting equipment for the Pb-Bi loop (*exempli gratia* heat exchanger to the secondary system, pumps, coolant storage tank and heater) will be located on the reactor top. The mechanical support for the Pb-Bi loop will come primarily from the reactor top, by running the loop through the upper access shield ring plug. From a practical standpoint, routing the Pb-Bi loop through the core tank will dramatically simplify maintenance of both the reactor and the loop for personnel. Figure 13 shows a vertical diagram of the entire Fast Flux Trap loop.

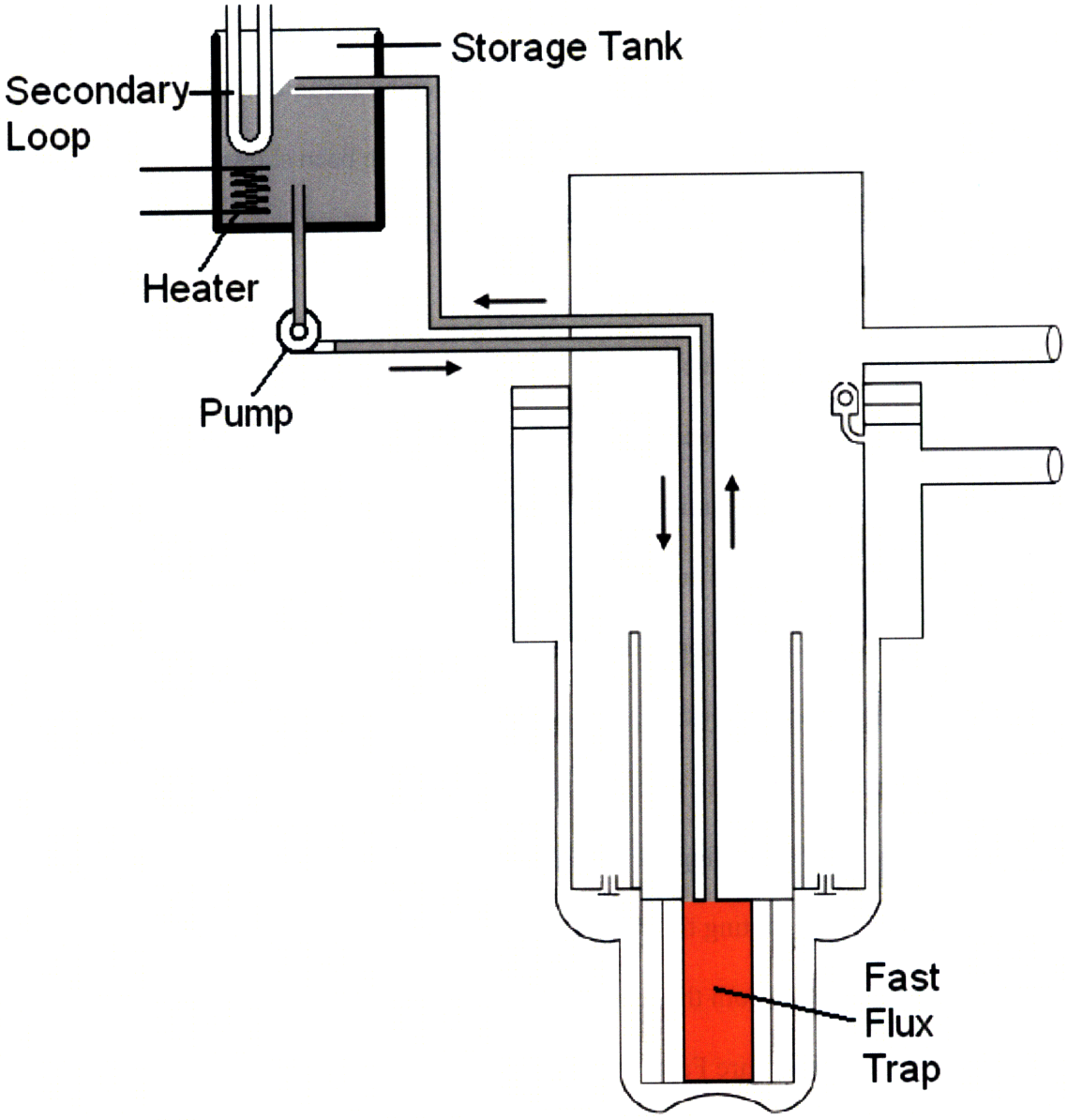

Figure 13: Vertical Diagram of Fast Flux Trap Loop

Chapter 3 – Neutronic Evaluation

3.1 Steady-state Analyses

This chapter covers the neutronic evaluation for both the Fast Flux Trap in the center of the core as well as rest of the core proper. As mentioned in the previous Chapter, two different UO_2 fissile material configurations, 20% enriched ^{235}U (F1 design) and 12% enriched ^{233}U (F2 design), were considered for the amplifier pins in the Fast Flux Trap. The results from both optimized designs are compared in each of the subsections. Although both designs showed fairly similar performance, the more exotic ^{233}U design was kept in order to allow for the option of burning down some of the existing stockpile of ^{233}U. Additionally, since the ^{235}U fuel has been extensively studied, this allows for faster implementation of the Fast Flux Trap design while the ^{233}U fuel awaits qualification for research reactor use. After the initial ^{235}U fueled Fast Flux Trap is spent, it can be replaced with a ^{233}U fueled design with no additional design changes.

The first subsection will highlight the boost in the fast flux as well as how the flux profile changes over the four rings of the Fast Flux Trap. This section also shows the power peaking factors of the amplifier pins, the optimization of the cadmium filter thickness, the reactivity worth of expected experimental samples and the power peaking profiles of all plates in the rest of the core. The second subsection describes the reactivity worth and system performance of anticipated transient scenarios such as initial insertion of the Fast Flux Trap, flooding of the central irradiation facility with water and gradual water flooding of the entire Fast Flux Trap assembly. The final subsection describes the

lifetime performance analysis of the Fast Flux Trap by depicting how the flux, heat production and actinide vector growth of the amplifier pins change over time.

3.1.1 Flux Spectrum Enhancement

Figure 14 shows how the neutron energy spectrum in the proposed MITR differs from that of the existing HEU core and LEU reference [Newton 2006] designs which were defined in Table 5. This neutron energy spectrum was tallied in the central irradiation facility (volume of 1244 cm^3) for the proposed MITR as well as in the LEU reference core. Since the HEU reference core does not have a dedicated in-core position for a central irradiation facility, the tally was taken in the A-3 fuel element spot, where in-core irradiation experiments are frequently located. The reference LEU and HEU design spectra differ by only ~5% above 0.1 MeV. However, as one moves down in energy from 100 eV to 10 eV, the difference between the two increases steadily due largely to resonance capture in the ^{238}U amply present in the LEU. The reference LEU design has less low energy, or thermal, flux than the reference HEU design because of the higher amount of ^{235}U in the core.

Both the F1 and F2 designs show increasingly reduced flux below 1 keV as compared to either the HEU or LEU reference design. This is because the central irradiation facility within the amplifier ring doesn't see as many of the neutrons thermalizing in the water primary coolant as the irradiation facilities in either the HEU or LEU reference designs do. Finally, for the F2 design, the large dip in the neutron flux spectrum just above 1 eV is due to a strong ^{233}U resonance absorption peak.

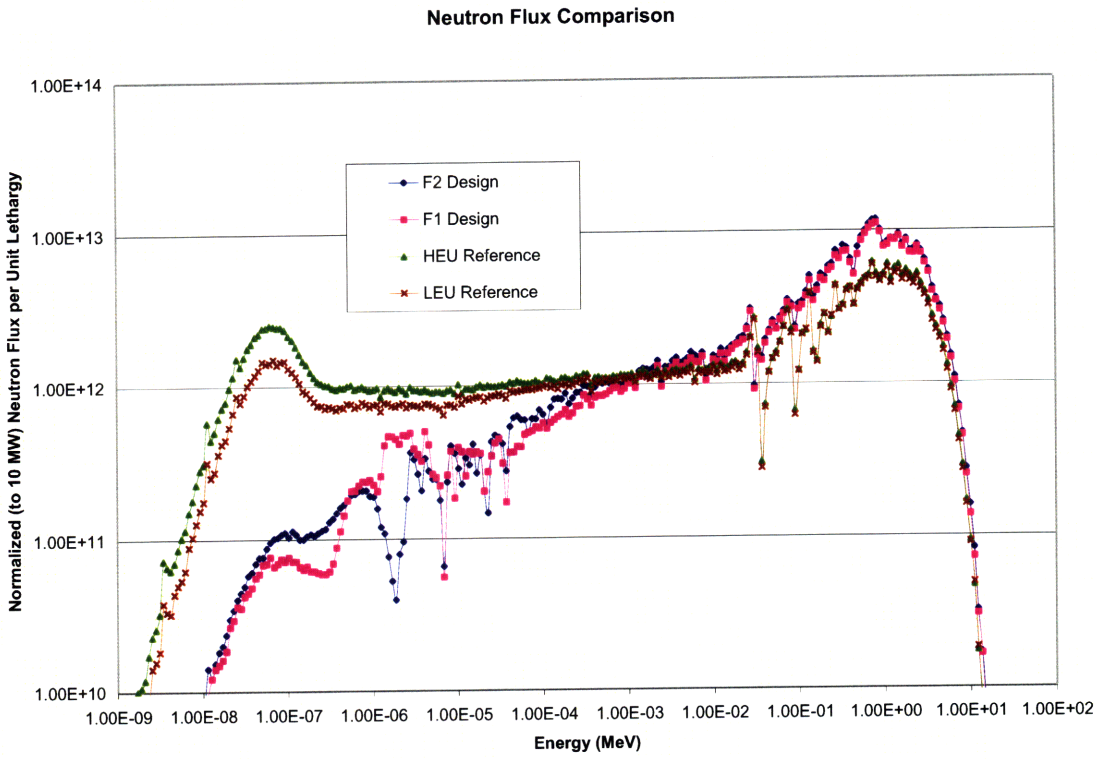

Figure 14: Flux Spectrum Comparison of F1, F2, and HEU/LEU Reference Designs for a 10 MW Core

As shown in Figure 14, both the ^{235}U (F1) and ^{233}U (F2) fueled amplifier ring resulted in appreciable increase in the fast flux capability of the MITR over both the previous LEU reference core as well as the current HEU reference core. It's important to note that both the LEU and HEU reference cores are normalized to 10 MWth for purposes of comparison. Since both the LEU and HEU reference cores operate at 5 MWth, the neutron flux values presented here for them should be divided by a factor of two for an explicit design comparison. If the HEU core were actually run at 10 MW, assuming that all supporting heat removal equipment were upgraded, then the reactor

would require refueling twice as often as it does now. This would shorten the typical HEU operational period from 3 months to 1.5 months.

Table 11 and Table 12 give a numerical breakdown of the difference in fast neutron flux levels between each Fast Flux Trap design and the reference designs compared above. The standard deviations for the fast flux data presented ranged from 0.00012 to 0.00009.

Table 11: Fast Flux Enhancement of F1 Design

Option	Power Level (MW)	Fast Flux (0.1-10 MeV)	% Fast Flux Enhancement of F1 Design over Design Option
F1 Design	10	2.64E+14	0%
HEU Reference	5	7.88E+13	235%
LEU Reference	5	7.50E+13	252%

Table 12: Fast Flux Enhancement of F2 Design

Option	Power Level (MW)	Fast Flux (0.1-10 MeV)	% Fast Flux Enhancement of F2 Design over Design Option
F2 Design	10	2.78E+14	0%
HEU Reference	5	7.88E+13	253%
LEU Reference	5	7.50E+13	271%

As shown in Table 11, the F1 design at 10 MW offer a 252% higher fast flux than the LEU reference design at 5 MW and a 235% higher fast flux than the HEU reference design at 5 MW. If the same comparison is made at an equivalent power level of 10 MW for all design options, in order to isolate the fast flux contribution from just the addition of the Fast Flux Trap, then the F1 design offers a 76% higher fast flux than the LEU reference design and a 67% higher fast flux than the HEU reference. Table 12 shows that the F2 design at 10 MW offers a 271% higher fast flux than the LEU reference design at

5 MW and a 253% higher fast flux than the HEU reference design at 5 MW. If the comparison is made at an equivalent power level of 10 MW for all design options, then the F2 design offers an 85% higher fast flux than the LEU reference design and a 76% higher fast flux than the HEU reference design. The F2 design does allow for a modest enhancement of fast flux over that of the F1 design. However, the value of burning down the existing legacy stockpile of ^{233}U will have to be weighed against the likely higher costs of new $^{233}UO_2$ fuel qualification in order to determine the viability of future adoption. Nevertheless, the F1 design offers a high performance, fast and likely more economical path to implementation because of the simpler fuel qualification requirements.

Figure 15 shows the numbering scheme for the four different amplifier pin rings. The neutron flux was tallied in each of the four different amplifier rings in order to better understand the relative flux contributions from the core proper and the amplifier pins.

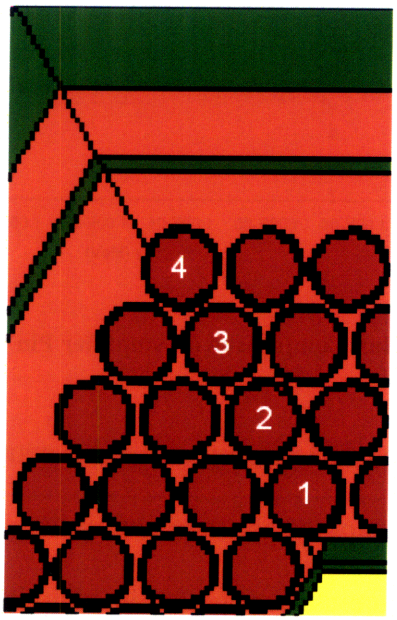

Figure 15: Numbering Scheme for Amplifier Pin Flux Profiles

Figure 16 shows the complete neutron energy spectrum for each of the four rings of ^{235}U fueled amplifier pins in the F1 design as well as for the center fuel plate in both B-6 and C-10 fuel elements, which are located radially outside of the tallied amplifier pins. The standard deviation for the calculated eigenvalue in the figure below is 0.00012. The error bars were omitted since they were too small for the scale of the figure.

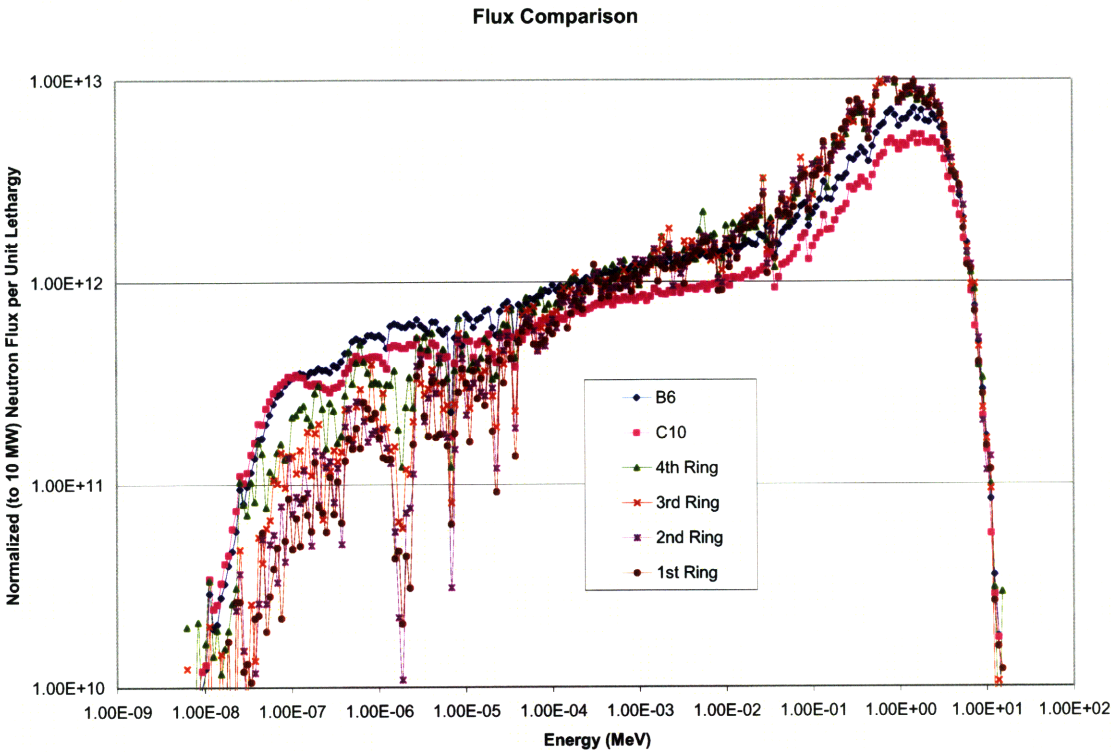

Figure 16: Neutron Flux Comparison of Amplifier Pin Rings and Core Elements

Table 13 presents a numerical summary of the neutron flux results given in Figure 16. As shown in the table, an appreciable amount of thermal flux comes into the amplifier pins of the Fast Flux Trap from the core proper in addition to the reflected fast flux from the Pb-Bi in the trap. The F2 design exhibited very similar trends to that of the F1 design

presented here, so it was not included. The fluxes shown in Table 13 have an error of 1% on average.

Table 13: Neutron Flux Profile across Rings of Amplifier Pins

		0 eV to 0.4eV	0.4eV to 3 keV	3keV to 0.1 MeV	0.1 Mev to 10 MeV
Outer	C10	7.57E+12	5.41E+13	4.05E+13	1.49E+14
	B6	8.29E+12	7.52E+13	5.91E+13	2.06E+14
	Ring # 4	4.50E+12	6.39E+13	6.73E+13	2.67E+14
	Ring # 3	1.96E+12	5.52E+13	6.60E+13	2.74E+14
	Ring # 2	1.04E+12	4.92E+13	6.53E+13	2.78E+14
Inner	Ring # 1	8.42E+11	4.66E+13	6.55E+13	2.77E+14

3.1.2 Power Peaking Profiles for Fast Flux Trap Amplifier Pins

The radial power peaking profiles (or the ratio of that particular pin power to the average pin power) of all 164 amplifier pins for both the F1 design as well as the F2 design are given in Figure 17 and Figure 18. The pin power statistical error ranges from 0.5% to 0.61%. The highest peaking for both designs always occurs in the lower right corner pin located in the outer-most ring of the amplifier pins. The F1 design has the highest radial power peaking factor of 1.53 (± 0.58%) while the F2 design has a radial power peaking factor of 1.49 (± 0.54%). Even though the Fast Flux Trap has a symmetrical axis, the core proper isn't necessarily symmetrical because of the differing orientations of the surrounding fuel assemblies. This causes a slight asymmetry in the outer peaking factor values for the amplifier pins. The sides of the Fast Flux Trap which face the "flat plate side" of the fuel assembly experience higher peaking than the sides which face the "plate-edge side" of the fuel assembly. Extra conservatism is added to

these results due to the fact that the pins here only have a 0.048 cm gap between the fuel pins. The final design has a 0.148 cm gap between the fuel pins. This larger gap will allow for reduced peaking along the rings since there is better neutron streaming between through the rings.

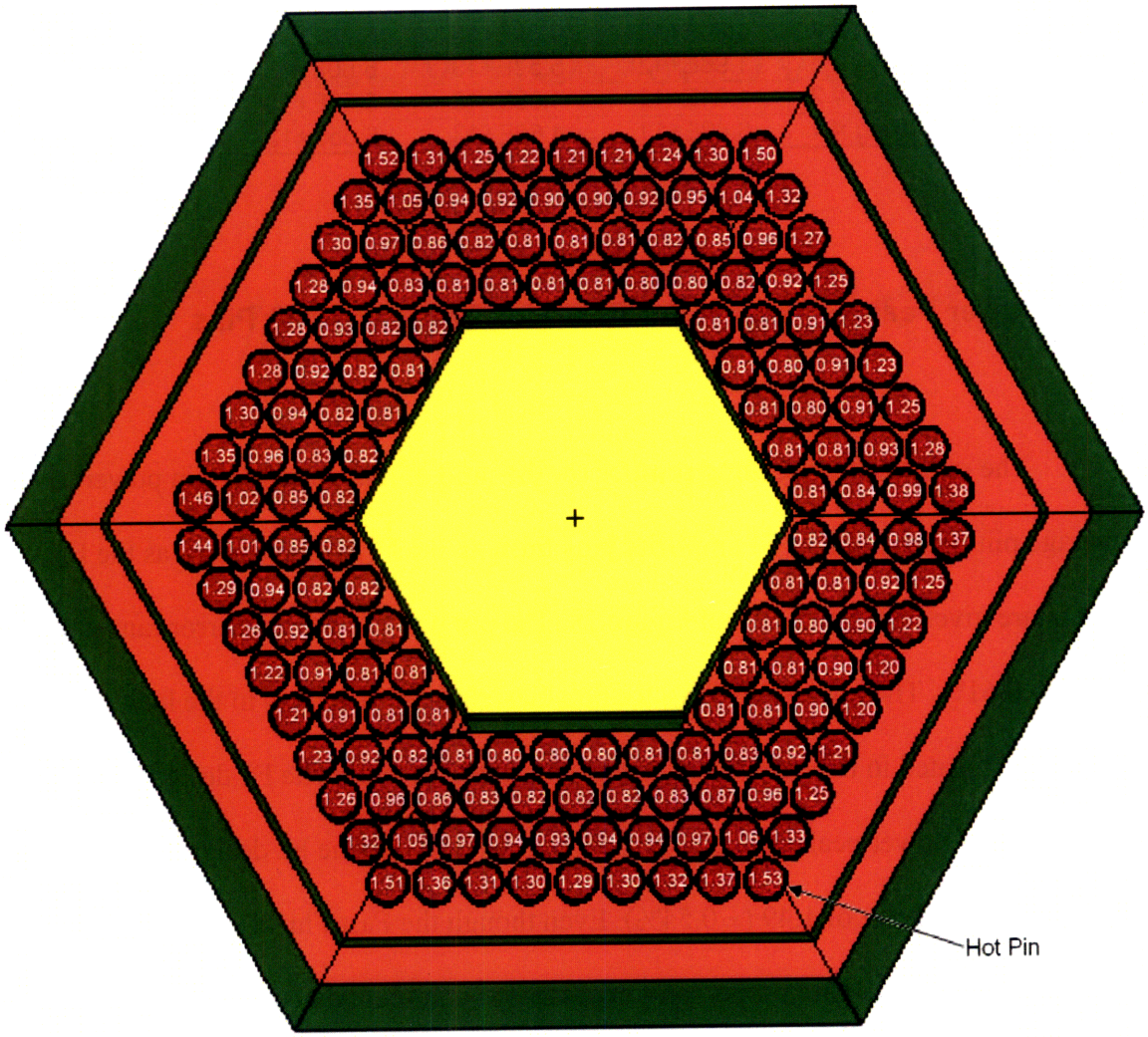

Figure 17: F1 Design Radial Peaking Factors

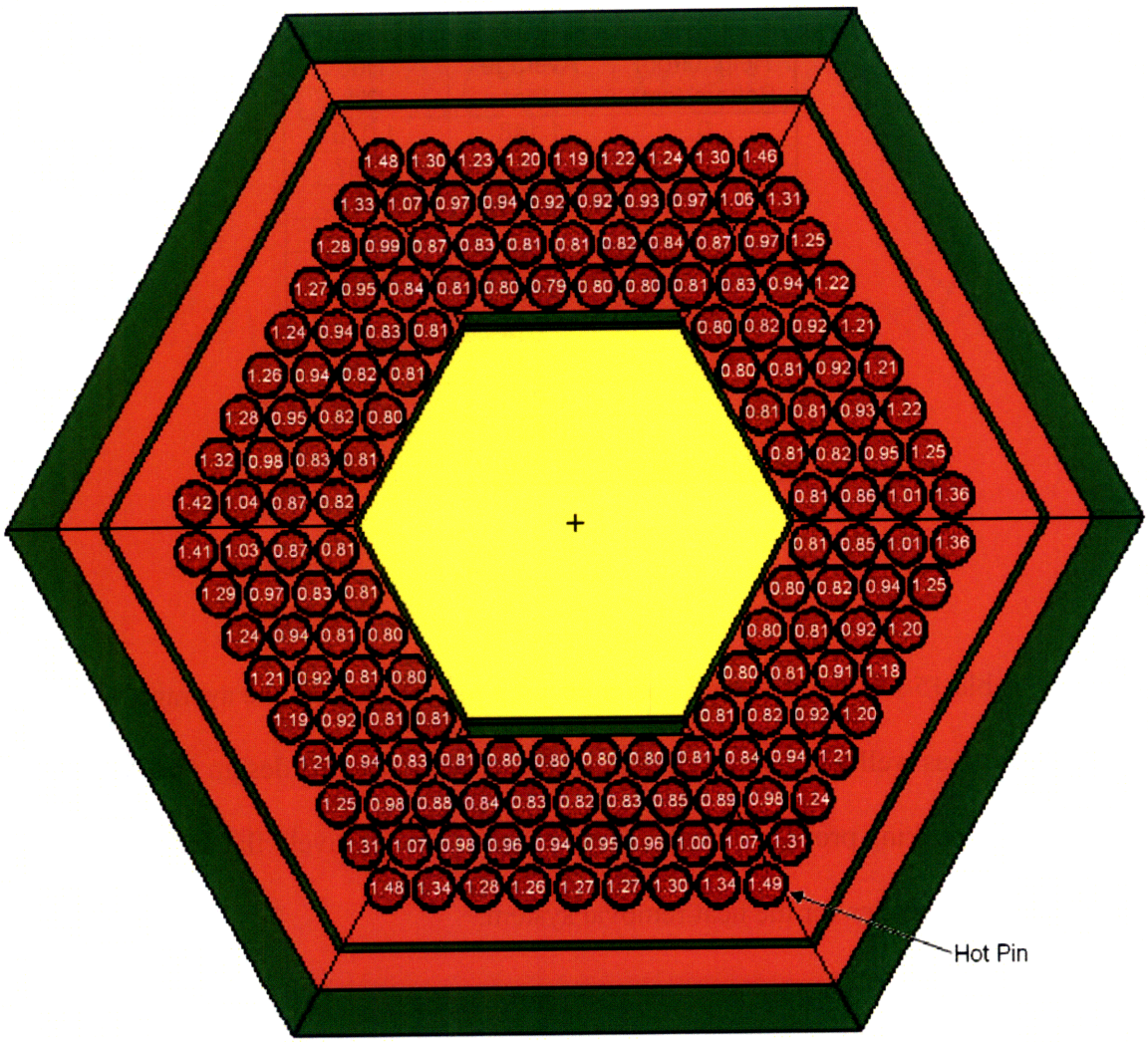

Figure 18: F2 Design Radial Peaking Factors

The F1 design axial power peaking profile, for both the average radial amplifier pin as well as the hottest radial amplifier pin, is shown in Table 14 (± 0.58%). The axial peaking values are given from the bottom of the amplifier pins (i.e. 0 cm) all the way up to the top at 37 cm. The axial peaking values for each pin have been normalized to an axial average of one, and the control blades are at a near critical height of 8.5 in.

Table 14: F1 Design Amplifier Pins Axial Peaking Profile

Height from Bottom (cm)	Average Pin	Hot Pin
0	1.148	1.070
4	1.014	0.987
8	1.034	1.007
12	1.034	0.977
16	0.996	1.027
21	0.996	1.012
25	1.014	1.058
29	0.945	1.002
33	0.888	0.940
37	0.931	0.921
Axial Average	1.000	1.000

Table 15 features the axial power peaking profile for both the average radial amplifier pin as well as the hottest radial amplifier pin for the F2 design (± 0.54%). The axial power peaking profiles in both Table 14 and 15 are relatively flat and present no significant challenges for the heat removal system.

Table 15: F2 Design Amplifier Pins Axial Peaking Profile

Height from Bottom (cm)	Average Pin	Hot Pin
0	1.136	1.049
4	1.007	1.000
8	1.020	1.007
12	1.034	1.007
16	0.993	1.007
21	1.003	1.041
25	1.016	1.057
29	0.966	1.006
33	0.893	0.927
37	0.931	0.899
Axial Average	1.000	1.000

3.1.3 Cadmium Filter Optimization

Since some experimenters might desire a more pure fast neutron spectrum, cadmium was considered for incorporation in the design. Cadmium is a very strong thermal neutron absorber and a comparatively weak neutron absorber at higher energies. This trait allows the usage of cadmium for an effective thermal neutron filter when incorporated around the perimeter of the central irradiation facility. Early in the design process it was not known how thick to make the cadmium filter, so an optimization study was conducted. Table 16 shows the results of the cadmium filter optimization study (error ±1%).

Table 16: Cadmium Filter Thickness Affect Study

Cd Filter Thickness (cm)	Thermal Flux 0 to 0.4eV	0.4eV to 3 keV	3keV to 1 MeV	Fast Flux 1 Mev to 10 MeV
0.00	0%	0%	0%	0%
0.01	-55%	0%	-2%	-2%
0.02	-65%	-1%	-2%	-3%
0.05	-69%	-2%	-2%	-4%
0.07	-71%	-2%	-1%	-4%
0.08	-72%	-5%	-1%	-4%
0.13	-73%	-5%	-2%	-5%
0.21	-73%	-6%	-2%	-8%

As shown in Table 16, an exceedingly thin layer of cadmium is able to reduce the thermal flux by well over 50% while the fast flux decreases by a couple of percent. The question of how thick to make the cadmium filter depends on the needs of the experiment, since different objectives will have different needs; some will want to reduce the thermal flux significantly while others will want solely to maximize the fast flux.

Since this facility aims to accommodate as many different experiments as possible, the cadmium filter was not permanently incorporated into the Fast Flux Trap design. If an experimenter wishes to significantly reduce the number of thermal neutrons, then it would be easy enough to incorporate a thin cadmium wrapper around the experimental sample assembly. The thickness would be dictated by the magnitude of thermal neutron reduction desired by the experimenter. For an example neutron energy spectrum, Figure 19 shows the effect of a 0.01cm thick cadmium filter on the flux inside of the central irradiation facility.

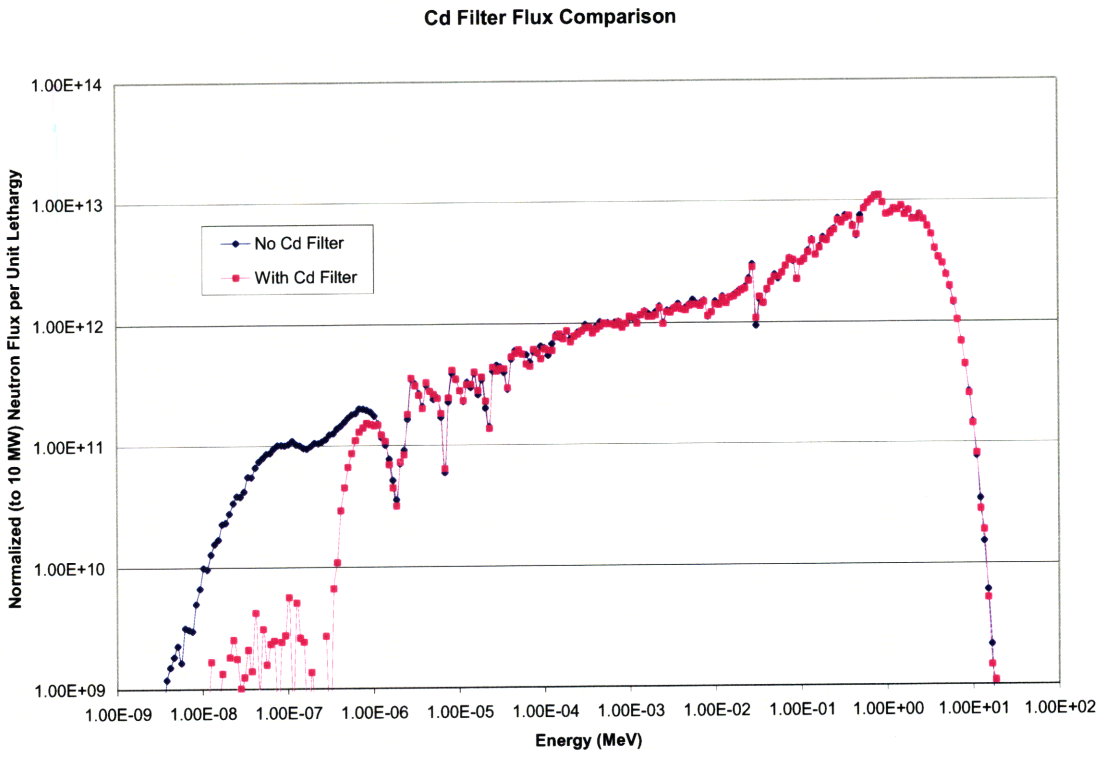

Figure 19: Cadmium Filter Effect on the Neutron Flux Spectrum

3.1.4 Reactivity Worth of Typical Experimental Samples

As mentioned in the introduction, there is a strong need for a capability to test advanced materials' behavior in a fast neutron spectrum. Some of the representative candidate materials for tests were simulated inside of the central irradiation facility to understand the effect on core reactivity. Table 17 gives a listing of the various candidate materials along with their corresponding effect on the reactivity of the core. The control blades are set at a position of 8.5 inches.

Table 17: Reactivity Effect of Various Samples

Sample Material	Keff	ρ Difference (ΔK/K)	Heat Production (W/g)
No Sample Material	0.99230 ±0.00012	0	0.00
Stainless Steel	0.99212 ±0.00012	-0.0002 ±0.0003	0.07 ±1%
HT-9	0.99208 ±0.00012	-0.0002 ±0.0003	0.84 ±1%
Graphite	0.99243 ±0.00012	0.0001 ±0.0003	1.89 ±1%
Tungsten	0.99205 ±0.00012	-0.0003 ±0.0003	1.31 ±1%
Titanium	0.99215 ±0.00012	-0.0002 ±0.0003	0.84 ±1%

The 5 cm long cylindrical samples with a 0.25 cm radius were placed in the middle of the central irradiation facility. The heat deposition in the samples was also tracked and the amount observed was lower than the ~2 W/g observed in the current HEU core. This result was expected since the thermal flux in the Fast Flux Trap is roughly an order of magnitude less than the thermal flux in the HEU core and the total absorption cross sections of the experimental sample materials investigated here have a much larger thermal absorption cross section than fast absorption cross section. The one exception to this was graphite which has a significant total absorption cross section (0.1

barns) at energies above 5 MeV. This was reflected in Table 17 which showed that Graphite had the highest heat production at 1.89 W/g. The total absorption cross sections for all experimental samples investigated here are shown and further discussed in Appendix D.

As also shown in the table, the samples had a negligible effect on the core average reactivity. The ~ 9% underestimation of the equilibrium fast flux by transitioning from the fresh to the equilibrium core (discussed further in section 3.1.5) will likely have a small reduction effect on the reactivity results presented here. Thus irradiating the proposed sample materials should not present any significant neutronic or thermal hydraulic challenges. If sample heating is desired, the coolant system design of the Fast Flux Trap can easily accommodate up to 100 kW of excess heat.

Uncertainty in the MCNP generated eigenvalue was reported as 'Std Dev' or the value of one standard deviation. For the reactivity difference (ρ_{diff}) calculations, the error was propagated through the calculations [Palmer 2003]. The ρ difference was calculated by the following formula:

$$\rho_{diff} = \frac{(k_1 - k_{ref})}{(k_{ref})}$$

The uncertainty was propagated through by summing the standard deviation of the k_1 and k_{ref} eigenvalues in the numerator (since they are being subtracted) and then adding the fractional uncertainty of the numerator $\frac{\delta(k_1 - k_{ref})}{|k_1 - k_{ref}|}$ and denominator $\frac{\delta(k_{ref})}{|k_{ref}|}$ as shown in the following formula:

$$U_{\Delta\rho} = \frac{\delta(k_1 - k_{ref})}{|k_1 - k_{ref}|} + \frac{\delta(k_{ref})}{|k_{ref}|}$$

This list of experimental materials is not exhaustive. Advanced fast reactor fuels can also be tested in the Central Irradiation Facility as well. The Fast Flux Trap was designed to be able to remove ~500 kW worth of heat. Since the F1 design produces a maximum of ~400 kW worth of heat at beginning of life, there is at least 100 kW of cooling capability for any fueled experimental sample. The F2 design produces a maximum of ~450 kW worth of heat at beginning of life so the available cooling capacity is 50 kW, or roughly half that of the F1 design. The specific reactivity limits associated with experimental fuel irradiations in the equilibrium core (with appropriate safety margins) will have to be determined for the new Safety Analysis Report of the upgraded core.

3.1.5 Power Peaking Profiles for Fuel Plates

Normally, the highest plate peaking occurs in the outer periphery of the C-ring which faces the D_2O reflector. This is because when the fast neutrons leak out of the core, they slow down in the D_2O and are then reflected back into the core as more thermalized neutrons. Hence, the D_2O reflector acts as a 'source' of thermal neutrons. For extra design conservatism, the hot channel factors described below are given for a completely fresh core. With previous LEU designs, fresh cores can have up to 10% higher hot channel factors than a comparable equilibrium core. Also in the equilibrium core, more of the power is shifted to the B-ring which provides for higher flux, approximately 4% thermal and 9% fast, in the Fast Flux Trap. Thus, the fast flux increase cited in this dissertation for the fresh core is likely to underestimate the actual equilibrium core fast

flux by ~9%. The power peaking for the amplifier pins in the Fast Flux Trap is affected by less than 1%, whether the core is fresh or at equilibrium.

In order to limit the hot channel factors at the periphery of the C-ring for simulations in the fresh core, a small amount of cadmium (3%) was added to the outermost plate #20 in the C-1, C-2, C-3, C-6, C-7, C-8, C-11, C-12 and C-13 assemblies. The inclusion of the cadmium will add some additional complexity to the current fuel cycle where all fuel elements are unpoisoned. The poisoned elements in the C-ring may have to only be used in the C-ring during their in-core lifetime so as to prevent potential excessive power peaking if shuffled to the B-ring. Extra studies will be needed to ascertain the impact of the cadmium on the power peaking of the poisoned elements after the first fuel cycle. The cadmium may not be needed for the equilibrium core since the hot channel factors at the periphery could be minimized by placing the oldest previously burned fuel at the corner positions in the C-ring (C-3, C-8 and C-13) and by orientating the other fuel elements in the C-ring to have their plate edges face the D_2O reflector as opposed to their plate faces. The hot channel factor profiles of all 480 plates for both the F1 design (±0.31%) as well as the F2 design (±0.25%) are given in Table 18 and Table 19, respectively. It's important to note that the hot channel factor values given here are calculated to the average core plate and not to the average assembly plate (i.e. the hot channel values are normalized to the total number of plates). In the following two tables, only the power produced in the core plates is included in the hot channel calculations. The power produced in the Fast Flux Trap is excluded.

Table 18: Core Plate Hot Channel Factors for the F1 Design

Plate #	B1	B2	B3	B4	B5	B6	B7	B8	B9	C1	C2	C3
1	1.31	1.24	1.37	1.33	1.24	1.36	1.30	1.20	1.32	1.10	1.11	1.01
2	1.20	1.19	1.22	1.21	1.19	1.22	1.20	1.16	1.19	1.03	1.05	0.96
3	1.17	1.16	1.17	1.17	1.17	1.17	1.16	1.14	1.14	0.99	1.02	0.94
4	1.15	1.15	1.14	1.16	1.16	1.14	1.15	1.13	1.11	0.97	0.99	0.93
5	1.14	1.15	1.13	1.15	1.15	1.13	1.15	1.13	1.10	0.94	0.97	0.91
6	1.14	1.13	1.12	1.15	1.15	1.13	1.15	1.13	1.09	0.92	0.95	0.91
7	1.14	1.13	1.12	1.15	1.14	1.13	1.14	1.12	1.09	0.90	0.93	0.90
8	1.13	1.12	1.12	1.15	1.13	1.12	1.14	1.12	1.10	0.88	0.91	0.89
9	1.13	1.12	1.12	1.15	1.13	1.12	1.14	1.12	1.10	0.86	0.90	0.88
10	1.13	1.12	1.12	1.15	1.12	1.12	1.14	1.11	1.10	0.84	0.87	0.88
11	1.12	1.11	1.12	1.14	1.12	1.12	1.13	1.11	1.10	0.83	0.86	0.87
12	1.12	1.11	1.12	1.13	1.11	1.13	1.12	1.11	1.10	0.81	0.84	0.86
13	1.11	1.11	1.13	1.13	1.11	1.13	1.13	1.11	1.11	0.80	0.82	0.85
14	1.10	1.10	1.13	1.12	1.11	1.14	1.11	1.10	1.11	0.78	0.81	0.85
15	1.09	1.09	1.14	1.11	1.10	1.14	1.10	1.09	1.12	0.77	0.79	0.84
16	1.09	1.09	1.14	1.11	1.10	1.15	1.10	1.09	1.13	0.77	0.78	0.83
17	1.08	1.09	1.15	1.10	1.10	1.16	1.09	1.08	1.14	0.75	0.77	0.82
18	1.08	1.09	1.17	1.10	1.10	1.17	1.09	1.09	1.15	0.74	0.74	0.79
19	1.09	1.10	1.18	1.10	1.11	1.19	1.10	1.09	1.16	0.70	0.70	0.74
20	1.12	1.13	1.23	1.13	1.14	1.24	1.13	1.13	1.20	0.71	0.69	0.77
Plate #	**C4**	**C5**	**C6**	**C7**	**C8**	**C9**	**C10**	**C11**	**C12**	**C13**	**C14**	**C15**
1	1.06	1.34	1.11	1.12	1.02	1.06	1.32	1.11	1.11	1.00	1.05	1.23
2	1.02	1.11	1.05	1.06	0.97	1.02	1.11	1.05	1.05	0.96	1.01	1.04
3	1.00	1.03	1.01	1.03	0.94	1.00	1.03	1.01	1.01	0.94	0.99	0.97
4	0.99	0.99	0.98	1.00	0.93	1.00	0.98	0.98	0.99	0.92	0.98	0.94
5	0.99	0.97	0.96	0.98	0.92	0.99	0.97	0.95	0.97	0.91	0.97	0.92
6	0.98	0.96	0.94	0.96	0.91	0.98	0.96	0.93	0.95	0.91	0.97	0.91
7	0.98	0.95	0.92	0.94	0.90	0.98	0.95	0.91	0.93	0.89	0.97	0.92
8	0.98	0.95	0.89	0.92	0.89	0.98	0.95	0.89	0.91	0.89	0.96	0.92
9	0.97	0.95	0.88	0.90	0.89	0.97	0.94	0.88	0.89	0.88	0.97	0.91
10	0.97	0.95	0.86	0.88	0.88	0.97	0.94	0.86	0.88	0.87	0.96	0.92
11	0.97	0.95	0.84	0.87	0.87	0.97	0.95	0.84	0.86	0.86	0.96	0.92
12	0.96	0.95	0.83	0.85	0.87	0.97	0.95	0.83	0.84	0.86	0.96	0.93
13	0.96	0.96	0.82	0.84	0.86	0.97	0.96	0.81	0.83	0.85	0.96	0.94
14	0.96	0.96	0.81	0.82	0.86	0.96	0.96	0.80	0.81	0.85	0.96	0.94
15	0.96	0.97	0.80	0.80	0.85	0.96	0.96	0.79	0.80	0.84	0.96	0.94
16	0.96	0.97	0.79	0.79	0.84	0.97	0.96	0.79	0.79	0.83	0.95	0.95
17	0.96	0.98	0.78	0.77	0.82	0.96	0.98	0.78	0.77	0.81	0.96	0.96
18	0.96	0.99	0.77	0.75	0.80	0.97	0.99	0.76	0.75	0.79	0.96	0.97
19	0.98	1.01	0.73	0.71	0.75	0.98	1.01	0.73	0.70	0.74	0.98	0.99
20	1.02	1.05	0.76	0.70	0.78	1.02	1.06	0.75	0.70	0.76	1.01	1.04

Table 19: Core Plate Hot Channel Factors for the F2 Design

Plate #	B1	B2	B3	B4	B5	B6	B7	B8	B9	C1	C2	C3
1	1.33	1.24	1.37	1.34	1.25	1.37	1.32	1.20	1.32	1.10	1.11	1.01
2	1.21	1.19	1.23	1.22	1.20	1.23	1.21	1.16	1.19	1.04	1.05	0.96
3	1.18	1.17	1.17	1.18	1.17	1.17	1.18	1.15	1.14	1.00	1.02	0.94
4	1.16	1.16	1.14	1.17	1.16	1.15	1.16	1.14	1.12	0.97	0.99	0.92
5	1.15	1.15	1.13	1.16	1.15	1.13	1.15	1.14	1.11	0.94	0.97	0.91
6	1.15	1.14	1.13	1.16	1.15	1.13	1.15	1.13	1.10	0.92	0.95	0.90
7	1.14	1.14	1.13	1.16	1.14	1.13	1.15	1.13	1.10	0.90	0.93	0.90
8	1.14	1.13	1.12	1.15	1.13	1.13	1.15	1.12	1.10	0.88	0.91	0.89
9	1.13	1.13	1.12	1.15	1.13	1.13	1.15	1.12	1.10	0.86	0.89	0.88
10	1.13	1.12	1.12	1.15	1.13	1.13	1.14	1.12	1.10	0.84	0.87	0.87
11	1.12	1.12	1.13	1.14	1.13	1.13	1.14	1.11	1.11	0.82	0.85	0.87
12	1.12	1.11	1.13	1.13	1.12	1.13	1.13	1.11	1.11	0.81	0.84	0.86
13	1.11	1.11	1.13	1.13	1.11	1.14	1.13	1.10	1.11	0.79	0.82	0.85
14	1.10	1.10	1.14	1.12	1.11	1.14	1.12	1.10	1.12	0.78	0.81	0.84
15	1.10	1.09	1.14	1.11	1.10	1.15	1.11	1.09	1.12	0.77	0.79	0.83
16	1.09	1.09	1.15	1.11	1.10	1.15	1.11	1.09	1.13	0.76	0.78	0.82
17	1.08	1.09	1.16	1.10	1.09	1.16	1.10	1.09	1.14	0.75	0.76	0.82
18	1.08	1.09	1.17	1.10	1.10	1.18	1.10	1.09	1.15	0.73	0.74	0.79
19	1.09	1.10	1.19	1.11	1.10	1.20	1.10	1.10	1.16	0.69	0.70	0.74
20	1.12	1.13	1.24	1.14	1.14	1.25	1.13	1.13	1.20	0.70	0.69	0.76
Plate #	**C4**	**C5**	**C6**	**C7**	**C8**	**C9**	**C10**	**C11**	**C12**	**C13**	**C14**	**C15**
1	1.06	1.33	1.10	1.12	1.02	1.06	1.33	1.11	1.12	1.00	1.04	1.22
2	1.02	1.11	1.04	1.05	0.98	1.02	1.11	1.05	1.05	0.95	1.00	1.04
3	1.00	1.03	1.02	1.00	0.95	1.00	1.02	1.01	1.01	0.93	0.98	0.97
4	0.99	0.99	0.98	0.99	0.93	0.99	0.98	0.98	0.99	0.92	0.97	0.94
5	0.98	0.96	0.95	0.97	0.92	0.99	0.97	0.95	0.97	0.91	0.97	0.92
6	0.98	0.96	0.94	0.96	0.91	0.98	0.95	0.93	0.95	0.90	0.97	0.92
7	0.97	0.95	0.91	0.93	0.90	0.98	0.94	0.91	0.93	0.89	0.97	0.91
8	0.97	0.95	0.89	0.92	0.89	0.98	0.95	0.89	0.91	0.88	0.96	0.91
9	0.97	0.95	0.88	0.90	0.89	0.98	0.94	0.87	0.90	0.88	0.96	0.91
10	0.97	0.95	0.85	0.86	0.89	0.97	0.94	0.86	0.88	0.87	0.96	0.91
11	0.96	0.95	0.84	0.85	0.88	0.96	0.95	0.84	0.86	0.86	0.96	0.92
12	0.96	0.95	0.82	0.84	0.87	0.97	0.95	0.82	0.84	0.86	0.95	0.93
13	0.96	0.95	0.80	0.82	0.85	0.96	0.95	0.81	0.83	0.85	0.95	0.93
14	0.96	0.96	0.80	0.82	0.84	0.96	0.95	0.80	0.81	0.84	0.95	0.93
15	0.96	0.96	0.79	0.81	0.83	0.96	0.96	0.80	0.80	0.84	0.95	0.94
16	0.96	0.97	0.79	0.78	0.83	0.96	0.97	0.78	0.78	0.82	0.95	0.94
17	0.96	0.98	0.78	0.77	0.82	0.96	0.98	0.78	0.77	0.81	0.95	0.96
18	0.96	0.99	0.76	0.75	0.80	0.97	0.99	0.76	0.75	0.79	0.96	0.97
19	0.98	1.01	0.72	0.71	0.74	0.98	1.01	0.73	0.70	0.74	0.97	0.99
20	1.01	1.05	0.76	0.71	0.77	1.02	1.05	0.75	0.69	0.76	1.01	1.04

The axial power production profile for a representative element in both the B and C-rings are given in Table 19. The F1 and F2 designs gave rise to less than a 1%

difference in axial power production profile for the fuel plates so just the results from the F1 design are reported below. As shown in Table 20 the axial power production profile (±0.31%) is not appreciably different from that of the LEU or the HEU reference core designs.

Table 20: Axial Power Production Profile for Core Plates in the F1 Design

B4 Element Axial Peaking				
	Height	F1 Design	LEU Reference	HEU Reference
	Top	0.49	0.52	0.54
		0.70	0.71	0.72
		0.89	0.88	0.89
		1.07	1.04	1.04
		1.18	1.17	1.17
		1.26	1.25	1.24
		1.31	1.27	1.22
		1.21	1.22	1.22
		1.03	1.08	1.08
	Bottom	0.84	0.86	0.89
C6 Element Axial Peaking				
	Height	F1 Design	LEU Reference	HEU Reference
	Top	0.45	0.48	0.49
		0.68	0.66	0.67
		0.86	0.84	0.84
		1.02	0.99	1.00
		1.15	1.13	1.13
		1.26	1.25	1.23
		1.31	1.32	1.31
		1.27	1.27	1.27
		1.11	1.15	1.14
	Bottom	0.90	0.91	0.92

It's important to point out that the neutron energy spectrum in the surrounding B-ring is not considerably different from that of the LEU reference core. So if a thermal in-core irradiation needed to be performed, then an element spot in the B-ring could be used. Figure 20 shows how the neutron energy spectrums differ in the water of the middle

coolant channel of the B-6 fuel element between the F1 design and the LEU reference. The F1 design neutron energy spectrum is ~5% less than that of the LEU reference.

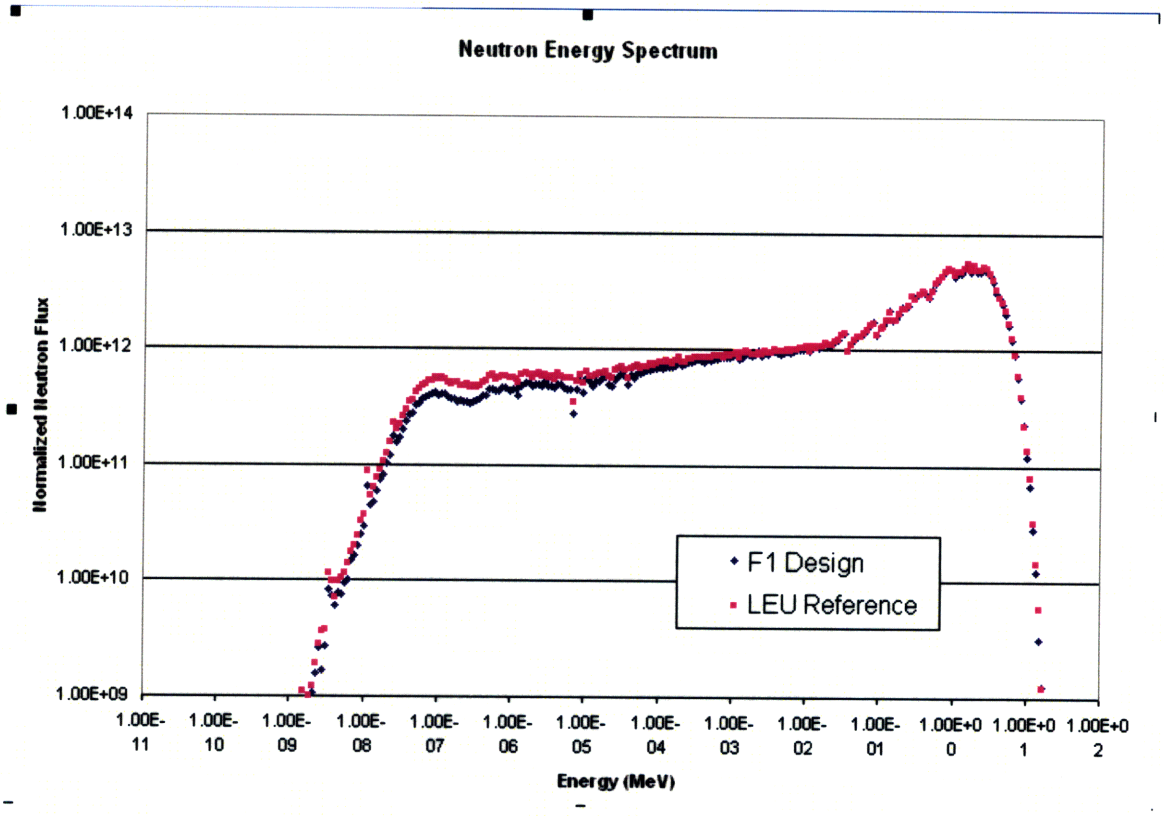

Figure 20: Neutron Energy Spectrum in the Middle H2O Channel in the B-6 Fuel Element

3.2 Reactivity Insertion Analyses

3.2.1 Initial Fast Flux Trap Insertion

The first reactivity insertion that the Fast Flux Trap must undergo is the initial placing into the core. This first calculation assumes all fresh fuel in the completely filled B and C-rings, all absorbers are fully inserted and the reflector is completely dumped. For the flooded case it is assumed that water is completely filling the entire A-ring space, as it would prior to insertion of the Fast Flux Trap loop. As shown in Table 21, the core is subcritical both before and after insertion of the Fast Flux Trap loop.

Table 21: Reactivity Difference from Installation of Fast Flux Trap Loop

	Keff	ρ Difference (ΔK/K)
Proposed core design with H2O in place of FFT	0.94766 ±0.00009	0
Proposed core design with F1 installed	0.94307 ±0.00009	-0.0048 ±0.00029
Proposed core design with F2 installed	0.95080 ±0.00009	0.0033 ±0.00029

3.2.2 Reactivity Worth of Fast Flux Trap

In order to determine exactly how much reactivity the Fast Flux Trap was worth, the entire Fast Flux Trap loop was replaced with helium which is an inert material relatively transparent to neutrons. For this calculation the control rods were held at the 'near critical' position in order to determine the reactivity worth at criticality for the

proposed Fast Flux Trap designs. As shown in Table 22, the F1 design is worth 0.0176 ΔK/K, while the F2 design is worth about 40% more at 0.0247 ΔK/K.

Table 22: Reactivity Worth of Fast Flux Trap

	Keff	ρ Difference (ΔK/K)
Proposed design with He in place of FFT	0.97495 ±0.00009	0.0000
F1 FFT design	0.99212 ±0.00009	0.0176 ±0.00028
F2 FFT design	0.99902 ±0.00009	0.0247 ±0.00028

3.2.3 Reactivity Worth of Control Mechanisms

Since the Fast Flux Trap does add an appreciable amount of reactivity, it's important to determine the affect on the total control worth of the core. Table 23 shows the LEU reference core along with both proposed Fast Flux Trap designs where all six shim blades and regulating rod have been fully inserted.

Table 23: Control Rod Insertion Worth

	Keff	ρ Difference (ΔK/K)
LEU reference core	0.97331 ±0.00013	0.0000
F1 Design	0.96951 ±0.00009	-0.0039 ±0.00032
F2 Design	0.97680 ±0.00009	0.0036 ±0.00032

Table 24 shows the same designs with all absorbers fully inserted as featured in Table 23, however now the D_2O heavy water reflector is completely dumped.

Table 24: Control Rod Insertion plus Reflector Dump Worth

	Keff	ρ Difference (ΔK/K)
LEU reference core	0.93927 ±0.00010	0.0000
F1 Design	0.94307 ±0.00009	0.0040 ±0.00030
F2 Design	0.95080 ±0.00009	0.0123 ±0.00030

Table 25 shows how the shutdown margin of the control blades in the LEU reference core design compares to the core with the F1 and F2 designs. While the shutdown margin of the control blades with the Fast Flux Trap design is smaller than that of the LEU reference, it is still sufficient to keep the core subcritical. This decreased shutdown margin for the Fast Flux Trap designs was expected since the neutron spectrum is significantly harder than that of the LEU reference.

Table 25: Control Blade Shutdown Margin Calculation of FFT and LEU Reference Designs

	Blade Height (in)	Keff	ρ Difference (ΔK/K)
LEU reference core	8.3	1.01795 ±0.00009	0.0000
	Fully Inserted	0.97331 ±0.00009	-0.0439 ±0.00027
F1 Design	8.5	0.99230 ±0.00009	0.0000
	Fully Inserted	0.96951 ±0.00009	-0.023 ±0.00027
F2 Design	8.5	0.99879 ±0.00009	0.0000
	Fully Inserted	0.97680 ±0.00009	-0.022 ±0.00027

3.2.4 Pb-Bi/Primary H_2O Leakage Effects

The next scenario investigated was that of leakage between the Pb-Bi coolant loop and the H_2O cooled core. Fortunately Pb-Bi is chemically inert in the presence of both water and air so there is no chance of a violently exothermic reaction as in the case of sodium coolant. Furthermore, since the temperature of the primary water is well under the freezing point of Pb-Bi at 125°C, any Pb-Bi coolant which manages to leak out of the Fast Flux Trap would instantly harden and reduce if not plug up the leak. It is because of this trait that a large sustained leak of Pb-Bi into the primary coolant is not considered to

be a likely scenario. However, due to the damage that solid Pb-Bi chunks could cause to the primary pumps, it would be wise to install a system which is capable of detecting Pb-Bi leaks to the primary system.

In the highly unlikely event of water ingress into the Pb-Bi reflector region, the water/steam will collect near the top of the Fast Flux Trap, since the Pb-Bi is heavier than water. Table 26 shows the difference in reactivity for both the F1 and F2 designs assuming that 25% of the Pb-Bi coolant has been replaced with water.

Table 26: Fast Flux Trap Water Ingress Reactivity Difference

	% Pb-Bi	% H2O	Keff	ρ Difference (ΔK/K)
F1 Design	100	0	0.99212 ±0.00009	0.0000
	75	25	0.99470 ±0.00009	0.0026 ±0.00027
F2 Design	100	0	0.99902 ±0.00009	0.0000
	75	25	1.00197 ±0.00009	0.0030 ±0.00027

3.2.5 Flooding of the Central Irradiation Facility

The final scenario investigated here is the replacement of the central irradiation facility with water. Compared to the other scenarios investigated here, this transient will be relatively common, given that it will occur whenever the central irradiation facility is loaded with a new sample material. Table 27 and Table 28 show the reactivity insertion from the complete flooding of the central irradiation facility for both the F1 and F2 designs respectively. For this calculation all control rods have been inserted and the reflector was dumped, in accordance with current standard operating procedures for in-core work. As shown in both tables the reactor core is safely subcritical, despite the reactivity insertion from the water.

Table 27: F1 Design Flooded Central Irradiation Facility Reactivity Insertion

	Keff	ρ Difference (ΔK/K)
Normal Central Irradiation Facility	0.94307 ±0.00009	0.0000
H2O flooded Central Irradiation Facility	0.96332 ±0.00009	0.0215 ±0.00028

Table 28: F2 Design Flooded Central Irradiation Facility Reactivity Insertion

	Keff	ρ Difference (ΔK/K)
Normal Central Irradiation Facility	0.95080 ±0.00009	0.0000
H2O flooded Central Irradiation Facility	0.97708 ±0.00009	0.0276 ±0.00028

3.3 Lifetime Analyses

The FFT materials performance in an irradiation environment is not likely to be a design limitation. T91 can survive fluences of 30-50 dpa before any significant swelling occurs and the MIT reactor typically imparts a fluence of 1 dpa per year to the internal core components [Kohse 2008b]. Since T91 was used for the Fast Flux Trap cladding and internals, materials issues should not begin to negatively impact performance until 30-50 years of operation at the earliest.

In order to understand how the neutronic and thermal hydraulic performance change with time, the amplifier pins of the Fast Flux Trap design were depleted in MCODE Version 2.2. This code is a linkage program which combines the continuous-energy Monte Carlo code MCNP-4C with the one-group depletion code ORIGEN2 to perform burnup calculations for nuclear fission reactor systems [Xu and Hejzlar 2008]. MCODE is described more fully in Appendix C.

MCODE allows for depletions to be carried out at either constant power or constant flux. Since we were interested in how the fast flux would change with time, the depletion was carried out at a constant power level of 10 MW. The only region which was depleted was the fissile material in the amplifier pins of the Fast Flux Trap. Therefore, as the power decreased in the Fast Flux Trap, it was increased by the code in the rest of the core. The power decrease results reported in Table 31 and Table 34 are only for the Fast Flux Trap. Since the flux from the core elements served as a neutron source for the Fast Flux Trap depletion, the core elements were arranged to approximate the flux coming in from the equilibrium core.

For both the F1 and F2 design depletions, the control rods were held at a near critical height, the fuel is fresh and all other systems were placed in their normal operational configurations. Since the MITR typically operates for 290 days out of the year this same capacity factor was assumed for the depletion simulation. This is a fairly conservative assumption since the reactor does not necessarily operate at full power for all of the 290 days that it is up.

3.3.1 F1 Fast Flux Trap Design Lifetime Analysis

The neutron energy spectrum for the F1 design in the Central Irradiation Facility over a 35 year operational lifetime is shown in Figure 21 (average standard deviation of k_{eff} 0.00010). The LEU and HEU reference spectra are included for comparison purposes.

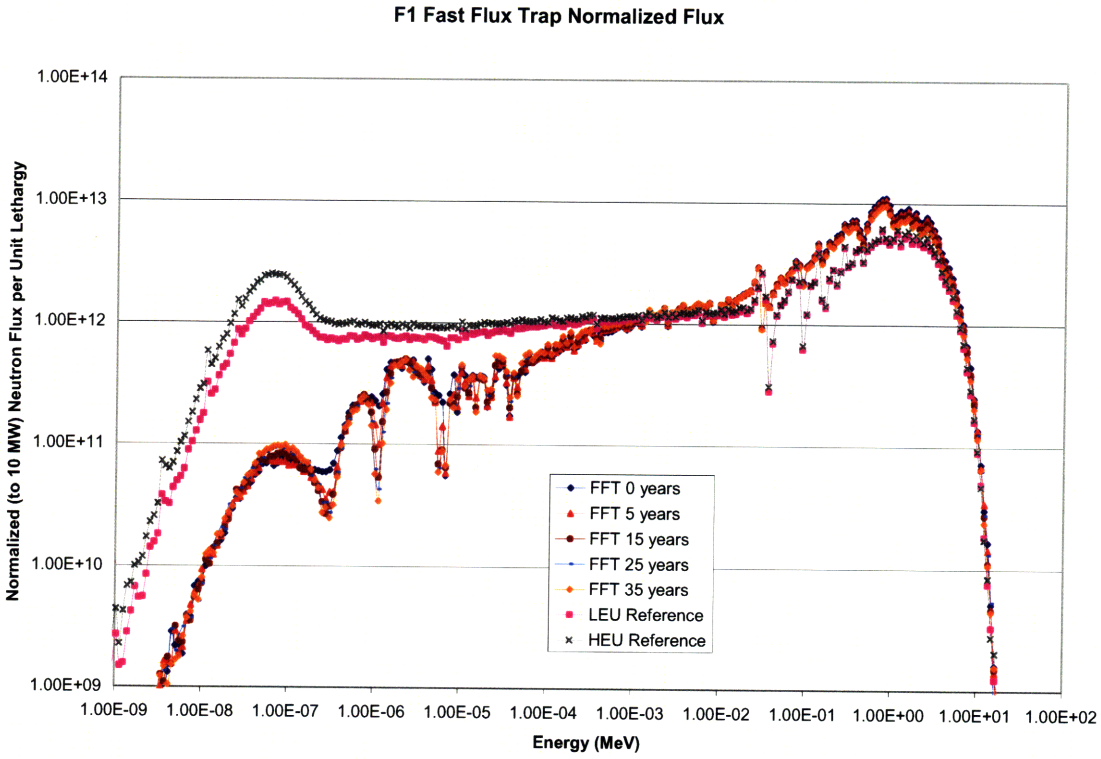

Figure 21: F1 Design Neutron Spectra in the Central Irradiation Facility during Operational Lifetime

Table 29 shows the same information described in Figure 21 broken up into thermal, epithermal and fast energy ranges.

Table 29: Neutron Flux Changes during Operational Lifetime of the F1 FFT

Depletion Time (years)	0 to 0.4eV	0.4eV to 3 keV	3keV to 0.1 MeV	0.1 Mev to 10 MeV
0	2.01E+12	4.88E+13	6.40E+13	2.64E+14
1	1.94E+12	4.84E+13	6.37E+13	2.60E+14
2	1.89E+12	4.85E+13	6.38E+13	2.58E+14
3	1.90E+12	4.86E+13	6.38E+13	2.56E+14
4	1.87E+12	4.84E+13	6.39E+13	2.54E+14
5	1.86E+12	4.85E+13	6.38E+13	2.53E+14
10	1.90E+12	4.89E+13	6.36E+13	2.45E+14
15	1.91E+12	4.94E+13	6.37E+13	2.39E+14
20	2.02E+12	4.98E+13	6.37E+13	2.34E+14
25	2.08E+12	5.01E+13	6.35E+13	2.30E+14
30	2.10E+12	5.04E+13	6.36E+13	2.27E+14
35	2.11E+12	5.06E+13	6.32E+13	2.25E+14

Both Figure 21 and Table 29 show a steady decrease in the total flux with time of roughly 0.5% per year. The fast flux decreases at a slightly faster steady rate of 0.7% per year.

Table 30 shows how the major fissile and fertile isotope vectors change over the lifetime of the F1 design. The ^{235}U steadily decreases from 19.75 wt% at BOL to ~2.6 wt% at 35 years while the ^{239}Pu steadily increases from 0 wt% at BOL to ~3 wt% after 35 years.

Table 30: Fissile and Fertile Vector Changes during Operational Lifetime of the F1 FFT

In-Core Time (years)	U-234	U-235	U-238	Pu-239
0	6.12E+19	4.84E+21	1.96E+22	0.00E+00
1	6.12E+19	4.55E+21	1.95E+22	6.39E+19
2	5.60E+19	4.29E+21	1.94E+22	1.20E+20
3	5.37E+19	4.04E+21	1.93E+22	1.70E+20
4	5.16E+19	3.80E+21	1.92E+22	2.15E+20
5	4.95E+19	3.58E+21	1.92E+22	2.54E+20
10	4.06E+19	2.64E+21	1.87E+22	3.97E+20
15	3.38E+19	1.94E+21	1.83E+22	4.78E+20
20	2.85E+19	1.40E+21	1.79E+22	5.24E+20
25	2.49E+19	1.00E+21	1.75E+22	5.47E+20
30	2.25E+19	7.16E+20	1.71E+22	5.57E+20
35	2.13E+19	5.08E+20	1.67E+22	5.58E+20

By contrast, the fission heat production of the Fast Flux Trap experiences the largest decrease of 4.26% after the first year of operation and follows a consistently decreasing rate throughout its subsequent years of operation. The calculated change of the fission heat production in only the Fast Flux Trap of the F1 design with time is described in Table 31. The calculated reduction in heat generation is much more than the reduction in the fast flux. Thus the lifetime of the FFT, if limited to 20 years, implies a rise in the power of the core proper by about 2%.

Table 31: Heat Production Changes during Operational Lifetime of the F1 FFT

Burn-up (MWd/kg)	In-Core Time (years)	Heat Production (W)	Cumulative % Change from BOL
0	0	398784	0.00%
9.42	1	381811	-4.26%
18.456	2	370023	-7.21%
27.172	3	358746	-10.04%
35.586	4	348676	-12.56%
43.745	5	336492	-15.62%
81.137	10	294394	-26.18%
113.099	15	260642	-34.64%
141.943	20	231932	-41.84%
167.198	25	210368	-47.25%
189.958	30	191787	-51.91%
210.829	35	178860	-55.15%

3.3.2 F2 Fast Flux Trap Design Lifetime Analysis

The neutron energy spectrum for the F2 design in the Central Irradiation Facility over a 35 year operational lifetime is shown in Figure 22 (average standard deviation of

k_{eff} 0.00010). The LEU and HEU reference spectra are included again for purposes of comparison.

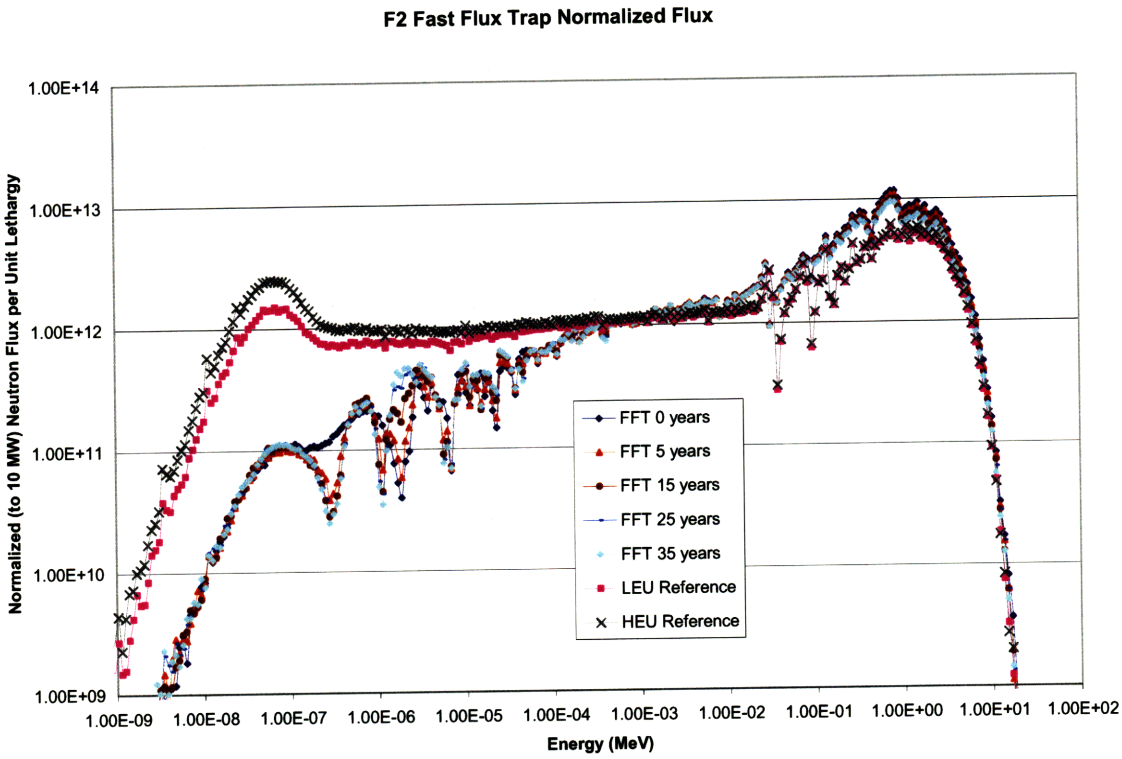

Figure 22: F2 Design Neutron Spectra in the Central Irradiation Facility during Operational Lifetime

As was the case with the F1 design, there is not a drastic change in the neutron energy spectrum over the lifetime of the Fast Flux Trap. Table 32 shows the same information described in Figure 22 broken up into thermal, epithermal and fast energy ranges.

Table 32: Neutron Flux Changes during Operational Lifetime of the F2 FFT

Depletion Time (years)	0 to 0.4eV	0.4eV to 3 keV	3keV to 0.1 MeV	0.1 Mev to 10 MeV
0	3.00E+12	5.12E+13	6.80E+13	2.78E+14
1	2.65E+12	5.12E+13	6.78E+13	2.72E+14
2	2.54E+12	5.14E+13	6.76E+13	2.69E+14
3	2.51E+12	5.15E+13	6.74E+13	2.66E+14
4	2.44E+12	5.17E+13	6.72E+13	2.63E+14
5	2.43E+12	5.17E+13	6.73E+13	2.61E+14
10	2.39E+12	5.27E+13	6.66E+13	2.50E+14
15	2.41E+12	5.35E+13	6.61E+13	2.41E+14
20	2.44E+12	5.40E+13	6.60E+13	2.36E+14
25	2.43E+12	5.42E+13	6.54E+13	2.32E+14
30	2.46E+12	5.40E+13	6.53E+13	2.29E+14
35	2.41E+12	5.41E+13	6.52E+13	2.27E+14

Both Figure 22 and Table 32 show a slightly more varied decrease in the total flux with time between 0.5% and 1.5% per year. The fast flux decreases at a slightly steadier rate of 0.9% per year. If the value of the fast flux is desired not to decrease more than 20% over the lifetime, then the lifetime should not exceed 35 years.

Table 33 shows how the major fissile and fertile isotope vectors change over the lifetime of the F2 design. The ^{233}U steadily decreases from 12 wt% at BOL to ~0.6 wt% at 35 years while the ^{239}Pu steadily increases from 0 wt% at BOL to ~3 wt% after 35 years.

Table 33: Fissile and Fertile Vector Changes during Operational Lifetime of the F2 FFT

In-Core Time (years)	U-233	U-238	Pu-239
0	2.94E+21	2.16E+22	0.00E+00
1	2.68E+21	2.15E+22	7.50E+19
2	2.45E+21	2.13E+22	1.40E+20
3	2.23E+21	2.12E+22	1.96E+20
4	2.03E+21	2.11E+22	2.45E+20
5	1.85E+21	2.10E+22	2.88E+20
10	1.14E+21	2.05E+22	4.37E+20
15	6.85E+20	2.00E+22	5.16E+20
20	3.94E+20	1.95E+22	5.57E+20
25	2.22E+20	1.91E+22	5.75E+20
30	1.23E+20	1.86E+22	5.82E+20
35	6.76E+19	1.82E+22	5.83E+20

By contrast, the fission heat production of the Fast Flux Trap experiences the largest decrease of 5.92% after the first year of operation and follows a consistently decreasing rate throughout its subsequent years of operation. The calculated change of the fission heat production in only the Fast Flux Trap of the F2 design with time is described in Table 34.

Table 34: Heat Production Changes during Operational Lifetime of the F2 FFT

Burn-up (MWd/kg)	In-Core Time (years)	Heat Production (W)	Cumulative % Change from BOL
0	0	451930	0.00%
10.018	1	425166	-5.92%
19.45	2	404962	-10.39%
28.415	3	386881	-14.39%
36.969	4	367827	-18.61%
45.151	5	351685	-22.18%
81.146	10	288699	-36.12%
110.241	15	243690	-46.08%
135.535	20	209691	-53.60%
157.383	25	187642	-58.48%
177.204	30	174091	-61.48%
195.71	35	165721	-63.33%

3.3.3 Coolant Activation

Another important factor to consider when working with Pb-Bi Eutectic coolant is the radiological hazard associated with coolant activation. The ^{209}Bi can capture a neutron and β^- decay to become ^{210}Po which has a 140 day half life and is a relatively toxic alpha emitter. The equilibrium coolant activity due to neutron activation (A) is given by the formula from [Buongiorno, *et al.* 2008]:

$$A = \frac{\Phi \sigma N_t \left(e^{\lambda t_c} - 1\right)}{e^{\lambda (t_c + t_{oc})} - 1}$$

Where Φ is the neutron flux, σ is the capture cross section (4.8 mb), N_t is the target nucleus number density (2.64E25), λ is the radioactive decay constant ($5.8*10^{-8}$ sec^{-1}), t_c is the in-core transient time (0.185 sec) and t_{oc} is the out of core residence time (14 sec). Assuming the neutron fluxes given for the F1 design in Table 29 and for the F2 design in Table 32, the equilibrium coolant activity due to neutron activation for the F1 design is 9.32E6 Bq/m^3 and for the F2 design is 9.85E6 Bq/m^3. It's important to point out that these are preliminary estimates of the activity level; the actual values will be determined after the final engineering has been completed on the rest of the system. These levels indicate that some shielding may be required for the Pb-Bi storage tank and supporting equipment on the reactor top, however the total required amount of shielding will again be determined after the final engineering is complete.

Chapter 4 – Thermal Hydraulic Evaluation

4.1 Coolant Selection

This chapter covers the thermal hydraulic evaluation for the Fast Flux Trap in the center of the core. In the early design phases of the Fast Flux Trap a wide variety of different coolants were considered. Table 35 features basic characteristics of several reactor coolants which were considered.

Table 35: Reactor Coolant Basic Characteristics [Todreas 2004]

Coolant	Atomic Mass (g/mol)	Relative Moderating Power	Neutron Absorption Cross-section (1 MeV)(mbarn)	Neutron Scattering Cross-section (barn)	Melting Point (°C)	Boiling Point (°C)	Chemical Reactivity (with air and water)
Pb	207	1	6.001	6.4	327	1737	Inert
Pb-Bi Eutectic	208	0.82	1.492	6.9	125	1670	Inert
Na	23	1.80	0.230	3.2	98	883	Highly Reactive
H2O	18	421	0.1056	3.5	0	100	Inert
D2O	20	49	0.0002115	2.6	0	100	Inert
He	4	0.27	0.007953	3.7	-	-269	Inert

Among the various factors considered, the most important characteristics were; a low moderating power since we were seeking to maximize the fast flux, a high heat transfer coefficient since we wanted to remove an appreciable amount of heat from a small volume and chemical inertness with water since the MITR primary coolant is water. The low moderating power requirement eliminated the H_2O and D_2O coolant options. The high heat transfer coefficient requirement eliminated the helium coolant option. The chemical inertness with water requirement eliminated the sodium coolant option. This left either the lead or lead-bismuth eutectic coolant options. Both lead and

lead-bismuth eutectic coolants have relatively high boiling temperatures, 1737°C and 1670°C respectively, so margin to boiling does not differ considerably between the two options. However, since lead-bismuth eutectic melts at a much lower temperature of 125°C than the lead coolant at 327°C, lead-bismuth was selected for the coolant in the Fast Flux Trap. The lower melting temperature of the lead-bismuth allows for lower operating temperature than a pure lead loop. This is desirable because operating at as low a temperature as possible would minimize the necessary thermal gradient between the primary water coolant in the MITR core and the lead-bismuth coolant in the Fast Flux Trap loop. Also lower temperatures put less of a demand upon the structural materials in the design.

Pb-Bi Eutectic coolant, which is made up of 45% Pb and 55% Bi, has been investigated for use in nuclear systems since the 1950s. It has a number of beneficial properties for reactor systems with a fast spectrum including a small parasitic neutron absorption cross section, high scattering cross section to prevent the neutrons from leaking out of the core, a small energy loss per collision to minimize moderation, a high boiling temperature, a high heat transfer coefficient (20,000 W/m^2 K) and acceptable corrosion/mechanical degradation with existing structural materials [CEA 2007]. Also, it does not undergo any volume change upon solidification/melting so its density remains constant at 10.5 g/cm^3.

4.2 Structural Material Selection

As mentioned in Section 2.4, the T91 alloy (Fe-9%Cr-1%Mo) was selected as the reference material for all materials facing the Pb-Bi coolant including the amplifier pin cladding, piping and all internal structures in the Fast Flux Trap. T91 has been found to have excellent performance with Pb-Bi coolant at temperatures below 500°C and coolant velocities below 3 m/sec [CEA 2007]. However, there is a new alloy (Fe-12%Cr-2%Si) being developed at MIT [Short 2007] for Pb-Bi Eutectic applications which promises to have improved resistance to corrosion at higher temperatures than T91. Preliminary laboratory experiments have confirmed acceptable resistance to corrosion at 650°C and higher temperature corrosion tests are currently being performed.

According to neutronic simulations, a complete replacement of all cladding and Fast Flux Trap internals with the new (Fe-12%Cr-2%Si) alloy has less than a 1% effect on neutron flux levels. Adoption of this alloy could allow for a significant thermal hydraulic and corrosion resistance benefit with a negligible effect on the neutronics. So provided this new alloy can be certified by the time that the Fast Flux Trap is ready to be constructed, and the cost is not appreciably different from T91 alloy, then this new (Fe-12%Cr-2%Si) alloy could allow for significantly higher safety margins in the Fast Flux Trap design.

4.3 Steady-state Analyses

A nodalization diagram of the Fast Flux Trap Pb-Bi loop, featured in Figure 23, was designed to develop the hydrodynamic model for RELAP5-3D version 2.3.6. The three pieces of information in each hydrodynamic component of the nodalization diagram are the three digit hydrodynamic component identification number, the name of the hydrodynamic component and the hydrodynamic component type (example: tmdpvol, tmdpjun, pipe, sngljun and branch). This nodalization diagram served as a blueprint to construct the full RELAP5-3D input file given in Appendix B. For this model the Pb-Bi coolant starts in a time dependant volume (hydrodynamic volume #215) called 'source.' The Pb-Bi then flows through a single time dependant junction 216 called 'srcjun' and into the down pipe (hydrodynamic volume #217) which is a 4 m long, 3.66 cm inner radius pipe. The Pb-Bi then travels through single junction #218 into the lower pipe (hydrodynamic volume #219). After traveling through the lower pipe single junction #220 the Pb-Bi enters the lower plenum (hydrodynamic volume #221). This lower plenum branches the coolant into four different sub-channels; the lumped average core sub-channel (hydrodynamic volume #222), the lumped partial corner sub-channel (hydrodynamic volume #223), the lumped full corner sub-channel (hydrodynamic volume #224) and the lumped side sub-channel (hydrodynamic volume #225). The Pb-Bi flow from these four parallel lumped sub-channels comes back together in the upper plenum (hydrodynamic volume #230). This upper plenum connects, via single junction #231, to the up pipe (hydrodynamic volume #232) which is a 3.49 m long, 3.12 cm inner

radius pipe. Finally, the Pb-Bi flows through single junction #233 into a time dependant volume (hydrodynamic volume #234) called 'sink.'

The mass flow rate was selected by applying the steady-state energy equation of $\dot{Q} = \dot{m}C_P\Delta T$ where $\dot{Q}$ is the heat production of the Fast Flux Trap (398784 W), C_P is the specific heat capacity of Pb-Bi (146 J/kg K), ΔT is the temperature difference (~50 K) across the core and $\dot{m}$ is the desired mass flow rate in kg/sec. The mass flow rate was calculated to be ~55 kg/sec. This calculated flow rate of ~55 kg/sec, with velocities of <2 m/sec, is well within the current pump state of the art. The required pumping power can be approximated as: $\dot{Q}_{pump} = \frac{\dot{m}\Delta P}{\rho}$. The ΔP values shown in Figure 24 (0.73 MPa) and Figure 27 (0.84 MPa), give pumping powers of 3.9 kW for the F1 design and 4.5 kW for the F2 design.

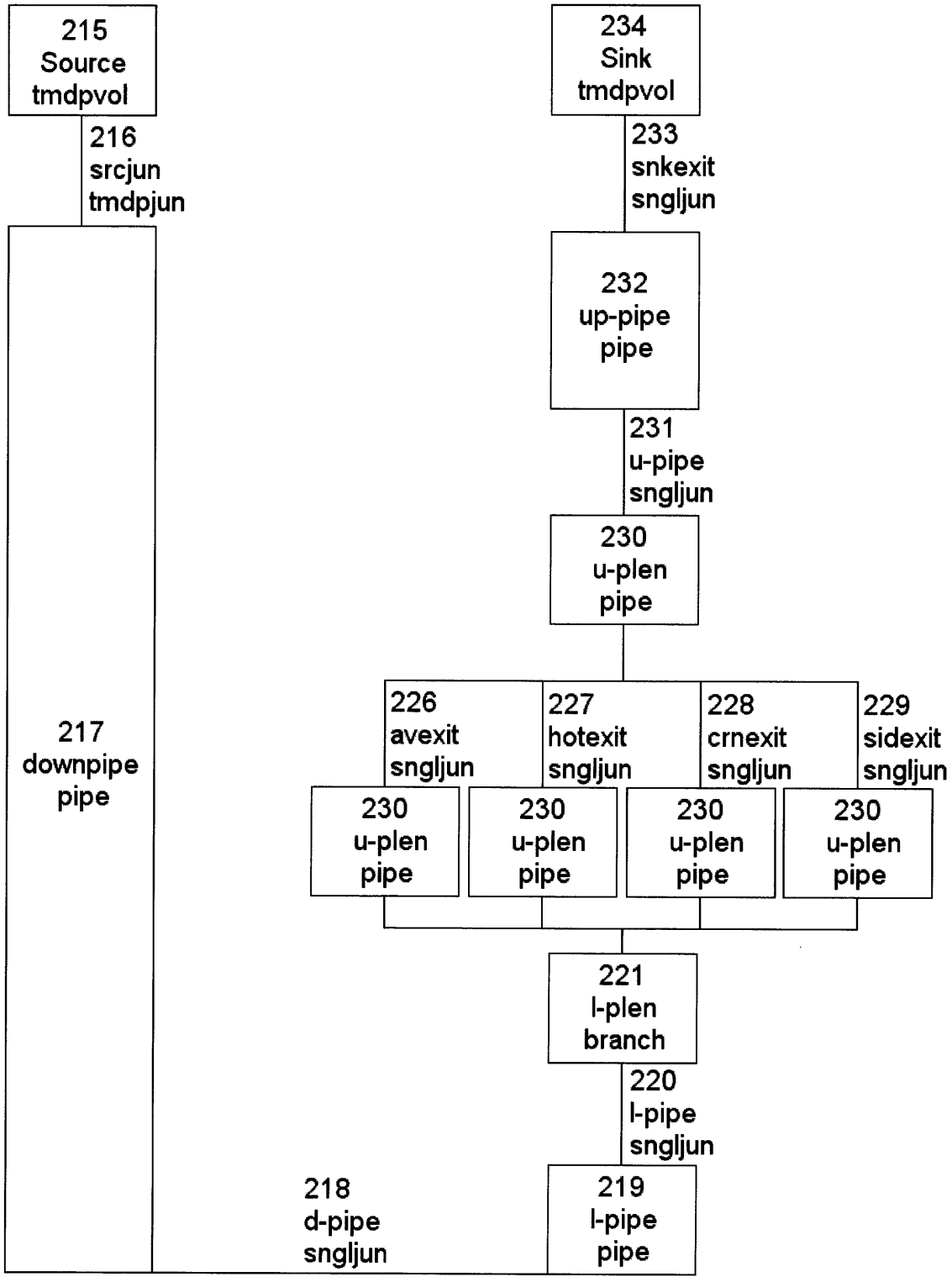

Figure 23: RELAP5-3D Fast Flux Trap Nodalization Diagram

The Fast Flux Trap core area was modeled by breaking the region up into four different parts: a lumped full corner sub-channel (which had the highest power peaking), a lumped partial corner sub-channel, a lumped side sub-channel and a lumped average core sub-channel. These four types of sub-channels are shown in Figure 24.

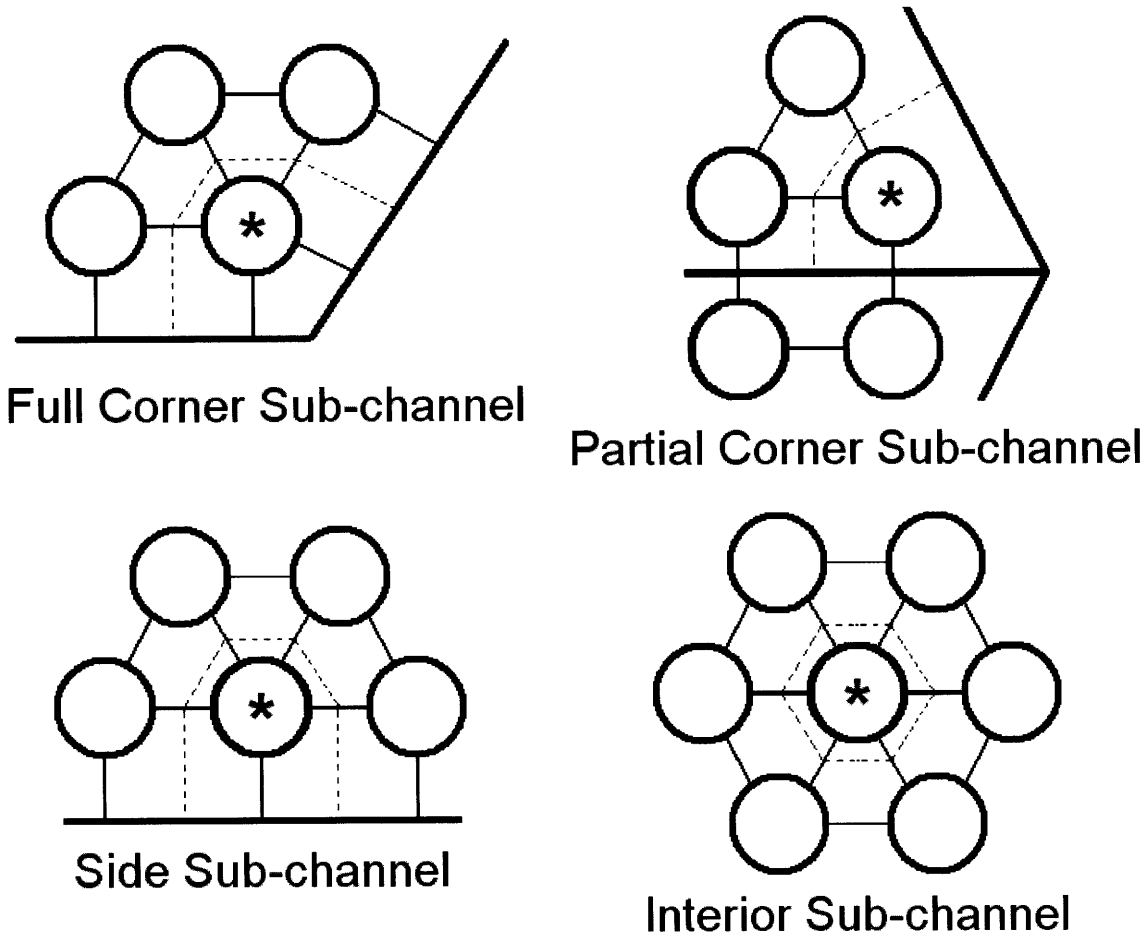

Figure 24: Sub-channel Geometry

As shown in Section 3.1.2, the hottest pins were all located in the outer-most amplifier ring. Since the lumped full corner (hot), lumped partial corner (corner) and lumped side (side) sub-channels represent all of the three types of sub-channels which exist in the hottest outer-most amplifier ring, these results, which used the highest power

peaking factors from each sub-channel category, represent the most challenging sites for heat removal in the entire Fast Flux Trap. Provided that the three hottest lumped sub-channels and the lumped average core sub-channel demonstrate acceptable temperature, pressure and coolant velocity profiles, then the Fast Flux Trap coolant loop should have no difficulty in rejecting the required heat. Both the F1 and F2 designs utilized the modified Unal, Lahey heat transfer correlation for subcooled liquid in the bubbly flow regime as given on page 3-195 of Volume I of the RELAP5-3D code manual [RELAP5 2005]. The Reynolds number for the coolant ranged from 15,000 to 21,000 in the outer channels and from 160,000 to 180,000 in the inner channels.

The steady-state coolant pressure, velocity and temperature profiles for the F1 design are featured in Figure 25, Figure 26 and Figure 27 respectively. As shown, the F1 design has a total coolant pressure drop of 1.01 MPa, a maximum coolant velocity of 2.22 m/sec and a coolant temperature difference of 47°K. These steady state parameters were given for a flowrate of 55.52 kg/sec through the Fast Flux Trap. Current liquid metal pumps can easily handle pressure drops in excess of 1 MPa and velocities up to 3 m/sec. The limiting parameter here is keeping the coolant velocity below 3 m/sec so that the flowing Pb-Bi doesn't erode the cladding material and protective oxide layers. All of these parameters are well within acceptable ranges for the current state of the art. The figures are arranged to give a graphical example of how the pressure, velocity and temperature change going around the loop.

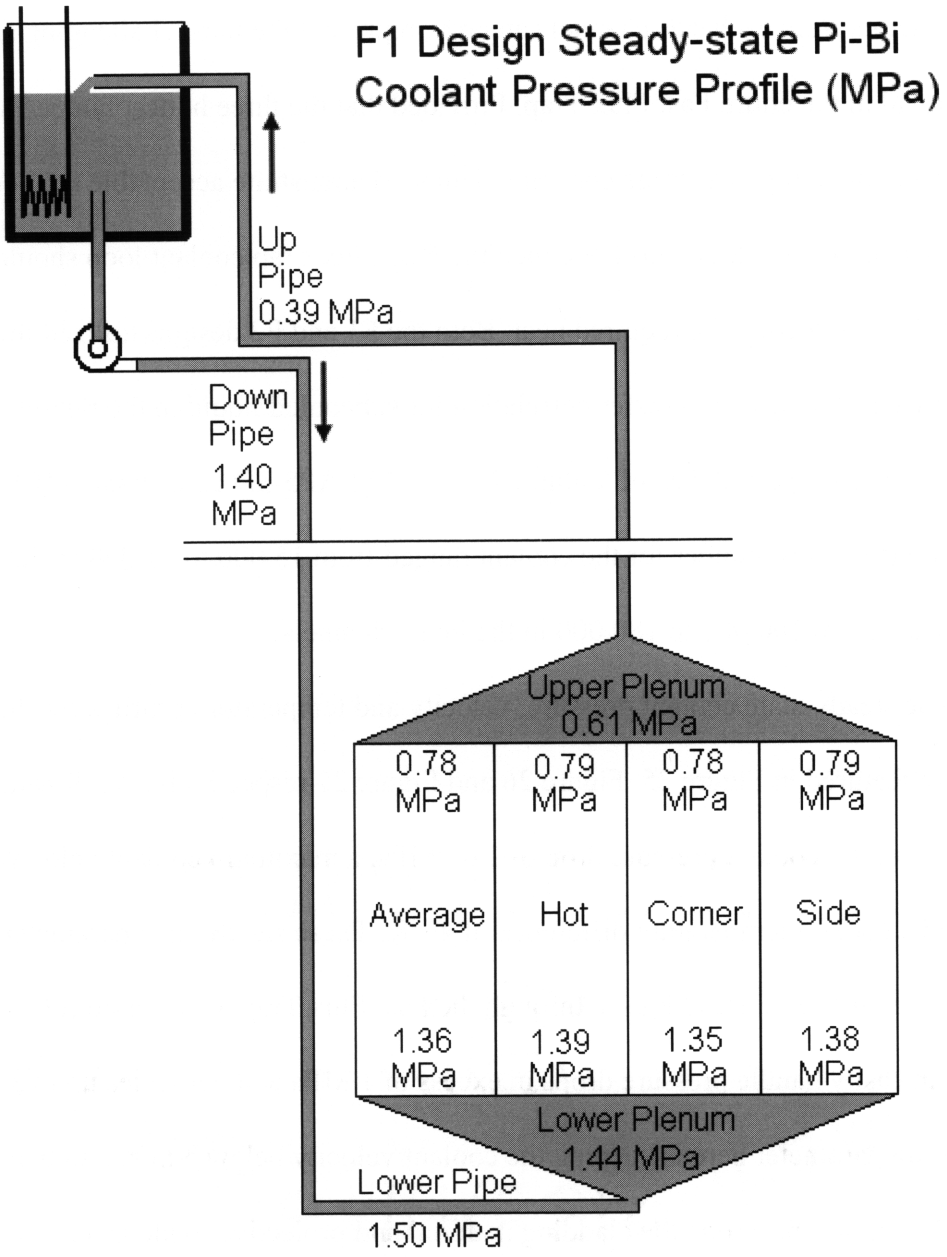

Figure 25: Steady-state Coolant Pressure Profile for F1 FFT

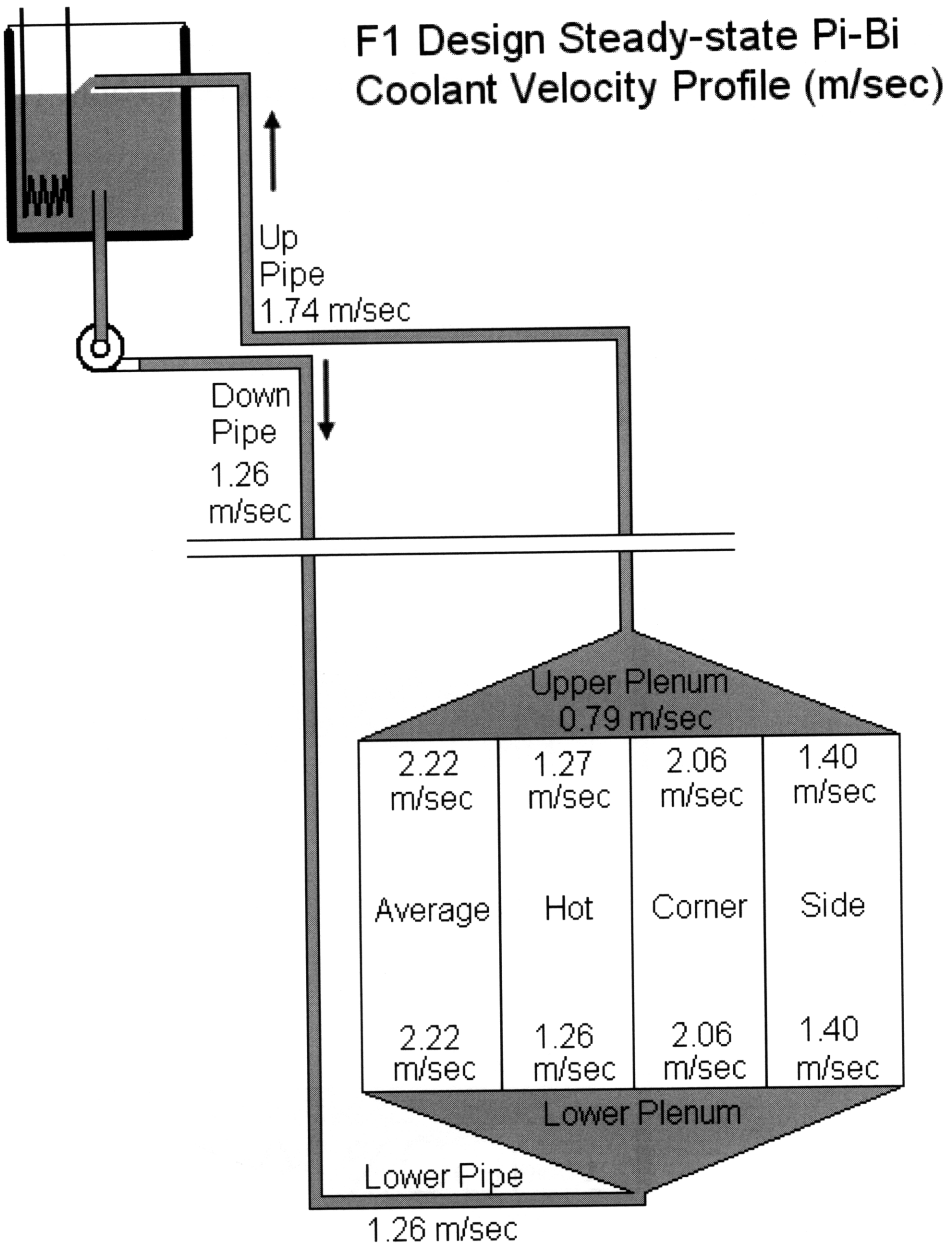

Figure 26: Steady-state Coolant Velocity Profile for F1 FFT

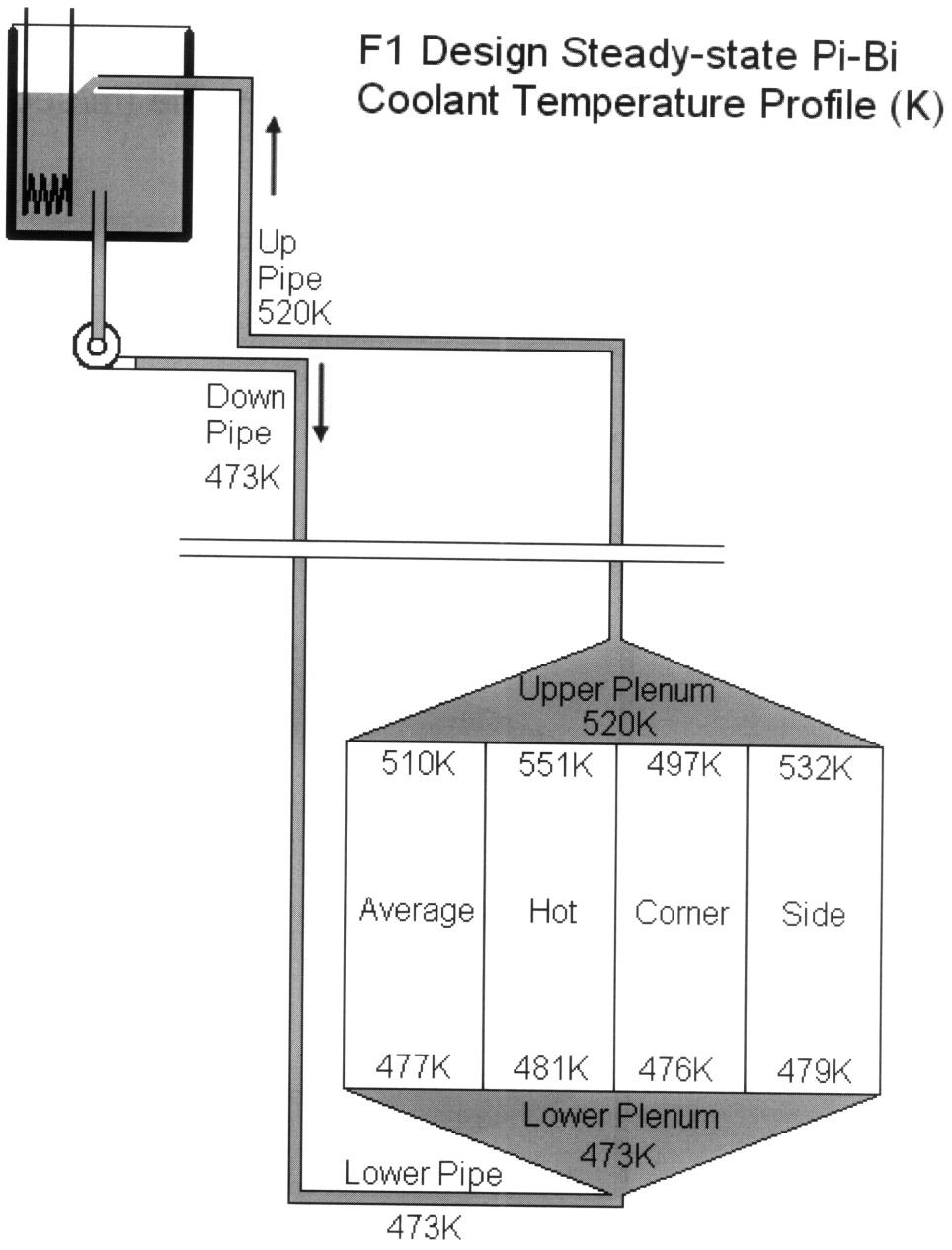

Figure 27: Steady-state Coolant Temperature Profile for F1 FFT

The steady-state coolant pressure, velocity and temperature profiles for the F2 design are featured in Figure 28, Figure 29 and Figure 30 respectively. As shown, the F2 design has a total coolant pressure drop of 1.01 MPa, a maximum coolant velocity of 2.23 m/sec and a coolant temperature difference of 53°K. All of these parameters are again well within the capability of current liquid metal pumps as well as below the 3 m/sec

coolant velocity limitation. These steady state parameters were also given for a flowrate of 55.52 kg/sec through the Fast Flux Trap.

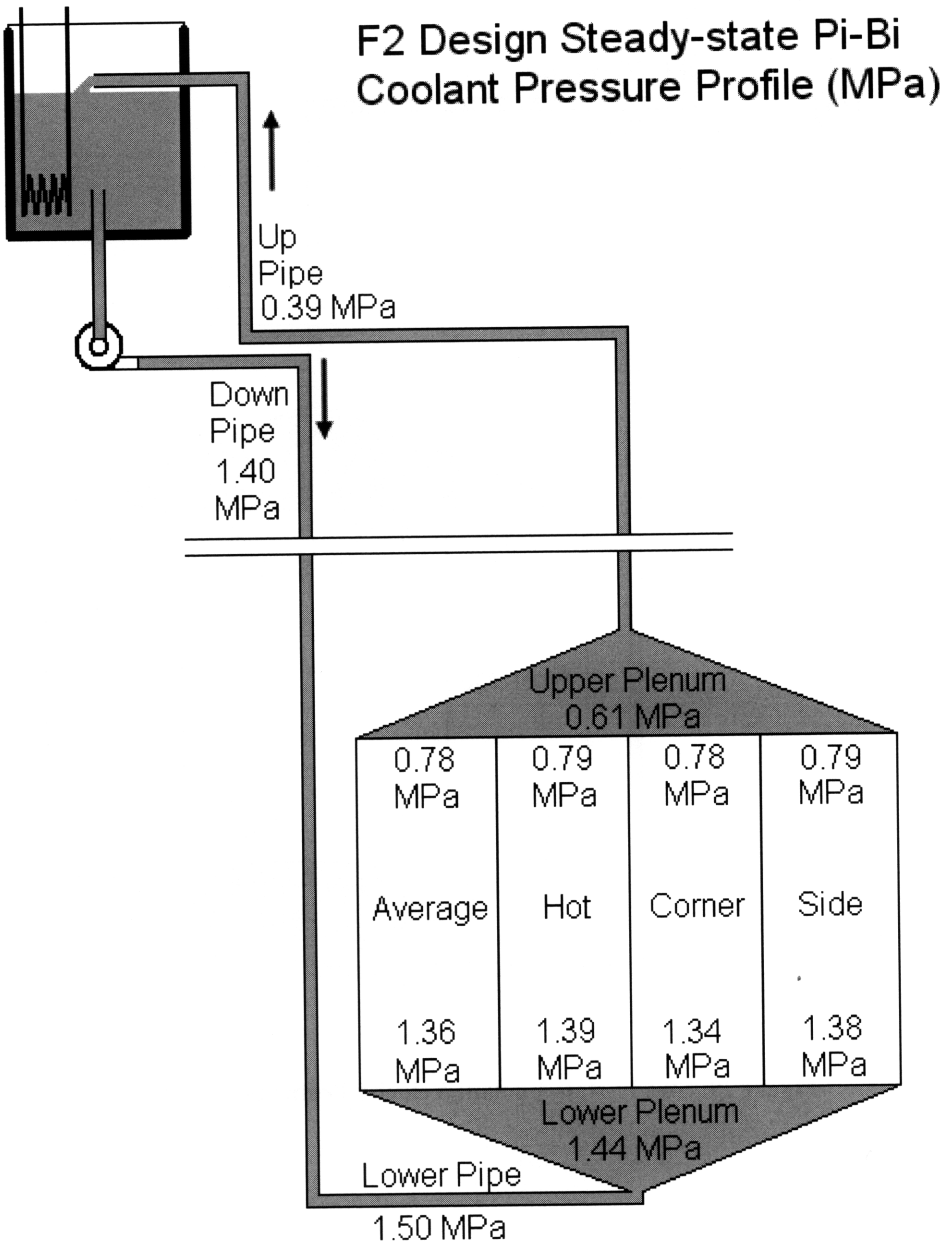

Figure 28: Steady-state Coolant Pressure Profile for F2 FFT

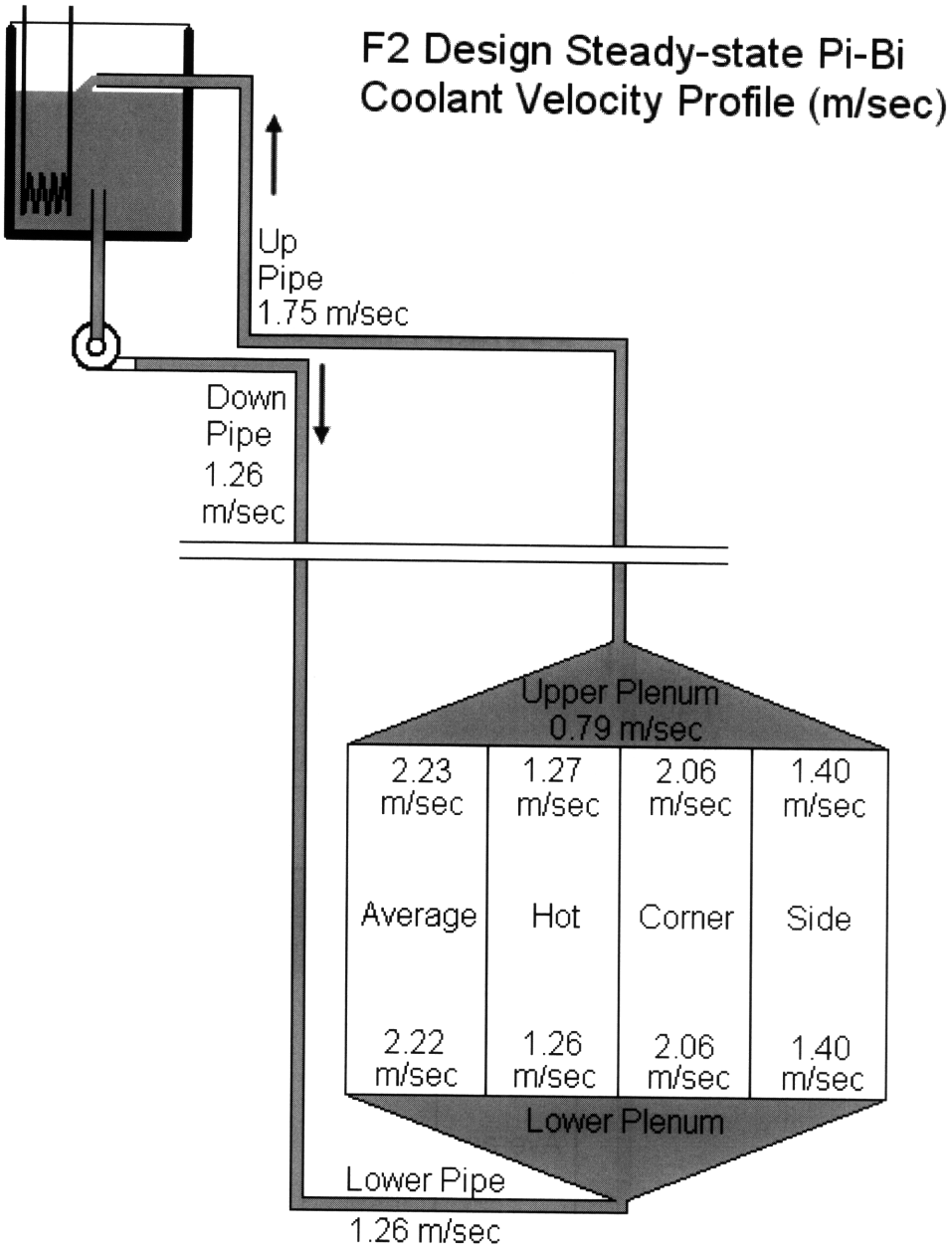

Figure 29: Steady-state Coolant Velocity Profile for F2 FFT

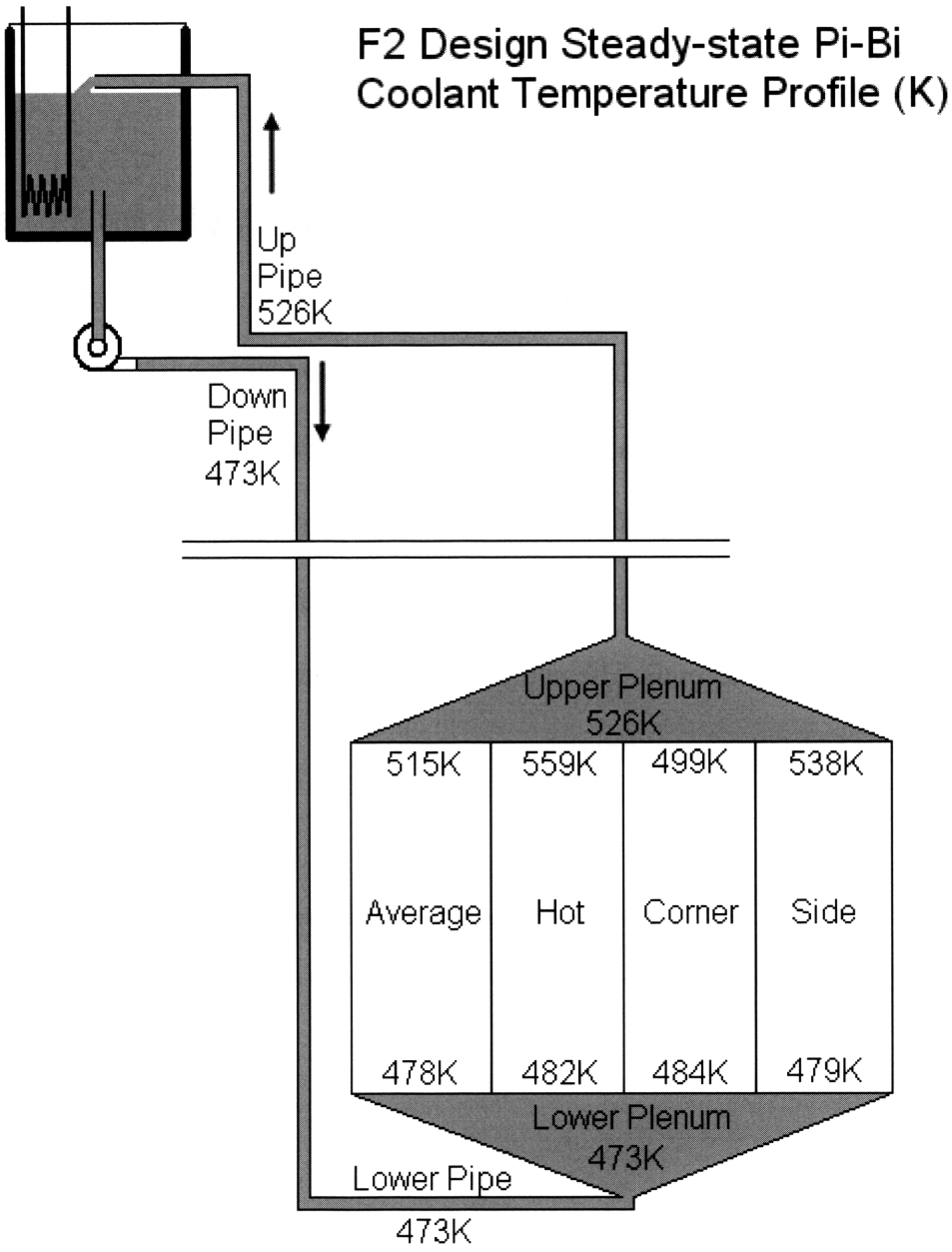

Figure 30: Steady-state Coolant Temperature Profile for F2 FFT

4.4 Transient Analyses

As shown in section 3.3, the Fast Flux Trap produces between 400-450 kW worth of heat. Therefore a trip of the Pb-Bi coolant pump must trigger an automatic scram of the MITR core so that the Fast Flux Trap does not approach any material temperature limits. Since the normal conservative time differential between receipt of a scram signal and insertion of the control rods is two seconds, this value was used to conduct a simulated pump trip transient. The transient assumed normal operation up until the pump trip which occurs at 50 seconds. The pump coast down curve used for this analysis is shown in Figure 31 [Memmott 2008].

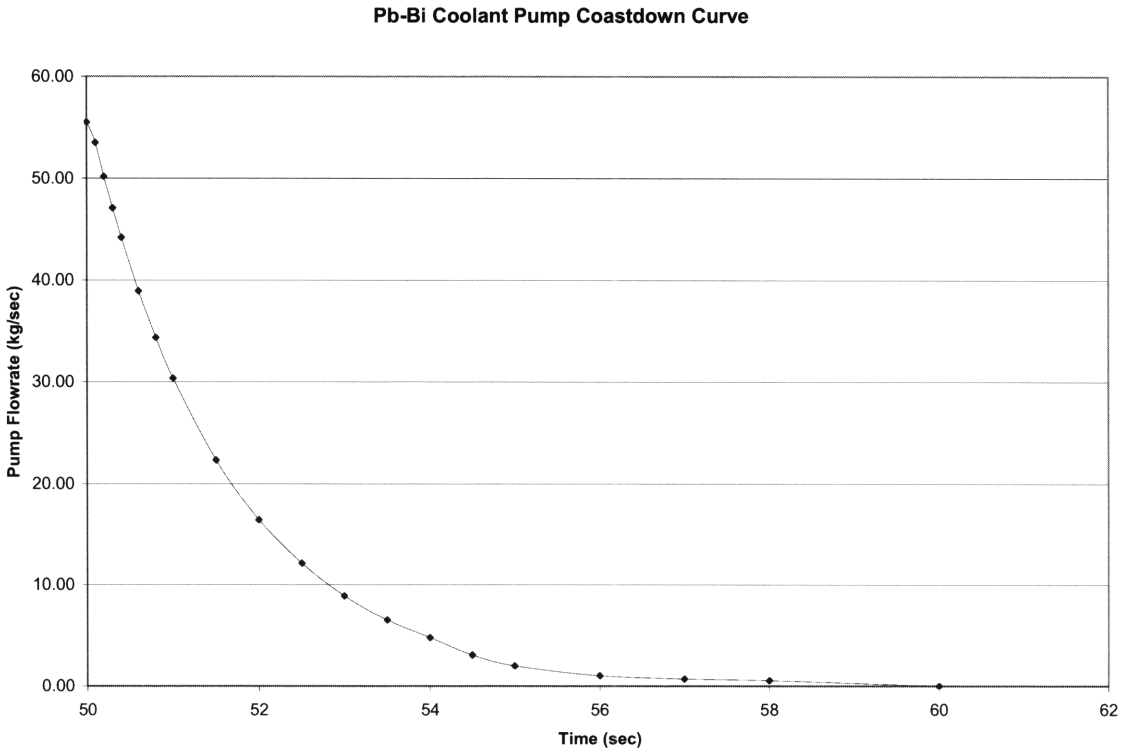

Figure 31: Pb-Bi Coolant Pump Coastdown Curve [Memmott 2008]

Two seconds after the Pb-Bi coolant pump trips the reactor is scrammed (at 52 seconds) and the heat production follows the respective decay heat curves given in Table 42. The total heat production for ^{235}U upon shutdown was given in the Nuclear Systems Volume I textbook [Todreas, Kazimi 1989] and the total heat production for ^{233}U upon shutdown was adapted from direct decay heat data measured by Yarnell and Bendt [Yarnell 1978] and discussed in [Kloosterman 2000].

Table 36: Decay Heat Curves for U-235 (F1) and U-233 (F2) FFT Designs

Time (sec)	Fractional Power for U-235 (F1)	Fractional Power for U-233 (F2)
52	100.00%	100.00%
53	12.89%	12.43%
54	12.64%	12.21%
55	12.49%	12.05%
56	12.33%	11.90%
57	12.18%	11.75%
58	12.03%	11.61%
59	11.88%	11.46%
60	11.73%	11.32%
61	11.59%	11.18%
62	11.45%	11.04%
72	10.11%	9.76%
82	8.92%	8.61%
92	7.88%	7.70%
102	6.96%	6.79%
112	6.14%	6.00%
172	3.11%	3.08%
232	1.58%	1.56%
292	0.81%	0.81%
352	0.41%	0.41%
412	0.21%	0.21%
472	0.11%	0.10%

For this heat production curve, the shutdown margin for the purposes of the prompt drop calculation was assumed to be 10%. Heat production curves utilizing a

shutdown margin of only 3% for the prompt drop calculation were also simulated and the results were approximately 15K higher than the temperatures reported in the following 6 figures. These values are still well within the thermal limits imposed on the structural components. The conclusions drawn should not be affected because these two curves sufficiently bound the uncertainty in the total heat production upon shutdown.

Since the full corner sub-channel experienced the largest temperature rise in both the F1 and F2 designs, it represented the most limiting place for heat rejection in the entire Fast Flux Trap flow loop system. The temperature near the end of the full corner sub-channel exit was tracked throughout the entire pump trip transient. The temperature profiles for the F1 design fuel, clad and coolant are presented in Figure 32, Figure 33 and Figure 34 respectively along with the associated temperature limit for each material.

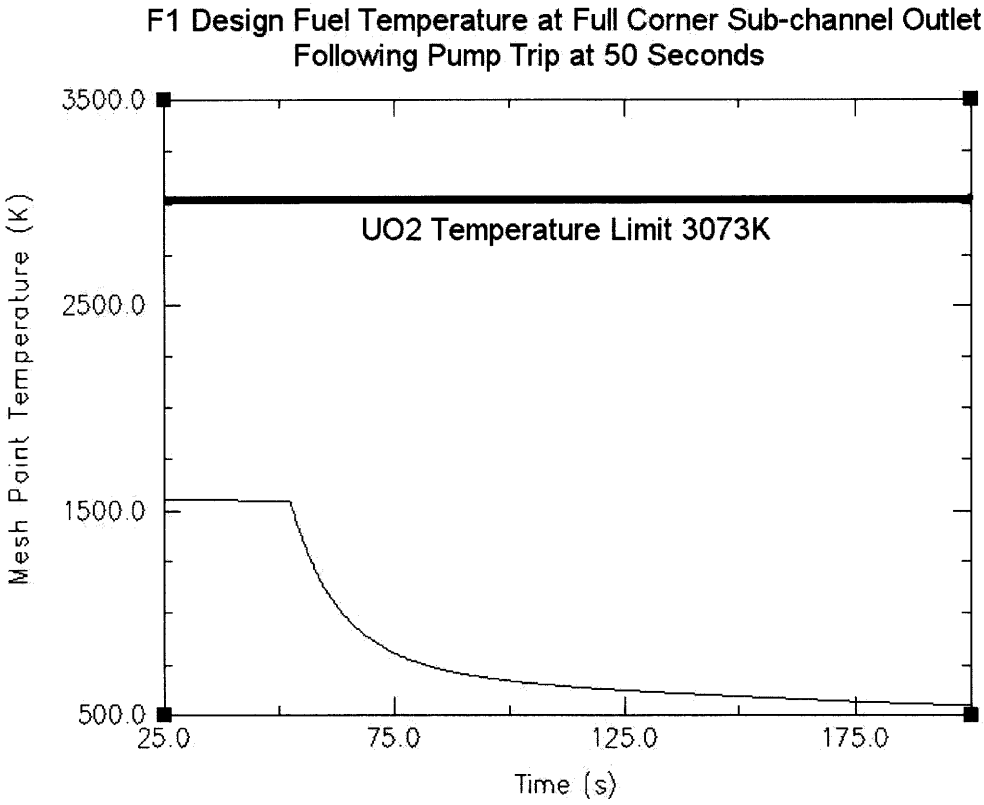

Figure 32: F1 FFT Design Fuel Temperature at Side Sub-channel Outlet

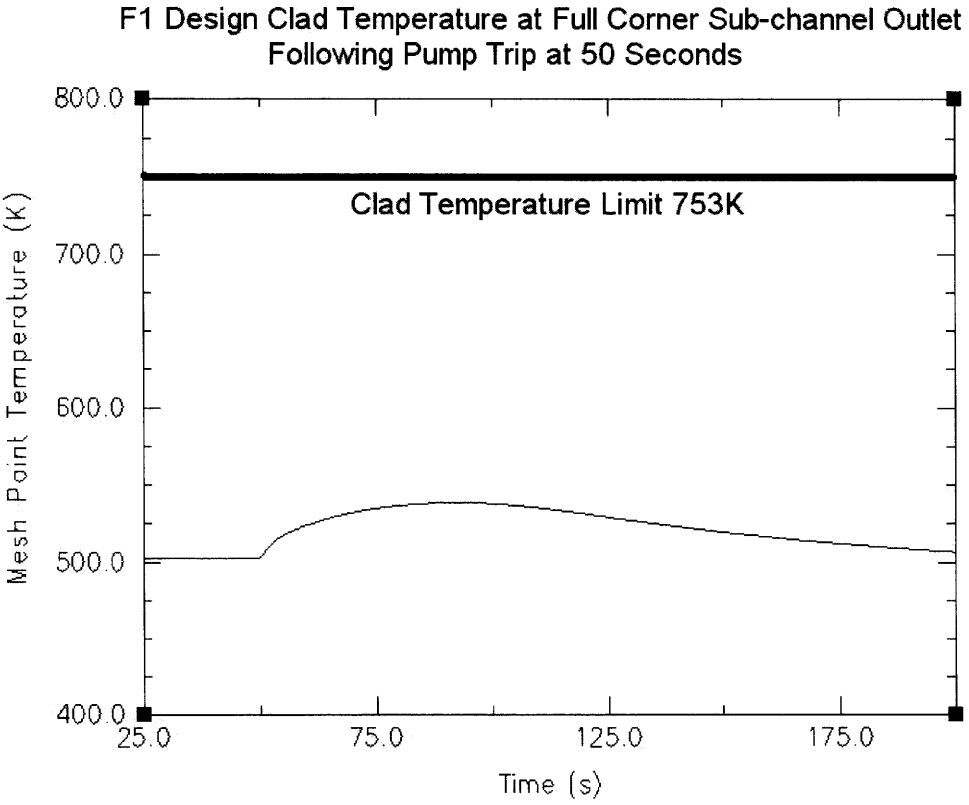

Figure 33: F1 FFT Design Clad Temperature at Side Sub-channel Outlet

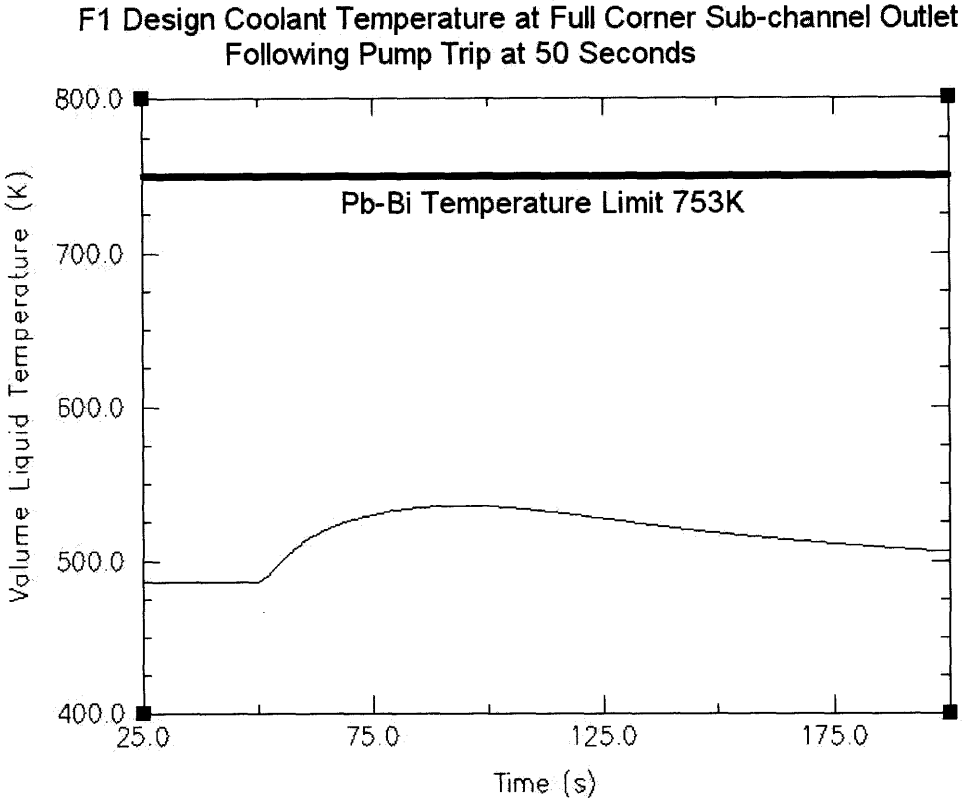

Figure 34: F1 FFT Design Pb-Bi Temperature at Side Sub-channel Outlet

As shown in the prior figures, the F1 design has a large thermal margin to the temperature limits of the materials utilized in this design. Over the course of the entire pump trip transient, the UO_2 fuel has a large ~1450K minimum margin to melt while the Pb-Bi coolant has a ~210K margin to the onset of corrosion with the T91 clad. The most limiting parameter during this transient for the F1 design is the temperature of the T91 clad which has a minimum margin of ~200K until the temperature regime where corrosion can start to become a problem.

The temperature profiles for the F2 design fuel, clad and coolant are presented in Figure 35, Figure 36 and Figure 37 respectively along with the associated temperature limit for each material.

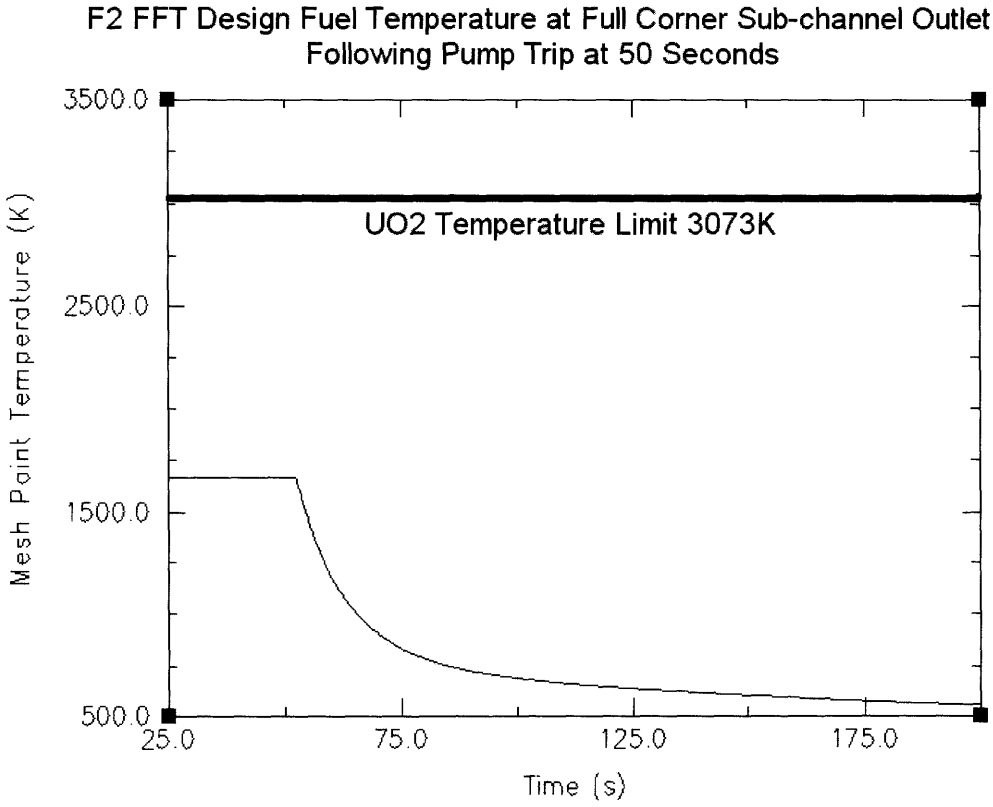

Figure 35: F2 FFT Design Fuel Temperature at Side Sub-channel Outlet

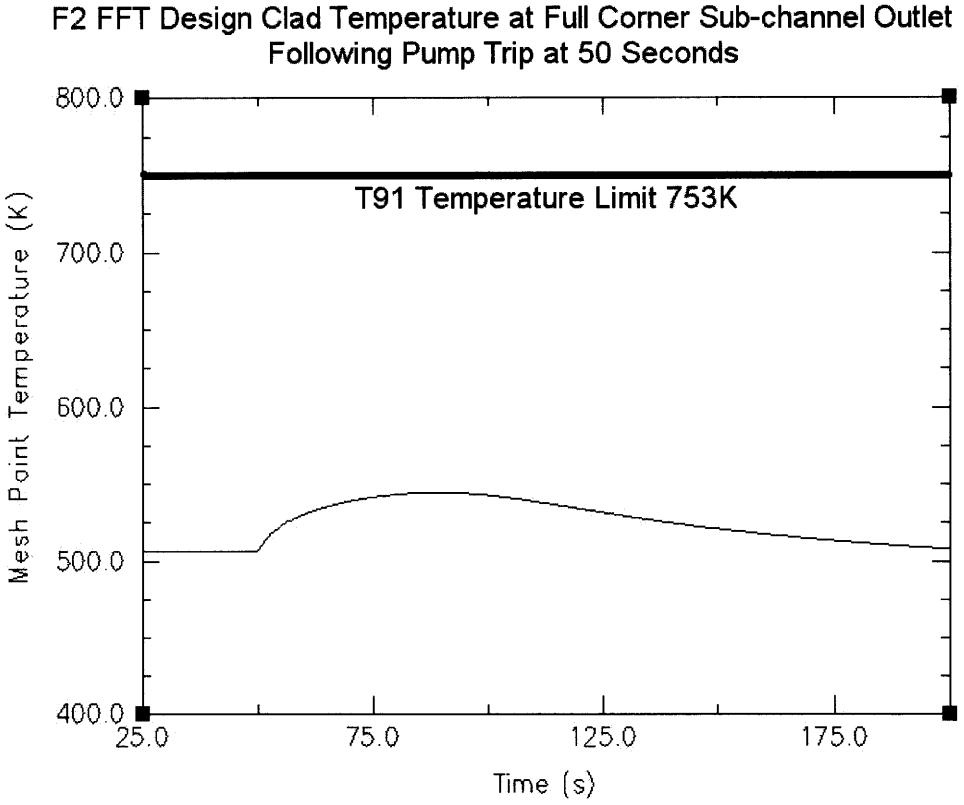

Figure 36: F2 FFT Design Clad Temperature at Side Sub-channel Outlet

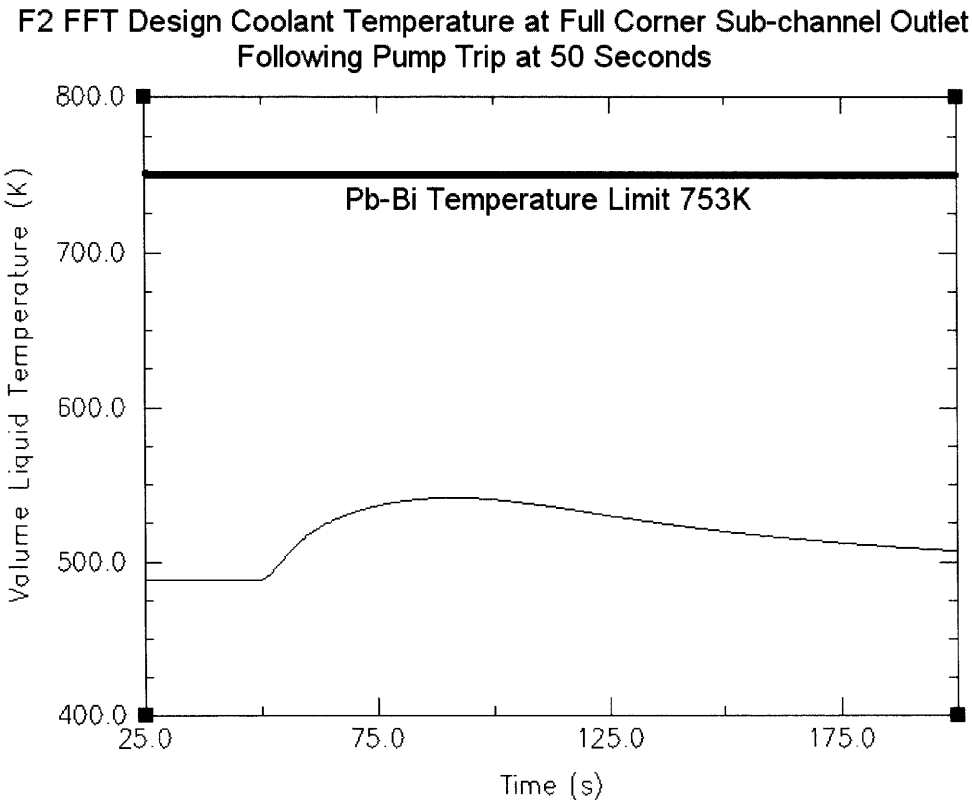

Figure 37: F2 FFT Design Pb-Bi Temperature at Side Sub-channel Outlet

As shown in the prior figures, the F2 design also has a large thermal margin to the temperature limits of the materials utilized in this design. Over the course of the entire pump trip transient, the UO_2 fuel has a large ~1370K minimum margin to melt while the Pb-Bi coolant has a ~210K margin to the onset of corrosion with the T91 clad. The most limiting parameter during this transient for the F2 design is again the temperature of the T91 clad which has a minimum margin of ~200K until the temperature regime where corrosion can start to become a problem.

In summary, this section has proven that both the F1 and F2 Fast Flux Trap designs can safely survive a Pb-Bi pump trip transient assuming a 2 second delay time between the trip of the pump and the scram of the reactor. However, in order to prevent

appreciable temperature gradients in the Pb-Bi, the pump should be restarted as soon as possible after the pump trip so that the heated coolant from the storage tank on the reactor top can continue to circulate through the Fast Flux Trap loop. After the reactor is shutdown, the decay heat will continue to be removed by the secondary loop on the reactor top via forced convection. The coolant pump should be connected to its own emergency power supply so that interruptions in power from Cambridge Electric do not affect operation of the coolant pump. The Pb-Bi coolant is prevented from freezing by a heating element installed in the storage tank on the reactor top.

Chapter 5 - Summary

5.1 Conclusions

This study sought to develop an innovative core design concept which could provide a significantly higher fast neutron flux than the previously proposed designs with low enrichment fuel for the MIT research reactor. The goal of enabling the performance of a wider variety of experiments for advanced technological development was achieved by proposing a design capable of a significantly higher fast flux than both the existing HEU core as well as previously proposed LEU cores. This new core design has a fast flux which is closer to the other much larger test reactors and hence will allow the MIT Nuclear Reactor Laboratory to participate with these other facilities for fast irradiation. Table 43 shows how the fast flux in this design compares to both the Advanced Test Reactor [Chang, *et al.* 2008] and the High Flux Isotope Reactor [Ellis, *et al.* 2008]. It is important to note that both the ATR and HFIR have not published any information on how the necessary conversion of their facilities from HEU to LEU will affect their maximum achievable fast flux. This conversion process could decrease their fast flux numbers quoted in the table below unless the power density is uprated and/or other major modifications are implemented.

Table 37: Fast Flux Comparison between the MITR-III FFT Design, ATR and HFIR

	Power Level (MW)	Fast Flux (0.1-10 MeV)	Fuel
MITR-III F1 Design	10	2.64E+14	LEU
MITR-III F2 Design	10	2.78E+14	LEU
HFIR	85	8.50E+14	HEU
ATR	250	5.00E+14	HEU

The F1 design was also shown to offer a 252% higher fast flux than the 5 MW LEU reference MITR design and a 235% higher fast flux than the currently operating 5 MW HEU reference design. The F2 design offers a 271% higher fast flux than the 5 MW LEU reference MITR design and a 253% higher fast flux than the currently operating 5 MW HEU reference design. Additionally, the F2 design includes an aspect which allows it to contribute to the strength of the international nuclear non-proliferation regime while permitting for a modest enhancement of fast flux over the F1 design. The inclusion of the ^{233}U isotope into this current Fast Flux Trap design can help to burn-down some of the existing two metric ton stockpile of highly enriched ^{233}U currently stored at Oak Ridge National Laboratory. However, the value of helping to burn down the existing legacy stockpile of ^{233}U will have to be weighed against the likely higher costs of new $^{233}UO_2$ fuel qualification in order to determine the viability of future adoption. Nevertheless, the F1 design offers a high performance, fast and likely more economical path to implementation because of the simpler fuel qualification requirements.

The neutronic evaluation in the third chapter showed that the proposed Fast Flux Trap design performs well in steady-state, reactivity insertion and lifetime analyses. The steady-state analyses highlighted the flux spectrum enhancement, showed how the thermal flux could be minimized via incorporation of a cadmium filter, demonstrated that the reactivity worth of typical experimental samples is very small and illustrated that the

power peaking profiles for both the core fuel plates as well as the Amplifier Pins in the Fast Flux Trap are suitable. The investigated reactivity insertion analyses showed that the initial insertion of the Fast Flux Trap into the core, leakage between the Pb-Bi and primary water coolant and flooding of the central irradiation facility do not present any insurmountable challenges. The lifetime analyses presented how the neutron flux and heat production change with time for both the F1 and F2 Fast Flux Trap designs so that an appropriate replacement schedule can be determined if needed.

The thermal hydraulic evaluation in the fourth chapter described why the Pb-Bi Eutectic was selected as the coolant as well as why the T91 alloy was selected as the structural material for the Fast Flux Trap. The steady-state analyses described the hydrodynamic model for the Pb-Bi loop in addition to showing that the temperature, pressure and velocity profiles during normal operation of the Fast Flux Trap are well within the acceptable operational capabilities of the materials utilized in this design. The F1 design had a total steady-state coolant pressure drop of 1.01 MPa, a maximum coolant velocity of 2.22 m/sec and a coolant temperature difference of 47°K. The F2 design has a total steady-state coolant pressure drop of 1.01 MPa, a maximum coolant velocity of 2.23 m/sec and a coolant temperature difference of 53°K. The transient analyses showed that the Fast Flux Trap can safely survive a Pb-Bi pump trip transient assuming a 2 second delay time between the trip of the pump and the scram of the reactor. The most limiting parameter during this transient was the peak temperature of the T91 clad, which was ~200K below the 753K temperature limit where corrosion starts to become a problem for both the F1 and F2 design.

Moving forward, the nuclear industry is going to depend upon the current fleet of research and test reactors for advanced technological development in the field so it is critical that these facilities treat this LEU conversion process as an opportunity to enhance their experimental capabilities. The innovations developed in this thesis allowed for a 10 MW research reactor to provide more economic fast neutron flux (i.e. higher flux per unit thermal power) than two other test reactors which have roughly an order of magnitude higher power level. While the specific design developed in this dissertation is particular to the MIT research reactor core, the Fast Flux Trap design concept can potentially be applied in other test reactor cores so that other research and test reactor facilities can benefit from this enhanced capability.

5.2 Recommendations for Future Work

Several practical aspects of implementing the Fast Flux Trap design into the current MITR core have been mentioned in this work. However, many more analyses will be needed to fully characterize the proposed core design for approval by the NRC. These include:

1) Development of an equilibrium core model will be required (in addition to the fresh core model presented here) to more accurately evaluate the reactor design throughout its service lifetime. This includes full characterization of the source term for the new design.

2) An installation feasibility analysis needs to be performed in order to address more of the practical mechanical engineering considerations associated with actual installation of the upgraded core.
3) The natural circulation capability of the proposed 10 MWth MITR core (not including the Fast Flux Trap) will have to be verified by future analyses. The larger decay heat source term in the proposed core should help to drive the natural circulation.
4) An in-depth transient analysis for the MITR core will also need to be conducted for the NRC certification, as well as a characterization of the changes in the fuel Doppler broadening reactivity effects between this and previous designs.
5) Finally, an economic analysis needs to be performed on the total cost for the upgrade so that the MIT Nuclear Reactor Laboratory knows if the upgrade is worth pursuing.

References

Buongiorno, J., Hu, L., Kim, S., Hannink, R., Truong, B., Forrest, E. "Nanofluids for Enhanced Economics and Safety of Nuclear Reactors: An Evaluation of the Potential Features, Issues, and Research Gaps." Nuclear Technology. Volume 162. p 80-91. April 2008

CEA. "Handbook on Lead-bismuth Eutectic Alloy and Lead Properties, Materials Compatibility, Thermal-hydraulics and Technologies." 2007 Edition. Available at: http://www.nea.fr/html/science/reports/2007/nea6195-handbook.html

Chang, G., Ambrosek, R. "Hardening Neutron Spectrum for Advanced Actinide Transmutation Experiments in the ATR." Radiation Protection Dosimetry. Volume 115. No 1-4. pp 63-68. 2005.

Chang, G., Lillo, M., Ambrosek, R. "Neutronic and Thermal Hydraulics Study for Using a Low-Enriched Uranium Core in the Advanced Test Reactor 2008 Final Report." INL/EXT-08-13980. Idaho National Laboratory. June 2008.

Department of Energy. "Neutron Flux Spectrum." Reactor Theory (Neutron Characteristics). DOE-HDBK-1019/I-93. p 34. 1993.

Eisenhower, D. "Atoms for Peace Speech" Before the General Assembly of the United Nations on Peaceful Uses of Atomic Energy. December 8, 1953.

Ellis, T., Newton, T. "Innovations in Design for the Enhancement of Experimental Neutron Flux at the Massachusetts Institute of Technology Research Reactor." International Congress on Advances in Nuclear Power Plants. Paper 8423. Anaheim, CA. June 8-12, 2008.

Ellis, R., Gehin, J., McDuffee, J., Hobbs, R. "Analysis of a Fast Spectrum Irradiation Facility in the High Flux Isotope Reactor." International Congress on the Physics of Reactors. Interlaken, Switzerland. September 14-19, 2008.

Farrel, K., King, R. "Tensile Properties of Neutron-Irradiated 6061 Aluminum Alloy in Annealed ad Precipitation-Hardened Conditions." Effects of Radiation on Structural Materials. ASTM STP 683. American Society for Testing and Materials. p 440-449. 1979.

Guillen, D., Yoder, T. "Thermal Hydraulic Effect of Fuel Plate Surface Roughness." Nuclear Engineering and Design. Volume 238. Issue 9. p 2480-2483. September 2008.

Hu, L., Kohse, G. "MITR Users Guide." MIT Nuclear Reactor Laboratory. Massachusetts Institute of Technology. Revision 1. p 23. June 2008.

International Atomic Energy Agency. "Research Reactor Core Conversion Guidebook." Volume 4: Fuels. Appendices I-K. IAEA-TECDOC-643. 1992.

Kazimi, M. "Thorium Fuel for Nuclear Energy." American Scientist. Volume 91. Number 5. p 408. September-October 2003.

King, R., Jostsons, A., Farrell, K. "Neutron Irradiation Damage in a Precipitation-Hardened Aluminum Alloy." Effects of Radiation on Substructure and Mechanical Properties of Metals and Alloys. ASTM STP 529. American Society for Testing and Materials. 1973. p 165-180.

Kloosterman, J. "Topic 3: Decay Heat Predictions: Experiments, Methods and Data. Integral Validation and Decay Heat Standards." IRI-131-2000-005. Frédéric Joliot/Otto Hahn Summer School in Reactor Physics. Cadarache, France. August 21-30, 2000.

Kohse, G. "Evaluation of Radiation Damage to the MITR-II Reactor Vessel – Effect on Pressure Rating." MIT Nuclear Reactor Laboratory LEU Conversion Project Internal Report. September 2008a.

Kohse, G. Personal Communication with the Author. MITR LEU Conversion Group Meeting. November 20, 2008b.

Ko, Y. "Thermal Hydraulics Analysis of the MIT Research Reactor in Support of a Low Enrichment Uranium (LEU) Core Conversion." Master of Science Thesis. Department of Nuclear Science and Engineering. Massachusetts Institute of Technology. January 2008.

Memmott, M. Personal Email Communication with the Author. August 10, 2008.

Newton, T. "Development of a Low Enrichment Uranium Core for the MIT Reactor." Doctor of Philosophy Dissertation. Department of Nuclear Science and Engineering. Massachusetts Institute of Technology. February 2006.

Palmer, M. "Propagation of Uncertainty through Mathematical Operations." Experimental Techniques in Fluids. School-wide Modular Program for Fluid Mechanics. Massachusetts Institute of Technology. 2003.

Pitcher, E. "The Materials Test Station: A Fast-Spectrum Irradiation Facility." Journal of Nuclear Materials. Volume 377. pp 17-20. 2008.

RELAP5-3D Code Development Team. "RELAP5-3D Code Manual." INEEL-EXT-98-00834. Revision 2.3. April 2005.

Short, M. "Functionally Graded Composites (FGCs) for Service in Advanced Lead-Bismuth Reactors." 2nd Tokyo Tech-MIT Symposium on Innovative Nuclear Energy Systems (TM-INES 2). Kamkura, Kanagawa, Japan. July 23-24, 2007.

Shwageraus, E., Ronen, Y., Friedman, E. "The Smallest Thermal Nuclear Reactor" Nuclear Science and Engineering. Volume 153. 2006. pp 90-92.

Todreas, N., Kazimi, M. "Nuclear Systems Volume I. Thermal Hydraulics Fundamentals." Second Edition. Hemisphere Publishing. December 1989.

Todreas, N., MacDonald, P., Buongiorno, J., Loewen, E. "Medium-power Lead Alloy Reactors: Missions for this Reactor Technology." Nuclear Technology. Volume 147. Number 3. 305. September 2004.

U.S. Department of Energy. "Reduced Enrichment for Research and Test Reactors." http://www.nnsa.doe.gov/na-20/rertr.shtml

Von Hippel, F., Kang, J. "U-232 and the Proliferation Resistance of U-233 in Spent Fuel." Science and Global Security. Volume 9. pp 1-32. 2001.

Wachs, D., et al. Idaho National Laboratory. Totev, T., et al. Argonne National Laboratory. Dunavant, R., et al. Y-12 National Security Complex. "Progress in US LEU Fuel Development." Research Reactor Fuel Management meeting. Hamburg, Germany. March 2008.

X-5 Monte Carlo Team. "MCNP – A General Monte Carlo N-Particle Transport Code, Version 5." LA-UR-03-1987. Los Alamos National Laboratory. April 24, 2003.

Xu, Z., "Design Strategies for Optimizing High Burnup Fuel in Pressurized Water Reactors." Doctor of Philosophy Dissertation. Department of Nuclear Science and Engineering. Massachusetts Institute of Technology. January 2003.

Xu, Z., Hejzlar, P. "MCODE, Version 2.2 – An MCNP-ORIGEN DEpletion Program." MIT-NFC-TR-104. Center for Advanced Nuclear Energy Systems. Massachusetts Institute of Technology. December 2008.

Y-12 National Security Complex. "The Y-12 Standard Specification Low Enriched Uranium Metal Supply to Research and Test Reactors." Y/GNSS/05-05. December 2005.

Yarnell, J., Bendt, P. "Calorimetric Fission Product Decay Heat Measurements for Pu-239, U-233 and U-235." LA-7452-MS. NUREG/CR-0349. Los Alamos National Laboratory. September 1978.

Appendix A: MCNP/MCODE Input Files

A.1 F1 Design

For the input file please see either Professor Mujid Kazimi at the MIT Department of Nuclear Science and Engineering or Dr. Thomas Newton at the MIT Nuclear Reactor Laboratory.

A.2 F2 Design

For the input file please see either Professor Mujid Kazimi at the MIT Department of Nuclear Science and Engineering or Dr. Thomas Newton at the MIT Nuclear Reactor Laboratory.

Appendix B: RELAP Input Files

B.1 F1 Design

For the input file please see either Professor Mujid Kazimi at the MIT Department of Nuclear Science and Engineering or Dr. Thomas Newton at the MIT Nuclear Reactor Laboratory.

B.2 F2 Design

For the input file please see either Professor Mujid Kazimi at the MIT Department of Nuclear Science and Engineering or Dr. Thomas Newton at the MIT Nuclear Reactor Laboratory.

Appendix C: Computational Modeling Tools

C.1 Neutronic Modeling Tools

The steady-state neutronic simulations were calculated using MCNP5 [X-5 2003]. MCNP is a general purpose Monte Carlo N-Particle code which can be used to simulate neutron, photon, electron or coupled particle transport which includes the capacity to determine the eigenvalue for critical systems. This code can model any three dimensional system using an array of different surfaces. The particular pointwise cross-section evaluation used for this analysis was the Joint Evaluated Fission and Fusion File (JEFF-3.1) data library. In order to obtain acceptable statistics, typical neutronic simulations were calculated using 10,000 particles for 9,000-10,000 cycles. The typical run time for a file was ~20 hours on a four socket AMD Opteron system running RHEL 5.0. The system has a Tyan s4985 motherboard and 4 OpteronT 8214 Dual-Core (2.2 GHz) processors and 8GB 667 MHz DDR2 memory. The heat production was calculated with a track length estimate of energy deposition (cell heating) F6 tally. The quantity which is actually scored by the F6 tally is as follows (in units of MeV/g):

$$H_t = \frac{\rho_\alpha}{m} \int dE \int dt \int dV \int d\Omega \sigma_t(E) H(E) \psi(\vec{r}, \hat{\Omega}, E, t)$$

This tally must then be normalized per starting particle. This normalized tally, for the example of the plate-type fuel element hot channel factor calculation, takes an average of all the other hot channel tallies for every fuel plate in the core and then divides each normalized hot channel tally by the core average hot channel tally in order to determine the final hot channel factor for each individual channel.

The depletion calculations were performed with MCODE [Xu and Hejzlar 2008]. MCODE Version 2.2 is a linkage program which combines the continuous-energy Monte Carlo code MCNP-4C and the one group depletion code ORIGEN2 to perform burnup simulations for nuclear fission reactor systems. MCODE uses MCNP to generate the neutron flux solution and detailed reaction rates in the defined depletion zones. MCODE then uses ORIGEN to perform multi-nuclide depletion calculations for each depletion zone and then uses the results from these calculations to update the material composition in the MCNP model. To further increase accuracy, MCODE employs a predictor-corrector approach for the MCNP/ORIGEN coupling. Again the JEFF-3.1 data library was used for all MCNP analyses and the neutronic simulations employed 10,000 particles for ~6000 cycles in order to achieve acceptable statistics. The typical run time for one MCODE depletion was ~4-5 days. Example MCODE input files are featured in Appendix A.

C.2 Thermal Hydraulic Modeling Tools

The steady-state and transient thermal hydraulic analyses for the liquid Pb-Bi cooled Fast Flux Trap were performed with RELAP5-3D [RELAP5-3D 2005]. This code

uses a nonhomogeneous and nonequilibrium model for the two-phase system which is solved by a fast, partially implicit numerical scheme to allow for efficient system transient calculations. Earlier versions of the RELAP5 code were developed to specifically analyze all transients and postulated accidents for LWR systems. However RELAP5-3D was developed as more of a generic code which can simulate a wide variety of hydraulic and thermal transients in both nuclear and non-nuclear systems involving mixtures of vapor, liquid, noncondensable gases and nonvolatile solute. In order to allow for the system to come to equilibrium for the specified flowrates the problem was run for ~2000 seconds. After the equilibrium profiles for temperature, pressure and velocity were determined, these parameters were entered into a subsequent input file for transient simulation. Example RELAP5-3D input files are featured in Appendix B.

Appendix D: Experimental Sample Total Absorption Cross Sections

Figure 38 shows the total absorption cross section of four different isotopes of Iron. The red colored line is ^{45}Fe, the green colored line is ^{56}Fe, the blue colored line is ^{57}Fe and the purple colored line is ^{58}Fe.

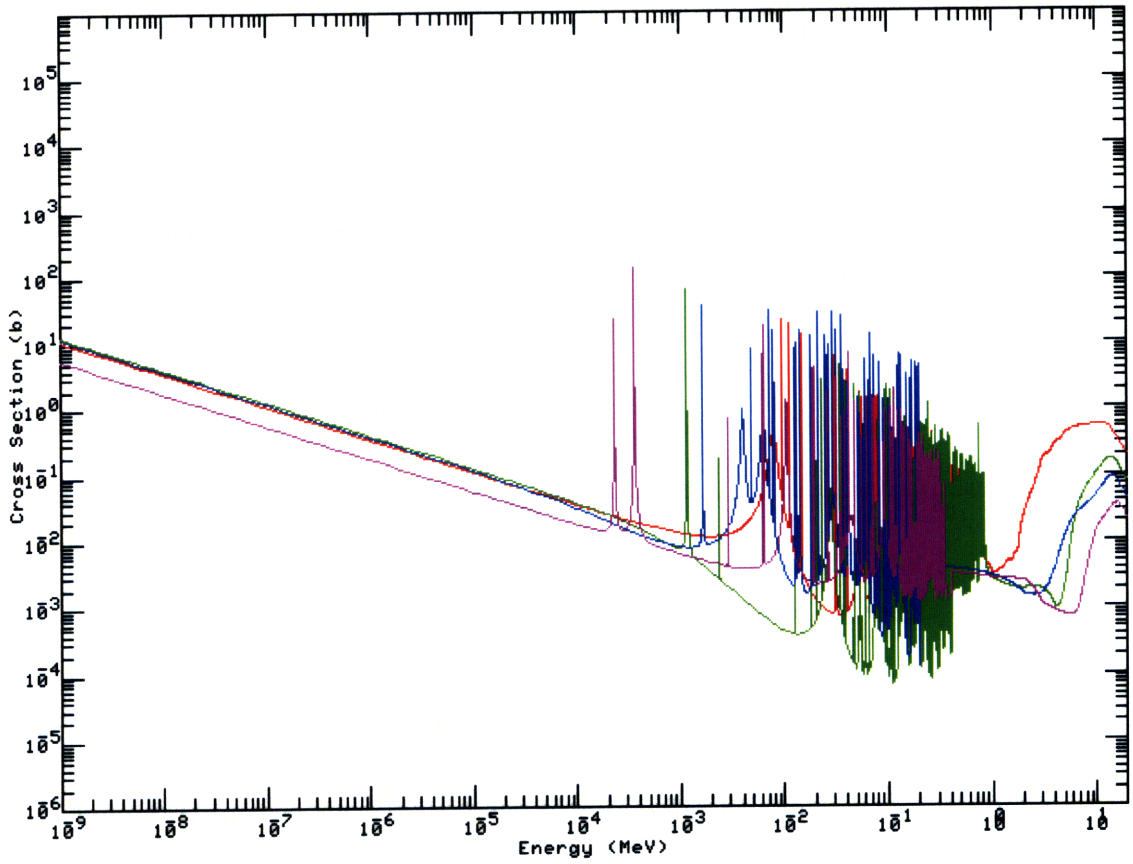

Figure 38: Total Absorption Cross Section for Isotopes of Iron

Figure 39 shows the total absorption cross section of four different isotopes of chromium. The red colored line is ^{50}Cr, the green colored line is ^{52}Cr, the blue colored line is ^{53}Cr and the purple colored line is ^{54}Cr.

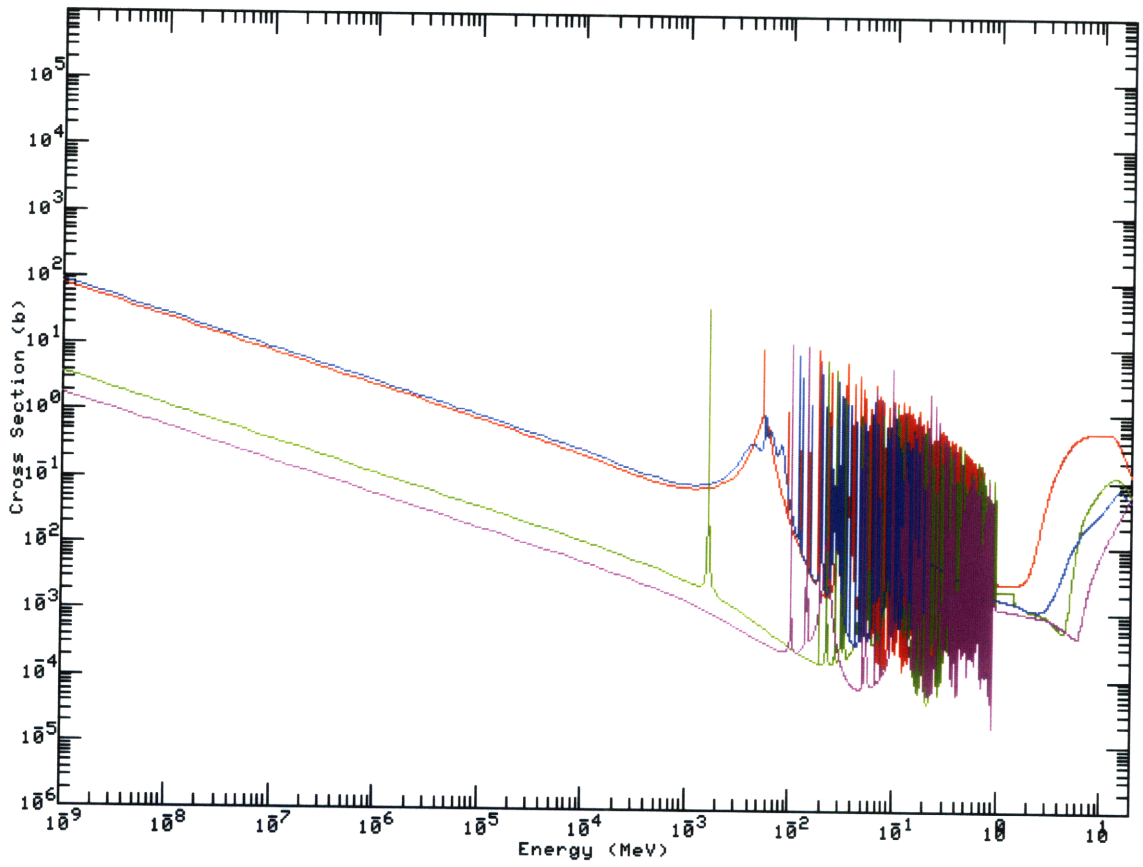

Figure 39: Total Absorption Cross Section for Isotopes of Chromium

Both stainless steel and HT-9 alloy are principally constituted of iron (~80%) and chromium (~15%) so the total absorption characteristics of each material should approximate a weighted combination of the two cross sections above.

Figure 40 shows the total absorption cross section of natural graphite.

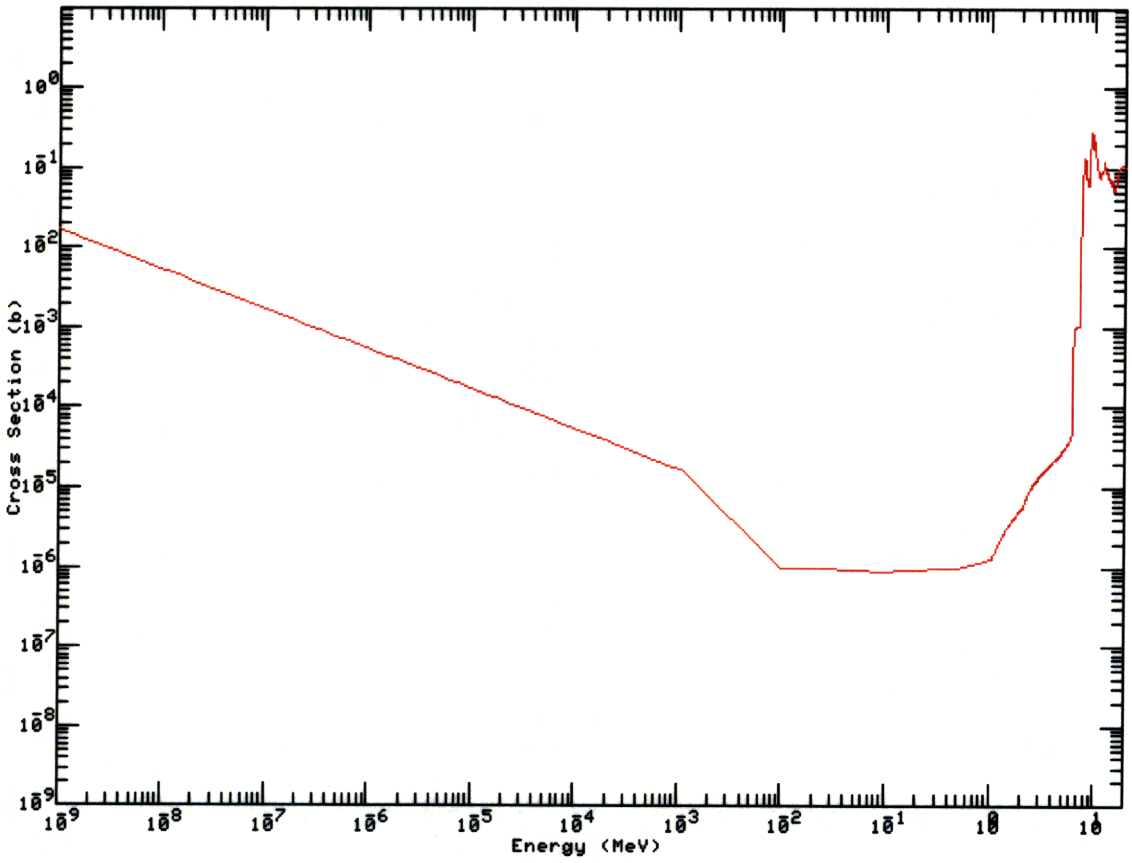

Figure 40: Total Absorption Cross Section for Natural Graphite

Figure 41 shows the total absorption cross section of natural tungsten.

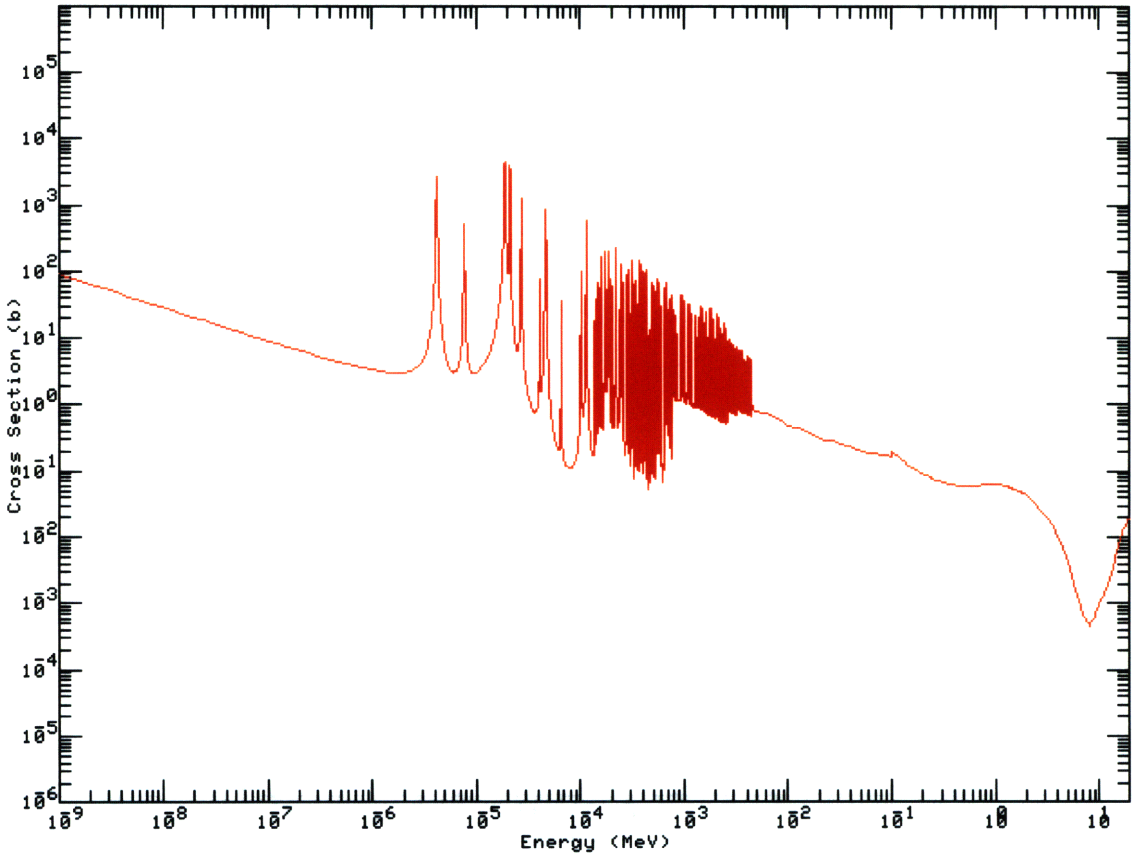

Figure 41: Total Absorption Cross Section for Natural Tungsten

Figure 42 shows the total absorption cross section of natural titanium.

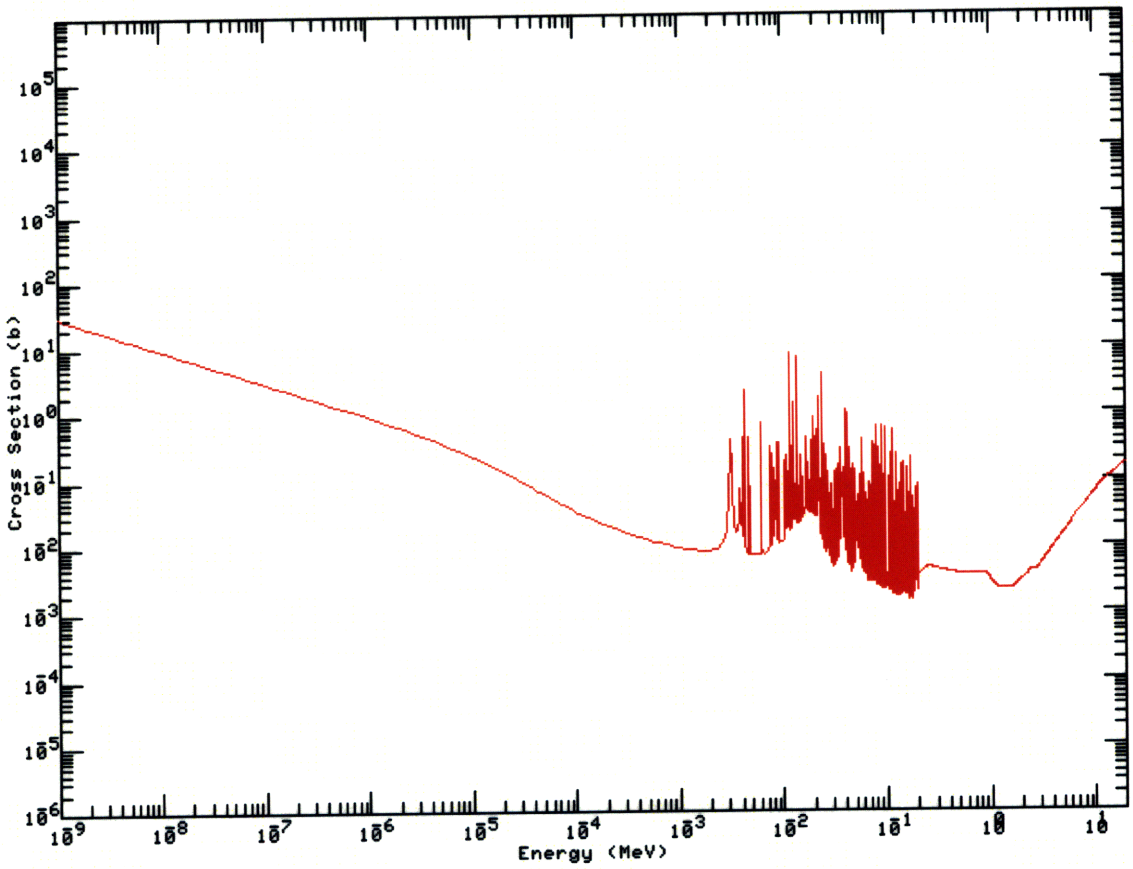

Figure 42: Total Absorption Cross Section for Natural Titanium